Novel Stability Problems in Pipe Flows

A Thesis
Submitted for the Degree of
Doctor of Philosophy
in the Faculty of Engineering

by

Kirti Chandra Sahu

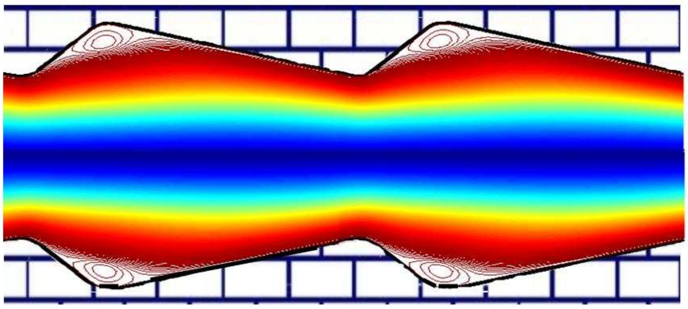

ENGINEERING MECHANICS UNIT
JAWAHARLAL NEHRU CENTRE FOR ADVANCED SCIENTIFIC RESEARCH
(A Deemed University)
Bangalore – 560 064

APRIL 2007

To my parents

DECLARATION

*I hereby declare that the matter embodied in the thesis entitled "***Novel Stability Problems in Pipe Flows***" is the result of investigations carried out by me at the Engineering Mechanics Unit, Jawaharlal Nehru Centre for Advanced Scientific Research, Bangalore, India under the supervision of* **Prof. Rama Govindarajan** *and that it has not been submitted elsewhere for the award of any degree or diploma.*

In keeping with the general practice in reporting scientific observations, due acknowledgement has been made whenever the work described is based on the findings of other investigators.

Kirti Chandra Sahu

CERTIFICATE

*I hereby certify that the matter embodied in this thesis entitled "***Novel Stability Problems in Pipe Flows***" has been carried out by* **Mr. Kirti Chandra Sahu** *at the Engineering Mechanics Unit, Jawaharlal Nehru Centre for Advanced Scientific Research, Bangalore, India under my supervision and that it has not been submitted elsewhere for the award of any degree or diploma.*

Prof. Rama Govindarajan
(***Research Supervisor)***

Acknowledgements

This thesis could not be possible without the help, guidance, and constant encouragement of my thesis advisor, Prof. Rama Govinadrajan. She is a great source of inspiration for me. Indeed she has taught me what research is all about. She has been much more than my thesis advisor; she has been a parent to me during my study at the Engineering Mechanics Unit, Jawaharlal Nehru Centre for Advanced Scientific Research, Bangalore. I will always fondly remember my conversations, scientific discussions with her. I am fortunate to have her as my thesis advisor.

I am grateful to Prof. Roddam Narasimha for valuable discussions and suggestions, which helped me in grasping the fundamentals in my area of research, and was essential for the completion of this thesis.

I would like to thank Dr. K. R. Sreenivas for his help and encouragement towards the thesis. His valuable suggestions and ideas about the practical situations helped me to think from the point of view of experiments. It is a pleasure to thank Dr. Meheboob Alam for his encouragement. I wish to thank Dr. Ganesh Subramanian for discussing several research problems with me including the one of wall-slip flows.

I thank Prof. S.P. Vanka for giving me a foundation in Computational Fluid Dynamics, for his keen interest in the work and many helpful suggestions to accelerate the rate of convergence of our Navier-Stokes solver. I thank him for sharing his multigrid algorithm with us.

I gratefully thank Prof. U. N. Sinha, Dr. T. N Venkatesh, Dr. V. R. Sarasamma, Dr. Rajalakshmy S., Mr. Amit and Dr. Jaganath for building the MK6 parallel machine and parallising our Navier-Stokes solver at the Flosover Unit, National Aerospace Lab, Bangalore.

I would like to thank Prof. A. K. Sood and Prof. G. Homsy for their helpful suggestions. I also wish to thank Dr. Narayanan Menon for many discussions. Grateful thanks to Prof. Tom Mullin for sharing his unpublished results of the developing flow in the entry region of a pipe and for discussions.

We acknowledge the Defence Research and Development Organisation, India for financial support. I would like to thank Council of Scientific and Industrial Research, India and Indian National Science Academy, India for providing me the financial support to attend the conference "Eleventh Asian Congress of Fluid Mechanics", Malaysia (2006). I also wish to thank International Center for Theoritical Physics, Italy for the financial support to attend the workshop "Introduction to Microfluidics", Italy (2005).

I would like to thank Dr. Jay Raj Kumar (Manipal Hospital) for many discussions on blood flow in human body. I really appreciate his encouragement. I thank Dr. Sameen for the collaboration to study the flow through a diverging channel with slip.

I would like to thank my lab mates: Sameen, Vinod, Vijay, Binaya, Mukund, Faraz, Subarna, Rajaram, Shreyas, Punit, Mani, Anubhab, Sanjeeb, Antina, Ratul, Harish, Pinaki, Kaushik, Ashish, Priyanka, Anjana and Gayathri for their constant supports, encouragement and creating a very good friendly and working environment in the Lab. Special thanks to Vijay, Kaushik and Raji for their help and encouragement.

I am ever grateful to my institute, JNCASR for providing the necessary infrastructure and financial support. I thank the office staff of JNCASR for their prompt and generous help. I would also like to thank the computer lab, JNCASR for providing excellent computation facilities. I am grateful to Dr. Umesh V Waghmare for allowing me to use all the complab facilities. I thank Rajesh, Shital, Ravi, Vikash, Masanam for helping me use the computer lab facilities.

During my Ph.D, I have come across many nice and friendly people. I would like to thank all of them whose presence have helped me a lot towards the completion of the thesis. I would like to thank Saswati, Gopal, Chandu, Jyoti, Sasmita and Jyotirmayee to make me feel homely at $\mathcal{JNCASR}$. Thanks to Asish, Prasant, Motin, Joydeep, Subrata, Krupa for their support and encouragement. I would also like thank Ram and Sutirth for their help and encouragement in many situations.

I would like to thank few people outside $\mathcal{JNC}$. I thank Amit Khatri (National Aerospace Lab) and Malik (Indian Institute of Science) for their encouragement. I am grateful to have friends like Subrat, Srikant, Om, Subudhi, Saroj and Sandeep. Special thanks to Subrat for several Spiritual and Philosophical discussions we have had. It indeed inspired me a lot.

Finally I would like to thank my parents for their constant care and blessings which helped me to grow in both professional and social life. I would like to thank my brother (Surya) and my sisters (Anu and Mami) for their love which gave me enough courage to face any problem. Last but not the least, I would like to thank Manisha for her support.

Synopsis

The main objective of this thesis is to study the instability and evaluate the likely mechanisms of transition to turbulence in divergent and small-scale (as discussed below) pipe flows. It was first demonstrated by Reynolds (1883) that pipe flow becomes turbulent at a particular value of a non-dimensional parameter which now bears his name. In recent times, this problem has received a lot of renewed attention [Faisst & Eckhardt (2003); Hof *et al.* (2003); Peixinho & Mullin (2006)]. With many demonstrations [see e.g. Hof *et al.* (2004)] that pipe flow may be maintained laminar up to high Reynolds numbers (of the order of hundred thousand), an understanding of the effect of variations in geometry and flow conditions are increasingly relevant.

Fully developed laminar flow (Hagen-Poiseuille flow) through a straight pipe is linearly stable at any Reynolds number, Re. In this case, nonlinear and transient growth mechanisms drive the transition to turbulence. However Hagen-Poiseuille flow is attained only when the pipe wall is straight and smooth and the pipe is long enough. The length required increases with Reynolds number. There are many variations from these conditions where linear instability can play a significant role in transition to turbulence. Some of these situations are addressed in this thesis. They are, flow through (i) a divergent pipe, (ii) a variety of diverging-converging pipes with constant average radius, (iii) diverging pipes/channels with velocity slip at the wall, and (iv) the entry region of a straight pipe. The instabilities of these spatially developing laminar flows is shown to be fundamentally different from flows that do not vary downstream. We have also studied separation in diverging channels and pipes.

It is not in general possible to derive analytical solutions for the laminar flows described above. We obtain the mean flow by solving the steady two-dimensional/axisymmetric Navier-Stokes equations exactly. For the accuracy desired, the computational time required for solving the elliptic equations is very large. A full-multigrid algorithm (FMG) is used to accelerate the convergence. The code is parallelised at the National Aerospace Laboratories, Bangalore. The FMG speeds up the solution by a factor of hundred as compared to many traditional algorithms like Gauss-Seidel and Jacobi iteration technique, and the parallel code (using an eight processor machine) gives a superlinear speed-up of 11 times over a single processor.

(i) The laminar flow through a divergent pipe is shown to be linearly unstable at any angle of divergence a, with the instability critical Reynolds number tending to infinity as the angle of divergence goes to zero. At small a $(< 1^\circ)$ the instability is determined by a parameter $S(x) \equiv a\mathrm{Re}$ describing the basic flow profile, and the mechanism is inviscid. The flow is linearly unstable to the swirl mode for $S > 10$. The instability critical Reynolds numbers are surprisingly low, e.g. about 150 for a divergence of 3°, which would suggest a role for such instabilities in the transition to turbulence.

For small angles of divergence and high Reynolds numbers, an axisymmetric Jeffery-Hamel equation (AJH) is derived to describe the mean flow. At larger angles of divergence (1° or greater) the axisymmetric Navier-Stokes equations are solved directly. The partial differential equations for non-parallel stability are solved as an extended eigenvalue problem by a novel technique. (ii) We then study the effect of local asymmetric convergence/divergence on laminar flow through a pipe of constant *average* radius. The main finding is that the instability behaviour can be changed dramatically by reversing the direction of flow. This is offered as a possible mechanism that could be operating in small-scale flows, due to the presence of wall roughness.

(iii) Fluid dynamics and the role of the walls at small-scale can be very different from that at large scales. We make a minor foray into this regime, by considering the effect of wall slip at Knudsen numbers less than 0.1. Recent studies indicate that a velocity slip at the wall dramatically stabilizes the linear mode in a plane two-dimensional channel, but has very little effect on the algebraic transient growth of disturbances [Lauga & Cossu (2005)]. At microscales, apart from slip, local divergences and convergences of the wall are frequently encountered, here we focus on the effect of divergence. Whereas transient growth is more important in a plane channel, at wall divergences of less than a degree, it is linear instability, taking place two orders of magnitude lower in Reynolds number than in a plane channel, which is dominant. Unlike in a plane channel, the effect of velocity slip at the wall is to reduce stability. Transient growth is shown to be an insignificant player in the process of transition to turbulence.

(iv) The laminar velocity profile through a circular pipe is parabolic once the flow is fully developed. However, the distance l_e required to reach this fully-developed state can be very long, and scales linearly with the Reynolds number, Re, roughly as $l_e/R \sim \mathrm{Re}/20$, where R is the pipe radius. Therefore high Reynolds number laminar flow through a pipe of limited length may never reach a parabolic state. We show that in such circumstances linear stability can play an important role in transition. We solve for the basic flow exactly, and conduct a non-parallel stability analysis, to show that flow can be linearly unstable even at a Reynolds number of 1000. In contrast to what is expected of a boundary layer type flow, disturbance growth is higher in the core region. Our results are consistent with that of experiment. Earlier theoretical studies predicted critical Reynolds number an order of magnitude higher than that observed in experiment and were in serious disagreement with each other.

(v) Some other studies which are in the preliminary stage are described at the end of the thesis. These include the study of pulsatile flow through a straight pipe. Prescribing time periodic velocity profiles at the inlet we have solved the Navier-Stokes equation directly using a full-multigrid algorithm on a parallel machine Venkatesh *et al.* (2005). We also studied separated flows in the diverging channel/pipe. At higher angles of divergence, we study flow separation in channels and pipes. The size, location and shape of the separated region for divergent angle varying from 0 to 90 degree are discussed in the thesis. In future, we are planning to conduct full non-parallel stability analysis e.g. global stability analysis of such flows without the approximations made in this thesis.

Refereed Publications

1. “Stability of flow through a slowly diverging pipe”, Kirti Chandra Sahu and Rama Govindarajan, *J. Fluid Mech.*, 531, 2005, 325 - 334.

2. “Super-linear speed-up of a parallel multigrid Navier-Stokes solver on Flosolver”, T. N. Venkatesh, V. R. Sarasamma, Rajalakshmy S., Kirti Chandra Sahu and Rama Govindarajan, *Current Science*, 88(4), 2005, 589 - 593.

3. “A possible linear instability mechanism in small-scale pipe flows”, Kirti Chandra Sahu, *Proceedings of Sixth IUTAM Symposium on Laminar-Turbulent Transition*, Springer, 2006, 127-132.

4. “Instability of entry flow in a pipe”, Kirti Chandra Sahu and Rama Govindarajan, *Proceedings of Eleventh Asian Congress of Fluid Mechanics*, May 22-25, 2006, Kuala Lumpur, Malaysia.

5. “Linear instability of the developing flow in the entry region of a pipe”, Kirti Chandra Sahu and Rama Govindarajan, *ASME Journal of Fluids Engineering*, to appear

Conference Paper

6. “Instabilities in decelerating pipe flow”, *Proceedings of STATPHYS 22*, Bangalore, July, 2004.

Preprints

7. “The relative roles of linear instability and transient growth in divergent channel flow with slip”, Kirti Chandra Sahu, A. Sameen and Rama Govindarajan, preprint

Nomenclature

Roman Letters

E : kinetic energy
H : shape factor
Kn : Knudsen number
L : half channel width
M : Mech number
R : radius of the pipe
R_i : radius of the pipe at the inlet
R_E : radius of the pipe at the smallest cross-section
Re : Reynolds number
Re_i : Reynolds number at the inlet
S : product of $Re \times a$ in diverging pipe
T : time period of the oscillation of the inlet velocity
U : axial velocity
V : radial velocity
W : azimuthal velocity
U_c : loacal centerline velocity
U_i : centerline velocity at the inlet
U_l : axial velocity scaled with the local centerline velocity (U_c/U_i)
V_l : radial velocity scaled with the local centerline velocity (U_c/U_i)
U_s : slip velocity at the wall
U_E : centerline velocity at the smallest cross-section
U_{PI} : axial velocity at piont of inflection
a : slope of the diverging pipe
c : phase speed of the disturbance
e : ellipticity of the pipe
f : is a function describing the boundary
g : growth of the disturbance kinetic energy
i : $\sqrt{-1}$
l_e : entry length for the flow in a straight pipe
l_s : slip length
u : disturbance axial velocity
v : disturbance radial velocity
w : disturbance azimuthal velocity
u_p : unsteady part of axial velocity in pulsatile flow
v_p : unsteady part of radial velocity in pulsatile flow
n : azimuthal wave numeber of the disturbance
p : disturbance pressure
r : radial coordinate

t : time
x : axial coordinate
y : wall normal coordinate

Greek Letters

α : axial wave number of the disturbance
β : spanwise wave number of the disturbance
ω : disturbance frequency
λ : mean free path
γ : ratio of specific heat
Ψ : streamfunction
Ω : vorticity
Ω_{rsd} : vorticity residue
ν : kinematic viscosity

Subscripts

cr : critical location, at which $g = 0$
d : dimensional quantity
r : real part of a complex quantity
i : imaginary part of a complex quantity

Superscripts

$'$: derivative in the radial direction
$\hat{\ }$: disturbance quantity
$\bar{\ }$: averaged quantity
$*$: complex conjugate

List of Figures

Contents

CHAPTER 1

Introduction

The complete route to turbulence of initially laminar pipe flow remains one of the oldest and as yet unsolved fundamental problems of fluid dynamics. In the laminar regime, the flow far from the ends of the pipe takes on an asymptotic limiting form, known as *Poiseuille flow*, which is steady and axisymmetric. The velocity is parallel to the pipe axis, and is a parabolic function of the radial coordinate. This simple flow is always a mathematical possibility in an infinite pipe, since it arises as an exact solution of the Navier-Stokes equations. In reality, however, the flow is subjected to perturbations coming from the inlet, imperfections and variations in the pipe walls, even if they are small. At low flow rates viscosity tends to damp out flow perturbations as they are convected downstream, resulting in Poiseuille flow at large downstream distances. However, once a certain flow rate is exceeded, the perturbations may instead be amplified, the flow is now unstable. Instability leads to the breakdown of Poiseuille flow and the resulting turbulent flow is no longer steady, parallel, or parabolic. The change from laminar to turbulent flow due to instability of the laminar state is referred to as *transition*.

While flow through straight pipes has been studied in every aspect for more than a century, there is not that much work on variations in geometry, such as diverging pipes. The flow in the entry region (where flow develops from a uniform to a parabolic velocity profile), as well as pulsatile flow, have been studied in somewhat greater depth, but here too there are aspects which have not been addressed. It is well known that fully-developed flow through a straight pipe is linearly stable for any Reynolds number, although in a standard experiment flow is turbulent at Reynolds number around 2000. Therefore along with direct numerical simulations, nonlinear analysis and algebraic growth have attracted lots of attention in the theoretical study of transition to turbulence in pipe flow. However, there are many situations of pipe flow, such as those mentioned above, when linear stability analysis could be important and can play a role in transition to turbulence. The heart of the thesis is in the study of such situations. We have considered a variety of spatially developing geometries, such as flow through steadily and converging/diverging pipes, developing flow in the entry region of a pipe, wall-slip flow through a diverging channel/pipe, and pulsatile flow in a straight pipe. In each case we have computed the basic flow by solving the two-dimensional/axisymmetric Navier-Stokes equations exactly and a non-parallel stability analysis is conducted.

The motivation to study the stability of these spatially developing and pulsatile flows is as follows. The transition to turbulence in pipe flows being an area of active interest [Hof *et al.* (2003, 2006); Peixinho & Mullin (2006)], and with many recent demonstrations [e.g., Hof *et al.* (2004); Huerre & Rossi (1998)] that pipe flow may be maintained laminar up to high Reynolds numbers (of the order of hundred thousand), an understanding of the instability of pipe flow with the variations in the geometry and flow conditions are increasingly relevant. A diverging pipe is more interesting than a diverging channel for several reasons: in the former, the critical Reynolds number is infinite for an angle of divergence of zero, the Reynolds number is a decreasing function of the streamwise (axial) coordinate x, the flow non-parallelism is larger for a given divergence, and the least stable disturbances are three-dimensional in nature. It is also interesting to explore what will happen in pipes with constant average radius, but with local divergences and convergences. This might be closer to real-life situations, especially in small-scale (order of mm) flow through rough pipes, than a divergence which continues for ever.

The situation is similar in a two-dimensional channel, although the laminar flow is linearly stable up to a Reynolds number of 5772 (based on the channel half-width and the centreline velocity), and the flow usually goes to turbulence at a much lower Reynolds number (between 1000 and 2000). Again the mechanisms leading to turbulence are accepted to be either directly nonlinear, or triggered initially by transient algebraic growth due to the superposition of linearly decaying waves. In a small-scale channel, wall roughness can be significant fraction of the channel width, making the flow locally divergent or convergent. The recent studies of Lauga & Cossu (2005); Min & Kim (2005) in a straight channel show that wall-slip dramatically stablises the linear modes of disturbance growth. Therefore the study of transition to turbulence in a diverging channel with slip boundary condition could be important in microfluidic and small-scale flows. Motivated further by the fact [Eagles (1965, 1972); Eagles & Weissman (1975)] that a small divergence of the wall can cause the critical Reynolds number for linear instability to plumet, we examine wall divergence in the presence of velocity slip at the wall.

The laminar velocity profile through a circular pipe is parabolic once the flow is fully developed. However, the distance l_e required to reach this fully-developed state can be very long [Ekman (1910); Reshotko (1958); Wygnanski & Champagne (1973)], and scales linearly with the Reynolds number Re, roughly as $l_e/R \sim \mathrm{Re}/20$, where R is the pipe radius. Therefore high Reynolds number laminar flow through a pipe of limited length may never reach a parabolic state. Thus, the entry region could play an important role in the transition to turbulence in a circular pipe.

The association of arterial diseases with flow related mechanisms has motivated the study of steady and pulsatile flow within a pipe. Arterial flow is of course very complicated but we confine ourselves here to the effect of flow non-parallelism on pulsatile flow. This study is in preliminary stage. The mean flow is computed and stability equations for sinusodally varying flows are given, with a future aim to study asymmetries, in the form of departures from sinusoidal.

1.1 Previous work

The present literature survey, though not exhaustive enough to cover all that has been done in the area of transition to turbulence in pipe flows, I hope is still quite representative of it. I have not discussed in any detail the recent advances in the physical understanding of transition to turbulence in straight pipes, except where relevant to the present work. Such insight is available in the bibliography at the end of this thesis, so I restrict myself to listing salient findings. I then discuss what is known about other geometries and pulsatile flow in a straight pipe.

1.1.1 Flow through a straight pipe: route to turbulence

Linear stability

Theoretical investigations of flow stability are based on the assumption that laminar flows are affected by certain small disturbances. Various linear stability analyses [Burridge & Drazin (1969); Corcos & Sellars (1959); Davey & Drazin (1969); Lessen *et al.* (1968)] have numerically shown that Hagen-Poiseuille flow is stable for any Reynolds number and secondly, that the Squire's (1933) theorem for two-dimensional flows is not applicable in the case of axisymmetric flows. In fact the Hagen-Poiseuille flow is less stable to non-axisymmetric small disturbances with azimuthal wavenumber $n = 1$ than to axisymmetric small disturbances ($n = 0$) [Gill (1973); Salwen *et al.* (1980)].

The eigen spectrum of channel and pipe flow consists of three branches of eigenvalues [Drazin & Reid (1981); Schmid & Henningson (2001)]. The eigenvalues c with real $(c) \approx 0$ correspond to wall modes, concentrated near the pipe wall and with low phase speed. The eigenvalues c with real $(c) \approx 1$ correspond to center modes, concentrated near the center of the pipe and with phase speed close to 1. The remaining eigenvalues, extending in a line with real $(c) \approx 2/3$ towards $-\infty$ in the complex plane. These are highly damped modes, having a phase speed $2/3$. It is known from the earlier studies [Burridge & Drazin (1969); Meseguer & Trefethen (2003); Salwen *et al.* (1980)] that the central mode is less stable than the wall mode for Hagen-Poiseuille flow.

In spite of the fully-developed flow being linearly stable, as first demonstrated by Reynolds (1883), transition to turbulence usually occurs at a Reynolds number, Re, based on the pipe diameter and mean velocity, of around 2000. However, by reducing the external disturbances, it is possible to achieve laminar flow up to $\mathrm{Re} \sim 10^5$ [Huerre & Rossi (1998)] when the pipe is smooth and the flow at the inlet very quiet. The Reynolds number up to which it is possible to keep the flow laminar varies inversely as the level of external disturbance [Hof *et al.* (2003)]. Modern theoretical research has followed basically two approaches to explain the disagreement between experiments and linearised theory for the flow in a straight pipe. The first approach has been to estimate the amplification of the small disturbances in a transient phase, until they reach a sufficiently large amplitude for nonlinear effects to become important. The second approach is to estimate the direct onset of nonlinearity through finite amplitude disturbances. We describe each one brifly.

Transient growth

In the past two decades the transient growth mechanism has attracted the attention of scientists in the field of hydrodynamic stability. It was recognized [Farrell (1988); Gustavsson (1991); Reddy & Henningson (1993); Schmid & Henningson (1994); South & Hooper (2001); Yecko & Zaleski (2005)] that the linear stability operators can support solutions that exhibit large transient growth in energy, although the eigensolutions of the operators are damped. This phenomenon is due to the non-normality of the linear stability operator, which results in a set of non-orthogonal eigenfunctions. There is thus a possibility of algebraic growth in the disturbance kinetic energy for short times, even when all the eigenfunctions are decaying. The physical mechanism of algebraic growth involves redistribution of the streamwise velocity due to wall normal motion [Ellingsen & Palm (1975); Landahl (1980)]. Although questions remain about the complete route to turbulence in a straight pipe, it seems likely that the spectrum of linear (stable) modes has a role to play via transient algebraic growth [Meseguer & Trefethen (2003); Schmid & Henningson (1994)] of disturbances.

Nonlinear effects

It has recently been demonstrated theoretically [Waleffe (1998, 2001); Faisst & Eckhardt (2003, 2004)] (and also experimentally as discussed later) that a nonlinear self-sustaining mechanism leads to the existence of travelling waves (and time-periodic states) that appear to play a key role in shear turbulence. Davey & Nguyen (1971) studied the stability of pipe flow to small but finite-amplitude axisymmetric disturbances. Their weakly nonlinear analysis showed that a center mode rather than a wall mode is more likely to cause nonlinear instabilities. It has also been known from numerical studies [Ma *et al.* (1999); Shan *et al.* (1999)] that the turbulent flow in the transition region is dominated by downstream flowing vortices and streaks. Wedin & Kerswell (2004) identify some well-defined flow features of travelling wave-like, two-dimensional streamwise rolls, streaks and three-dimensional streamwise-dependent waves for pressure-driven fluid flow throught a circular pipe.

By a spatial analysis, Tumin (1996) has shown the sensitivity of the eigenmodes to small distortions in the base flow. They have shown that the eigenvalues which show the highest sensitivity to infinitesimal variations in the base flow are the most affected, and can become unstable. By direct numerical simulations, Gavarini *et al.* (2004) studied the spatial growth of the flow in a straight pipe with a parabolic profile modified by a small axisymmetric and axially invariant distortion.

Reuter & Rempfer (2004) developed a hybrid finite-difference code for the simulation of unsteady incompressible pipe flows. They compared results of their simulation with the experimental data of Han *et al.* (2000). They have shown due to the periodic perturbations emanating from the pipe wall, Λ-like vortices with their head deflected towards the pipe axis are formed in the late stage of transition.

Experiments

In pipe flows the turbulent state arrives all of a sudden without any intermediate states. The recent discovery of travelling wave and periodic solutions [Waleffe (1998, 2001); Clever & Busse (1997); Kawahara & Kida (2001); Nagata (1990); Wedin & Kerswell (2004)] have suggested a new transition scenario for flow through a straight pipe. In a careful experiment Hof *et al.* (2004) confirmed these traveling waves. Experimental investigations carried out under controlled conditions [Darbyshire & Mullin (1995); Draad *et al.* (1998); Hof *et al.* (2003)] have shown that transition to turbulence is observed beyond a certain amplitude of the disturbance. The absolute amplitude of the critical perturbation decreases for increasing values of the Reynolds number as a power law with an exponent of -1. Regarding the exponent of this scaling, the authors in Hof *et al.* (2003) state that, “An exponent strictly less than -1 would indicate the importance of transient growth while -1 is expected from a simple balance between nonlinear advection and viscous dissipation....”. In a recent paper Hof *et al.* (2006) have shown that at extremely large times, all turbulent pipe flows decay and eventually the flow will always relaminarize.

According to Kovasznay *et al.* (1962) regions of highly concentrated vorticity occur near the centerline of the pipe at the initial stages of transition. A characteristic feature of these regions is a spike on a trace of a linearized hot-wire output. A spike of sufficiently large amplitude may brust into a turbulent spot [Elder (1960)]. As the spot travels downstream it may increase in size until its dimension becomes comparable with the radius of pipe [Lindgren (1969)]. The result is a turbulent slug, temporarily filling the entire cross-section of the pipe with turbulent flow. The slug is now restricted by the pipe diameter and can only grow in the axial direction. This regime has been studied in detail by Eliahou *et al.* (1998); Han *et al.* (2000); Wygnanski *et al.* (1975); Wygnanski & Champagne (1973). Eliahou *et al.* (1998) found that in the presence of high amplitude initial disturbances the stage of transient amplification can be bypassed and does not seem to play a role in the self-sustaining cycle. They also mentioned that transition to turbulence in a fully-developed Poiseuille flow can occur only after the parabolic velocity profile becomes distorted. Wygnanski & Champagne (1973) investigated transitional pipe flow and found two different types of turbulent structures. There are slugs generated at supercritical Re by the instability of the flow at the inlet, and puffs generated by large disturbances around the critical Re.

The structure of puffs was investigated by Wygnanski *et al.* (1975) with the help of strong momentary excitation introduced at the inlet. Actually, there are two distinctly different transition experiments to be considered: transition due to disturbances in the inlet region, and transition in fully-developed Poiseuille flow. The inlet region in laminar flow may extend over a few hundred diameters because its length depends on Reynolds number. Mackrodt (1971) suggested that the instabilities observed in fully-developed Poiseuille flow may be induced by swirl (originating from the fluid reservoir).

1.1.2 Spatially developing geometries

It is well known that a small change in the geometry of a pipe/channel can drastically affect the stability behaviour. A brief summary of flows in spatially developing geometries are given below. Creeping flow through pipes of varying radius has been studied by Sisavath *et al.* (2001). They consider a pipe having a sinusoidal variation of the radius as shown in figure (1.1). R_o is the average radius, λ and δ are the wavelength and amplitude of the constriction respectively. By using an asymptotic series solution method they computed the velocity profiles for various values of wavelength and amplitude of the geometry.

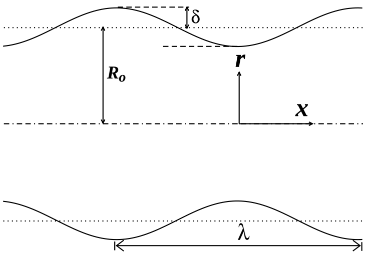

Figure 1.1: Sinusoidaly constricted tube.

Selvarajan *et al.* (1999) studied the temporal stability of a wavy-walled channel using the Floquet theory. The transition critical Reynolds number is shown to decrease with an increase of the wall amplitude to semi-channel height ratio. They have also shown that two-dimensional wavy channel flows can be modulated by a suitable frequency of wall excitation. Blancher *et al.* (2004) have shown that in a symmetric wavy channel flow is convectively unstable after it exceeds a Reynolds number of 100 based on centerline velocity and half channel width at the minimal section. Floryan (2003) studied the linear stability of the flow through a diverging-converging channel and showed that flow becomes unstable with respect to disturbances in the form of streamwise vortices at a Reynolds number much less than in a straight channel. His analysis of the mean flow circulation and the disturbance flow field suggest that the instability is driven by a centrifugal effect.

Sudden expansions have also attracted attention because of the recirculation zone they generate. In particular, Fearn *et al.* (1990) and Cherdron *et al.* (1978) study the length of the recirculation zone as a function of the Reynolds number, and Sreenivasan & Strykowski (1983) examine the oscillations of the recirculating bubble and their effect on the flow.

Coming to the specific geometry of our interests, Eagles (1965, 1972) and Eagles & Weissman (1975), analysed the Jeffery-Hamel flow generated by a slowly diverging channel, and showed by linear parallel stability analysis (the Orr-Sommerfeld equation), that the critical Reynolds number decreases by a large amount even for a small divergence angle.

1.1.3 Flow through non-circular/flexible pipes

Linear stability of flow through an elliptical pipe which is nearly circular is studied by Davey (1978); Davey & Salwen (1994); Kerswell & Davey (1996). The resulting perturbation problem was solved for the required eccentricity of the pipe necessary to destabilize the mean flow. Above an ellipticity of $e = 0.07$ exponentially growing solutions have been found. Davey (1978) analysis also showed that the temporal damping rates of non-axisymmetric wall modes monotonically decrease as the eccentricity of the pipe increases.

Many researchers [e.g. Carpenter & Garrad (1986); Davies & Carpenter (1997); Halpern & Grotberg (1992); Kumaran (1995*a*,*b*, 1998*a*,*b*)] have studied the stability of fluid flow in flexible tubes and channels. Shankar & Kumaran (1999) studied stability of flow through a flexible tube with velocity profiles very different from the parabolic Hagen-Poiseuille flow. Their results indicate that the flow becomes linearly unstable when the Reynolds number is increased beyond a critical value. Shankar & Kumaran (2000) also derived the inviscid stability criterion for flow in a flexible tube, with the rigid case included as the limiting one.

1.1.4 The developing flow in the entry region of a pipe

Observations in transitional pipe flow [Sarpkaya (1966, 1975); Wygnanski & Champagne (1973)] indicate that turbulent slugs and spots most often originate in the entry region. While fully-developed pipe flow is stable to linear perturbations at all Reynolds numbers, the entry flow (see figure 1.2) is not, and linear eigenmodes could enhance transition by the exponential growth of disturbances. Although many researchers, e.g., Da Silva & Moss (1994); Garg (1981); Gupta & Garg (1981); Sarpkaya (1975); Tatsumi (1952); Wilson (1969) have worked on this problem, there is significant discrepancy among the results. More important, all theoretical studies to our knowledge predict a critical Reynolds number at least two and half times higher than observed in experiment [Sarpkaya (1975); Williams (2001)]. These studies make two major approximations, (i) the basic flow, whose stability is being studied, is taken in an approximate form, usually of boundary-layer type, and (ii) the stability is studied under the assumption of locally parallel flow.

The mean velocity profiles used in the earlier studies are discussed first. Hornbeck (1964) used the finite-difference method for solving boundary layer type of equations. Sparrow *et al.* (1964) linearized the nonlinear inertial terms in the Navier-Stokes equations to get a series solution for the velocity profile. Another mean flow profile was proposed by Mohanty & Asthana (1979). They used the boundary layer equation in the initial region, and the Navier-Stokes equations in the filled region.

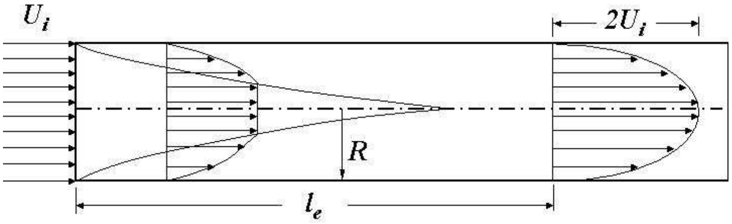

Figure 1.2: Schematic of the entrance region in a pipe; not to scale.

Next we briefly survey existing stability studies of the developing flow in the entry region of a pipe.

Tatsumi (1952), obtained a minimum critical Reynolds number of 9700 for axisymmetric disturbances. Later, Huang & Chen (1974) conducted a temporal stability analysis using Sparrow velocity profiles for the mean flow. They obtained critical Reynolds numbers 19900 and 19750 for axisymmetric and non-axisymmetric disturbances respectively, and suggested that Tatsumi's methods were not accurate enough. Garg (1981) performed a spatial stability analysis using Hornbeck mean flow profiles and reported a critical Reynolds number of 13250, and this number was modified to 11700 by Gupta & Garg (1981). They mention that for both Hornbeck and Sparrow profiles the wall mode exhibits instability but the central mode remains stable. All of the above are far from the experimental result of Sarpkaya (1975), who found the minimum critical Reynolds number to be about 3800. Williams (2001) investigated experimentally the response of the entry flow to finite-amplitude disturbances, and showed that the instability is inversely related to the amplitude of the perturbation. More recently Duck (2005) investigated the entry flow in two-dimensional channels as well as in pipes. His study was in the high Reynolds number limit, and was not aimed at predicting the critical Reynolds number. The non-parallel problem was considerably simplified by employing the boundary layer assumptions. It was shown that the transient growth of disturbances is significant, and suggests itself as an alternative mechanism for transition to turbulence. A better approximation of the mean flow [Mohanty & Asthana (1979)] was used. In the present study we solve for the mean flow exactly, derive the non-parallel equations from the Navier-Stokes equations and the focus is on exponential growth of disturbances.

1.1.5 Pulsatile flow

Pulsatile flow through a pipe has also been a topic of interest [Batchelor *et al.* (2000); Bertram & Pedley (1983); Davis (1976)] because of its relevance to the blood flow through arteries. Under standard physiological flow conditions, arterial flows are usually considered to be laminar, although always unsteady and often with separation. However, in the case of a stenotic pipe flow, the introduction of an inflection point into the velocity profile downstream of the contraction can lead to transition. This typically occurs for Reynolds numbers in the range of a few hundreds to a few thousands.

Linear stability of periodic flows is a relatively new (on the scale of a century!) topic in hydrodynamic stability. Grosch & Salwen (1968) studied the oscillatory plane Poiseuille flow and found it to be more stable than the steady flow in the sense that the growth (decay) rate of the principal disturbance mode was smaller (larger) in the unsteady flow. However, Hall (1975) has numerically shown that at very high frequencies the oscillations may destabilize the mean flow. Kerczek (1982) also studied oscillatory plane Poiseuille flow and found that, for sinusoidal oscillations the flow is more stable than when it is steady, for a wide range of frequencies. However, at very high and low frequency of oscillation the unsteady flow is less stable than the steady flow. This can be seen from their result that the critical Reynolds number for steady flow is 722 whereas the same for unsteady flow is 389.

Sherwin & Blackburn (2005) have examined the three-dimensional instabilities and transition to turbulence of steady and vascular pulsatile flow in a tube with a smooth 75% stenosis (reduction of diameter) using both linear stability analysis and direct numerical simulation. They have shown that for pulsatile flow instabilities occured at lower Reynolds number than the steady flow. Stability of pulsatile flow in a plane channel has been studed by Straatman *et al.* (2002) using a Floquet analysis [Iooss & Joseph (1989)]. They too find that pulsatile flow is always destabilising.

In a recent paper Fedele *et al.* (2005) have studied the stability of pulsatile pipe flow for axisymmetric disturbances and studied their transient energy growth. Although all eigen modes are decaying,

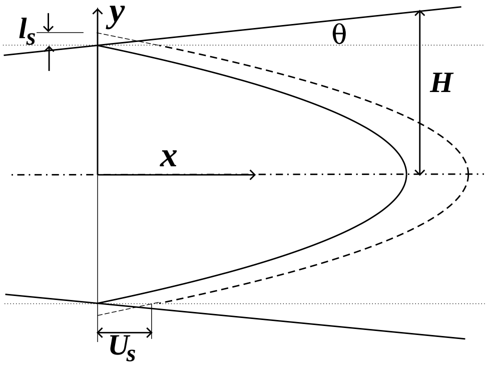

Figure 1.3: A schematic diagram showing the coordinate system, slip length (l_s) and slip velocity (U_s). H is the local half channel width, θ is the angle of divergence. The solid line and dashed line represent the velocity profiles when there is no-slip and finite velocty slip at the wall respectively.

a small transient growth of the disturbances was found for a short time. Pulsatile flow has also recently found renewed significance in its application to MEMS microfluidic engineering applications [Geng *et al.* (2001); Selverov & Stone (2001)].

1.2 Microflows

The dynamics of fluids and their interaction with surfaces in micro systems are very different from those in large systems [Karniadakis & Beskok (2002)]. In large scale flows, the velocity of a liquid immediately adjacent to a solid is taken equal to that of the solid. This is called the no-slip boundary condition, which seems to be confirmed in macroscopic experiments. However, it is diffcult to arrive at such a boundary condition using microscopic models. It has been noticed that, even in case of simple liquids, the no-slip boundary condition is not justified on a microscopic level. Therefore the no-slip boundary condition is not an exact law but a statement of what may be expected to happen under normal circumstances. On the other hand the wall-normal component of the velocity must of course vanish at an impermeable wall for kinematic reasons. In other words, it is possible microscopically for a velocity jump to exist at the wall, which could be described by a slip length l_s. The slip length for a simple shear flow is the distance behind the wall at which the velocity extrapolated to zero, as shown schematically in figure 1.3.

Maxwell (1879) first proposed a linear boundary condition at the wall which remains the standard characterisation of slip used today. Here the component of the fluid velocity tangent to the surface is taken to be proportional to the rate of strain at the surface.

$$U \pm Kn\frac{\mathrm{d}U}{\mathrm{d}y} = 0, \quad \text{at} \quad y = 0 \tag{1.1}$$

which defines a Knudsen number, Kn, typically used in liquid flows. This non-dimensional number is a very important parameter in small-scale flows. On the other hand, in gases, the Knudsen number is standardly defined as ratio of mean free path to the length scale, H. Depending on the Knudsen number the flow may be in the continuum, slip, transition or the free-molecular regime [Karniadakis & Beskok (2002)].

The flow regime for $Kn \leq 0.01$ is known as the continuum regime, where the Navier-Stokes equations with the no-slip boundary conditions govern the flow. The range $0.01 \leq Kn \leq 0.1$ is known as the slip flow regime. In this regime the flow is governed by the Navier-Stokes equations with slip boundary conditions at the wall. For $Kn \geq 0.1$ the Navier-Stokes equations are not valid. This is because the corrections to the Navier-Stokes equations appear at second order in Kn [Karniadakis & Beskok (2002)]. Upto $Kn = 10$ the flow is governed by the Burnett equations and is known as the transition regime. $Kn \geq 10$ is called free molecular flow regime. The flow now is governed by the Boltzmann equation.

Stemming from increasing interest in flow at small scales [Karniadakis & Beskok (2002); Lauga, Brenner & Stone (2005) and references therein], the instability of channel flow in the presence of wall-slip is receiving attention recently, see e.g. Gan & Wu (2006); Lauga & Cossu (2005); Min & Kim (2005). The consensus for a plane channel is that velocity slip at the wall hugely stabilizes the linear mode, but does not affect transient growth of instabilities much. Since the linear mode is not expected to play a dominant role in any case, no big change due to the smallness of scale is predicted in the early stages of the process of transition to turbulence.

At low Knudsen numbers, we take the Navier-Stokes equations to be valid in conjunction with the slip boundary condition of Maxwell (1879). The Maxwell slip model breaks down around $Kn = 0.15$ [Piekos & Breuer (1995)], so we, and others like Chu (2003); Gan & Wu (2006); Lauga & Cossu (2005); Min & Kim (2005) who use this model, restrict ourselves to values below this.

Incidentally the work of Lauga & Cossu (2005) set to rest a recent controversy over the effect of slip on the stability of channel flow. Chu (2000, 2003, 2004) had found a large destabilisation due to slip, in contrast to the earlier prediction of Gersting (1974) of a huge stabilisation. The conclusions of Gersting are confirmed by Lauga & Cossu (2005), who showed that there was a lapse in the application of the slip boundary condition in the work of Chu. There remains a small discrepancy in the effect of slip on transient growth, between the results of Lauga & Cossu (2005) and Min & Kim (2005). Both agree that the effect of slip is small, but the direction of the effect is stabilising in Min & Kim (2005) and destabilising in the other. We have checked that this discrepancy arises from a difference in the definition of Reynolds number, since the velocity scale used by Min & Kim (2005) decreases with increasing slip while that of Lauga & Cossu (2005) goes up with slip.

1.3 Non-parallel stability analysis of 2D flows

The parallel flow assumption; *i.e.,* $U = U(y), V \equiv W = 0$ with disturbances in the normal mode form applies exactly to developed flow through channels and pipes having straight boundaries. Under the parallel flow assumption, the stability of the basic flow is usually described by an ordinary differential equation in the wall normal coordinate, which is posed as an eigenvalue problem. With the inclusion of non-parallel effects (where the mean flow and therefore the amplitude of the disturbance vary in both normal and axial directions), the resulting stability equation is a partial differential equation and no longer a straightforward eigenvalue problem.

In the last two decades, many researchers [Bertolotti *et al.* (1992); Fasel & Konzelmann (1990); Gaster (1968, 1974, 2000); Govindarajan & Narasimha (1995*a*); Koch *et al.* (2000); Rao *et al.* (2004)] have studied boundary layer flows including non-parallel effects. They have used several techniques: the adjoint method of Gaster (1974), the Parabolized Stability Equations (PSE) of Bertolotti *et al.* (1992), a local trial and error method of Govindarajan & Narasimha (1995*b*), and also a method of adjoints of Govindarajan & Narasimha (2005). In all the above studies the disturbance quantities are split into two part: a rapidly growing wave like part and a slowly varying eigenfunction. By this conclusion only weakly non-parallel flows can be handled by these method. The term “weakly non-parallel” will be quantified later in the thesis. Theofilis *et al.* (2004, 2003, 2000) and others have developed a method to solve for general non-parallel flows. They do not make any assumption about the streamwise dependence of the disturbance amplitude. This results in a set of second order partial differential equations in two spatial directions. This approach is now known as global stability analysis. In this method we have to solve for the whole domain and which results in a very large eigenvalue problem. In the present thesis a different approach is followed to handle weakly non-parallel effects.

1.4 Outline of the thesis

It is well known from more than a century of research on transition to turbulence in pipe flows that there is a large gap between the classical linear stability theory and experiments. The main reason for this gap is the fact that Hagen-Poiseuille flow is linearly stable for any Reynolds number while flow is turbulent at Reynolds number around 2000 in a standard experiment. Hagen-Poiseuille flow is a special case which can be achieved only when pipe wall is very smooth, straight and long enough to obtain the fully-developed state. In the ideal condition of fully-developed pipe flow nonlinearities and transient growth analysis dominate the transition to turbulence. However, in reality there are many situations where pipe flow cannot reach the Hagen-Poiseuille flow state and linear instability can play a role in transition to turbulence.

A real pipe used in experiments can be a tapered one with very small divergence or it can be a diverging-converging pipe. In some situations of high Reynolds number the length of the pipe may be insufficient to get the fully-developed flow. For example the longest smooth pipe is 26 meter long [Hof *et al.* (2004)]. At a very high Reynolds number this length is also not sufficient to obtain the fully-developed flow and flow can be linearly unstable. Unsteadiness can also make the flow unstable in a straight pipe. We have addressed some of these situations in the thesis. They are flow through (i) a divergent pipe, (ii) a variety of diverging-converging pipes with constant average radius. (iii) the entry region of a straight pipe, (iv) diverging channel/pipe with velocity slip at the wall, and (v) pulsatile flow. We have also studied separations in diverging channels and pipes. These are spatially developing flows having a large streamwise dependence. The parallel flow assumptions (discussed in § 1.3) are not valid. In this thesis, we obtained the mean flow by solving the Navier-Stokes equations exactly, and a new approach has been followed to study the stability of these non-parallel flows. Below we have given a brief description of the main results and approches followed.

Flow through a diverging pipe is discussed in chapter 2. In this study a two-pronged approach has been employed for the mean flow. For small angles of divergence, an axisymmetric Jeffery-Hamel equation (AJH) is derived. At larger angles of divergence (1° or greater) the axisymmetric Navier-Stokes equations are solved directly. A full-multigrid algorithm is used to accelerate the convergence. At small angles of divergence and high Reynolds numbers (above 1000), a parallel flow stability analysis is conducted on the AJH profile, while at lower Reynolds numbers, the partial differential equations for non-parallel stability are solved as an extended eigenvalue problem. The main results for the flow in a divergent pipe may be summarized as follows. Although the critical Reynolds number for linear instability of the laminar flow in a straight pipe is infinite, it is shown here that it is finite for a divergent pipe, and approaches infinity as the inverse of the divergence angle. It is proved that flow through a pipe of any non-zero wall divergence satisfies the necessary conditions of inviscid instability. At divergences greater than 1°, non-parallel effects are found to be quite large, and a non-parallel analysis shows that the flow in a geometry containing a 3° divergence is linearly unstable to the swirl mode at Reynolds numbers as low as 150.

Flow through converging-diverging pipes is discussed in chapter 3. The laminar flow through a pipe of constant *average* radius is shown to display linear instability at low Reynolds number. This is offered as a possible mechanism that could be operating in small-scale flows. The effect of changing geometry, which could be a significant factor, is studied. The other main result for the case is that the instability behaviour can be changed dramatically by reversing the direction of flow. The above results motivate us to study the small-scale flows with the slip boundary conditions. In a small-scale flow, local divergence/convergence of the wall are common. Therefore the study of transition to turbulence in a diverging channel/pipe with slip boundary condition could have a major impact on microfluidic and small-scale flows. We have confined ourselves to $Kn \leq 0.1$ in this thesis. Our study of stability of slip flow through a diverging channel show that even for small levels of wall divergence, of less than a degree, transient growth of disturbances is likely to be unimportant. It is the linear instability that will probably begin the process of transition to turbulence. This linear instability will moreover take place at Reynolds numbers two orders of magnitude less than in a plane channel, when the divergence is a few degrees. This fact is significant for small-scale flows, where the typical Reynolds numbers are relatively small. These are discussed in chapter 4.

We study the developing flow in the entry region of a straight pipe in chapter 5. The axisymmetric Navier-Stokes equations are solved for a long entry region in an accurate manner using a parallel machine. Secondly, a complete non-parallel stability analysis, correct to $O\left(\mathrm{Re}^{-1}\right)$, is performed. We show that the behaviour of the instability critical Reynolds number is qualitatively the same as experimentally observed. The numerical value of 1000, at which we first find neutral disturbance growth, is lower than in the experimental value of Sarpkaya (1975). In a departure from earlier results we find that the most unstable disturbances are the central modes.

Some other studies which are in the preliminary stage are described in chapter 6. These include the study of pulsatile flow through a straight pipe. Prescribing time periodic velocity profiles at the inlet we have solved the Navier-Stokes equation directly using a full-multigrid algorithm on a parallel machine Venkatesh *et al.* (2005). We also studied separated flows in the diverging channel/pipe. Some important features of separation like length of the separation bubbles, separation and reattachment point for various angle of divergence from 0 to 60 degree are analysed. In chapter 7, we end the thesis with our main conclusions.

CHAPTER 2

Flow through a diverging pipe

The instabilities of spatially developing laminar flows are often fundamentally different from flows that do not vary downstream. The problems considered in the present thesis are of flows which change slowly as they progress downstream. They are flow through (i) a divergent pipe, (ii) a variety of diverging-converging pipes with constant average radius, (iii) diverging pipes/channels with velocity slip at the wall, (iv) the entry region of a straight pipe, and pulsatile flow. The first of these is discussed in this chapter. The term "slowly" will be quantified in each case. The streamwise variation may arise due to the geometry or the inlet conditions. The Orr-Sommerfeld equation, which is actually applicable only to strictly parallel flows such as fully-developed flow in a channel, has traditionally been used to study the stability of non-parallel flows as well. However, several authors [Bertolotti *et al.* (1992); Gaster (1968, 1974, 2000); Govindarajan & Narasimha (1995*a*); Koch *et al.* (2000); Theofilis *et al.* (2004)] have formulated theories that relax the parallel flow approximation as discussed in § 1.3. These non-parallel flow stability theories have usually sought to include all effects up to $O\left(\mathrm{Re}^{-1}\right)$. The resulting equations are partial differential equations, having two independent variables: the wall normal and streamwise coordinates. These flows have been solved by many different approaches e.g., the adjoint method of Gaster (1974), the Parabolized Stability Equations (PSE) of Bertolotti *et al.* (1992), a local trial and and error method of Govindarajan & Narasimha (1995*a*), and also a minimal composite theory (see e.g Govindarajan & Narasimha (2005)). Here we follow a new approach to solve the non-parallel equations by constructing a larger eigenvalue problem (Balachander *et al.* unpublished). The basic principle of the solution is the same as that in the PSE or an equivalent local solution.

2.1 Mean flow

Before we perform stability calculations, we need to compute the unperturbed laminar flow. The computation of mean flow for the above cases is difficult and extremely time consuming because of the following reasons. These are spatially developing flows having a significant axial dependence. As discussed below, one usually needs a long computational domain (for example, the entry length of the flow in a straight pipe is of the order of Re). To obtain the flow within and outside regions of separation if any also results in dramatic increase in computational time. Moreover stability calculations are extremely sensitive to the mean flow. To compute the mean flow and its derivatives accurately, a large number of grid points are required, which exponentially increases the computational time. For these reasons a mean flow code, which solves the axisymmetric Navier-Stokes equations using a full-multigrid algorithm (FMG) has been developed [Sahu (2003)]. It has been found that the convergence in the FMG is about hundred times faster than traditional algorithms. This code is then parallelised at the National Aerospace Laboratories, Bangalore, as discussed in subsection 2.1.1. The parallel code gives a superlinear speed-up of 11 times over the linear solver using an eight processor machine [Venkatesh *et al.* (2005)]. The formulation, method of solution and results of mean flow are described in § 2.1.

For the computation of mean flow in a diverging pipe, a two-pronged approach has been employed.

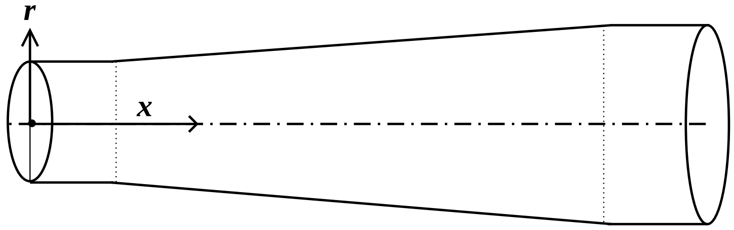

Figure 2.1: Schematic diagram of the divergent pipe used in the numerical simulations, not to scale.

At larger angles of divergence (1° or greater) the Navier-Stokes equations are solved directly in the axisymmetric geometry shown in figure 2.1, with a divergent portion of finite extent as described in § 2.1.1. At small angles of divergence, the velocity profiles may be obtained analytically by deriving an axisymmetric Jeffery-Hamel equation (AJH). The formulation of the AJH equation is discussed in subsection 2.1.2. In the next subsection, we describe the numerical computations of mean flow through a diverging pipe. The solution method is same for the other cases considered in the thesis as well. The non-dimensionalisation and boundary conditions are discussed separately for each problem.

2.1.1 Numerical solution

The geometry studied here is as shown in figure 2.1, with a straight pipe at the entry, followed by an axisymmetric divergent portion, which in turn is followed by a long straight exit portion. The length and velocity scales here are the radius R_i and the centerline velocity U_i at the inlet respectively. In the case discussed here, the divergent portion starts at $x = 9.4$ and ends at $x = 91$ with a 3° angle of divergence. The total length of the domain is 120. The axisymmetric Navier-Stokes equations for steady, incompressible, Newtonian flow in the streamfunction vorticity formulation are given in non-dimensional form by

$$\frac{\partial \Omega}{\partial t} + (\vec{U}.\nabla)\Omega = \frac{1}{\mathrm{Re}_i}\nabla^2\Omega, \tag{2.1}$$

$$\Omega = -\nabla^2\Psi, \tag{2.2}$$

$$U = \frac{1}{r}\frac{\partial \Psi}{\partial r}, \quad V = -\frac{1}{r}\frac{\partial \Psi}{\partial x}, \tag{2.3}$$

where $\mathrm{Re}_i \equiv U_i R_i/\nu$, $\Omega(x,r)$ is the azimuthal vorticity, $\vec{U}$ is the velocity vector, ν is the kinematic viscosity, and t is time. The solution is facilitated by a transformation of coordinates, given by

$$\zeta = x, \quad \eta = \frac{r}{f(x)},$$

where $f(x)$ is a function describing the boundary.

The boundary conditions at the centerline are $\Psi = \Omega = V = \partial U/\partial \eta = 0$. No-slip and impermeable boundary conditions are imposed at the wall. The functional forms of the streamfunction at the centerline, and the vorticity at the wall are described by employing fictitious points outside the domain. At the inlet, a parabolic velocity profile is prescribed, while at the outlet the Neumann boundary conditions: $\partial\Psi/\partial x = 0$ and $\partial\Omega/\partial x = 0$ are imposed. The reason for using a long exit section, and the consequent increase in computational effort, is due to the requirement that the Neumann condition be valid at the exit.

We begin with a guess solution, where the velocity profile is parabolic at every axial location. After setting up the initial and boundary conditions for the flow parameters, the vorticity distribution at each new time step is calculated from equation (2.1), adopting a first-order accurate forward differencing in time and second-order accurate central differencing in space, on a 34 × 514 grid. The vorticity distribution thus computed is used to solve the Poisson equation (2.2) by a Jacobi iterative scheme to obtain the streamfunction everywhere. This is the most time-consuming part in the program. If such spatially developing flows are to be solved within realistic time-frames (a few days for each case), a convergence acceleration technique is essential. Numerical acceleration is achieved by a six level full-multigrid technique [see e.g. Fletcher (1991*a*,*b*)]. Finally, the velocity components are calculated from the computed streamfunction. The procedure is repeated until the cumulative change in vorticity $\left(\Omega_{rsd} \equiv \sum_{i=1}^{n} \sum_{j=1}^{n} |\Omega^{r}_{i,j} - \Omega^{r-1}_{i,j}|\right)$ during the time step reduces to below = 10^{-10}. The method of solution, validation of the code, and typical results are available in Sahu (2003). A brief description of the full-multigrid technique is given below.

The multigrid method provides algorithms which can be used to accelerate the rate of convergence of iterative methods, such as Jacobi or Gauss Seidel, for solving elliptic partial differential equations. Iterative methods start with an approximate guess for the solution to the differential equation. The difference between the approximate solution and the exact solution is made smaller at every iteration. Algorithms like Jacobi or Gauss Seidel are local because the new value for the solution at any lattice site depends only on the value of the previous iterate at neighbouring points. Such local algorithms are generally only efficient in reducing short wavelength error components. In general, the error will be made up of components of many different wavelengths. The basic idea behind multigrid methods is to reduce long wavelength error components rapidly by working with blocks of grid points. The multigrid algorithm for the two-dimensional Poission equation is given in appendix I. A six-level multigrid technique with simple V-cycle algorithm was used in the present study.

The multigrid code was parallelised at the National Aerospace Laboratories (NAL), Bangalore, India. The parallel code (using an eight processor machine) gives a superlinear speed-up of 11 times over a single processor using the NAL FloSwitch for communication on a multigrid laminar Navier-Stokes code. In parallel computing, scalability is an important issue and getting linear speed-ups is difficult for most codes, whereas we are able to achieve superlinear speed-up. Both the hardware architecture and the parallel algorithm seem to contribute to this speed-up [Venkatesh *et al.* (2005)].

The parallel machine, called Flosolver (MK6) has eight processers. The machine consists of four Intel STL2 boards linked by the NAL FloSwitch. Each board has two Intel Pentium III processors with a clock speed of 1 GHz and 2 GB of shared RAM. The operating system on the nodes is Linux. The communication libraries include CCX[8], a small but efficient message passing library and an inhouse implementation of a subset of the MPI library.

The graph of speed-up versus the number of processors (figure 2.2) shows that there is significant superlinear speed-up beyond four processors. On eight processors, we get a speed-up of 11, *i.e.* a superlinear speed-up of 37.5 %. For comparison with superlinear speed-ups reported on similar problems in the literature, Stiller *et al.* (2004) obtained a speed-up of 140 on 120 processors (15% superlinearity). It should be noted though that the problem size also determines when the maximum speed-up is obtained. A general trend is that the number of processors at which the maximum speed-up is obtained increases with the problem size.

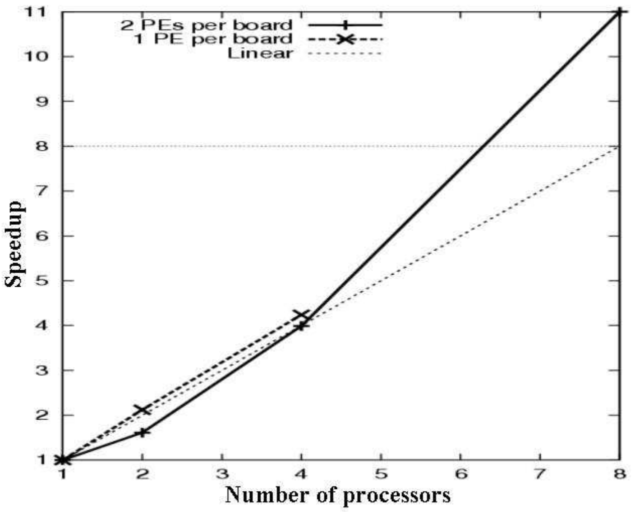

Figure 2.2: Speed-up of multigrid Navier-Stoke solver in Flosolver [Venkatesh *et al.* (2005)]

2.1.2 Axisymmetric Jeffery-Hamel equation

We begin by noting that unlike in a divergent two-dimensional channel, no similarity flow is possible in a divergent pipe. At very low angles of divergence, however, it is possible to derive a one-parameter family of velocity profiles, where the parameter

$$S \equiv a\mathrm{Re} \tag{2.4}$$

is taken to be slowly varying in the axial coordinate x. The Reynolds number (Re) is defined as

$$\mathrm{Re}(x_d) \equiv \frac{U_c(x_d)R(x_d)}{\nu}, \tag{2.5}$$

where R is the radius of the pipe, U_c is the centreline velocity and the subscript d stands for a dimensional quantity. It is assumed that the slope of the wall

$$a \equiv \frac{\mathrm{d}R(x_d)}{\mathrm{d}x_d} \ll 1, \tag{2.6}$$

Upon eliminating the pressure from the axisymmetric momentum equations, we obtain

$$-\frac{V_d}{r_d}\frac{\partial U_d}{\partial r_d} + U_d\frac{\partial^2 U_d}{\partial x_d \partial r_d} + V_d\frac{\partial^2 U_d}{\partial r_d^2} - \nu\left[\frac{\partial^3 U_d}{\partial r_d^3} - \frac{1}{r_d^2}\frac{\partial U_d}{\partial r_d} + \frac{1}{r_d}\frac{\partial^2 U_d}{\partial r_d^2}\right] = 0, \tag{2.7}$$

where r is the radial coordinate. For incompressible flow, the axial and radial velocities, U_d and V_d respectively, may be written in terms of a generalised streamfunction Ψ_d as

$$U_d = \frac{1}{r_d}\frac{\partial \Psi_d}{\partial r_d}, \qquad V_d = -\frac{1}{r_d}\frac{\partial \Psi_d}{\partial x_d}, \tag{2.8}$$

to satisfy continuity. Substituting these in equation (2.7), we get

$$3r_d\frac{\partial\Psi_d}{\partial x_d}\frac{\partial^2\Psi_d}{\partial r_d^2} - 3\frac{\partial\Psi_d}{\partial r_d}\frac{\partial\Psi_d}{\partial x_d} + r_d^2\frac{\partial\Psi_d}{\partial r_d}\frac{\partial^3\Psi_d}{\partial r_d^2\partial x_d} - r_d\frac{\partial\Psi_d}{\partial r_d}\frac{\partial^2\Psi_d}{\partial r_d\partial x_d} - r_d^2\frac{\partial\Psi_d}{\partial x_d}\frac{\partial^3\Psi_d}{\partial r_d^3} -$$

$$\nu\left[r_d^3\frac{\partial^4\Psi_d}{\partial r_d^4} - 2r_d^2\frac{\partial^3\Psi_d}{\partial r_d^3} + 3r_d\frac{\partial^2\Psi_d}{\partial r_d^2} - 3\frac{\partial\Psi_d}{\partial r_d}\right] = 0. \tag{2.9}$$

The above equation is non-dimensionalised using the local radius $R(x_d)$ and the centreline velocity $U_c(x_d)$ as scales, e.g., $\Psi_d = U_cR^2\Psi$. In particular,

$$\mathrm{d}x_d = R\mathrm{d}x. \tag{2.10}$$

The Reynolds number is assumed to be high and the divergence small enough, so that all terms of $O(\mathrm{Re}^{-2})$ or $O(a^2)$ and higher are negligible. The resulting equation in non-dimensional form becomes

$$[q\Psi - \eta a\Psi']\left[-3\Psi' + 3\eta\Psi'' - \eta^2\Psi'''\right] - \eta\Psi'\left[q\Psi' - \eta\Psi''a - \Psi'a\right] + \eta^2\Psi'\left[(q-2a)\Psi'' - \eta a\Psi'''\right]$$

$$-\frac{1}{\mathrm{Re}}\left[\eta^3\Psi^{iv} - 2\eta^2\Psi''' + 3\eta\Psi'' - 3\Psi'\right] = 0, \tag{2.11}$$

where

$$\eta = \frac{r_d}{R}, \quad q \equiv \frac{1}{U_cR^2}\frac{d}{dx_d}(U_cR^2),$$

and the primes refer to differentiation with respect to η. For the case of near-similar flow, given constant mass flow rate, we may set $q = 0$ to obtain

$$S\left[4\eta(\Psi')^2 - 4\eta^2\Psi'\Psi''\right] - \left[\eta^3\Psi^{iv} - 2\eta^2\Psi''' + 3\eta\Psi'' - 3\Psi'\right] = 0. \tag{2.12}$$

The mean flow is now a function of a single papameter S, as defined in equation (2.4). The above equation is integrated once with respect to η and scaled with the local centerline velocity (U_c/U_i) to give

$$\eta^2U_l''' = -\eta U_l'' + (1 - 4S\eta^2U_l)U_l', \tag{2.13}$$

where $U_l = \Psi'U_i/\eta U_c$.

This equation is satisfied by the parabolic velocity profile when $S = 0$. The boundary conditions are $U_l = 0$ at $\eta = 1$, and $U_l = 1,\ U_l' = 0$ at $\eta = 0$. From the continuity equation we obtain the expression for the radial velocity as

$$V_l = a\eta U_l. \tag{2.14}$$

In two dimensions at low angles of divergence, the incompressible laminar flow in a wedge-shaped channel is given by the Jeffery-Hamel equation [see e.g. Eagles (1965, 1972)]:

$$U_l''' + 2S\,U_lU_l' = 0, \tag{2.15}$$

The primes now denote derivative with respect to the normal coordinate, y. Here the half-channel width is the length scale. The normal velocity

$$V_l = ayU_l \tag{2.16}$$

from continuity. Note that η in equation (2.13) varies between 0 and 1. If we artifically set $\eta \to \infty$, equation (2.13) takes on the same form as equation (2.15) except for a change in the numerical factor, arising from the difference in geometries. The equations (2.13) and (2.15) are solved using Ranga-Kutta method of fourth order.

From global continuity we see that for diverging channel $U'_c/U_c = -a$ and

$$\frac{d\mathrm{Re}}{dx} = 0 \Rightarrow \mathrm{Re} = \text{constant}, \tag{2.17}$$

contrary to the diverging axisymmetric pipe where $U'_c/U_c = -2a$ and

$$\frac{d\mathrm{Re}}{dx} = -a\mathrm{Re} \Rightarrow \mathrm{Re} = \exp(-ax). \tag{2.18}$$

As seen above the Reynolds number in a diverging axisymmetric pipe decreases exponentially, although with a small exponent, as we go downstream. Therefore relaminarisation of the flow could take place as we go downstream due to decrease of local Reynolds number. This is in contrast to a diverging channel, where the Reynolds number is constant.

The axial and radial velocity profiles scaled with the local centerline velocity (U_c/U_i) for axisymmetric diverging pipe (AJH profiles), U_l and V_l, at different S are plotted in figures 2.3 and 2.4 respectively. It can be seen in figure 2.3 that separation starts approximately at $S = 10$. Therefore it might be intuitively expected that close to this value of S, the flow will be unstable. Similar behaviour is noted in figure 2.4 for the case of radial velocity. The comparison of U'_l at the wall for AJH and Jeffery-Hamel flow are shown in figure 2.5. It can be seen that flow just reaches the separation point for $S \approx 10$. Figure 2.6 shows the comparison of axial velocity profiles for axisymmetric pipe obtained from equation (2.13) with that of channel flow obtained by solving equation (2.15). The comparison of the corresponding radial velocity profiles are shown in figure 2.7. It can be seen that the reverse flow velocities are slightly larger for a channel than in a pipe for same S. However channel flow requires slightly larger S to come to the separation point than pipe.

We now discuss the numerically obtained velocity profiles in the geometry shown in figure 2.1. The numerically computed axial and radial velocity profiles at different downstream locations are compared with that of AJH profiles in figures 2.8 and 2.9 respectively. The Reynolds number, $\mathrm{Re}_i = 150$ and angle of divergence is 3°. It is seen that the AJH profile underpredicts the effect of divergence at $x = 22.9$ but overpredicts it at $x = 46.4$. It is relevant to mention that the AJH profiles do not correspond to flow through any particular geometry. However, at very low angles of divergence, axial variations are slow, and the AJH profiles are locally valid. It can be seen in figures 2.10 and 2.11 that for angles of divergence of a degree or less, the AJH profiles match very well with the numerically computed ones.

The variation of the axial and radial velocities obtained from numerical simulations (discussed in § 2.1.1) at different downstream locations are shown in figures 2.12 and 2.13 respectively. It can be seen in figure 2.12 that the flow has a tendency to separate, and a region of reverse flow is evident in the axial velocity profile. The divergence provides an adverse pressure gradient, so the region of separation increases as we go downstream in the diverging portion. Far downstream, the profile again becomes parabolic because of the existence of the long straight portion before the exit. It can be seen in figure 2.13 that the radial veloicty is maximum near the beginning of the diverging portion. In this neighborhood, the flow changes quite rapidly with axial distance, while far downstream, the radial velocity goes to zero as expected. The gradient of velocities in both radial and axial directions are given in figures 2.14 to 2.17. The features described above in the context of figures 2.12 and 2.13 can also be seen here. The axial variations in the flow, and in particular the departures from similarity, are evident in these plots. It is to be noted that at higher divergence, regions of separation are obtained to very good accuracy by the

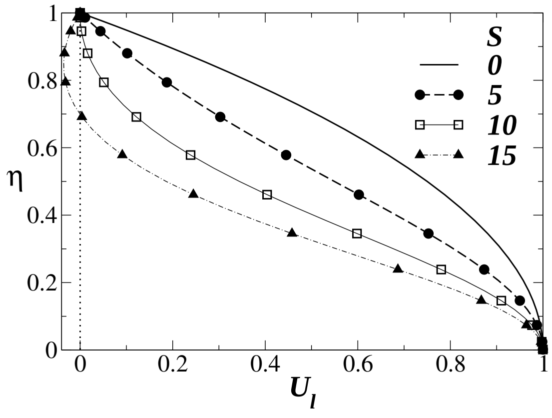

Figure 2.3: Axial velocity profiles scaled with the local centerline velocity for AJH flow at different S.

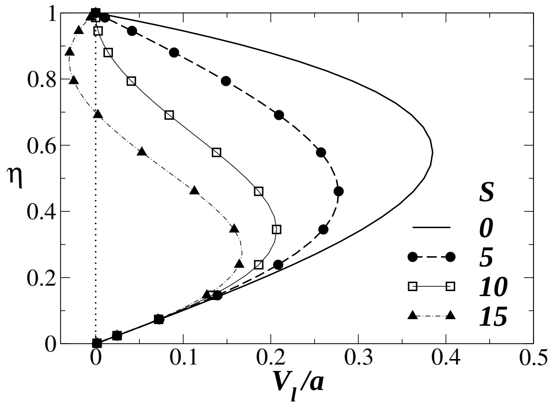

Figure 2.4: Radial velocity profiles divided by the wall slope, a for AJH flow for different S. The limiting value of $V_l/a = \eta U_l$ is shown for $S = 0$.

present method.

In the next section we discuss the formulation of the stability equations for this problem.

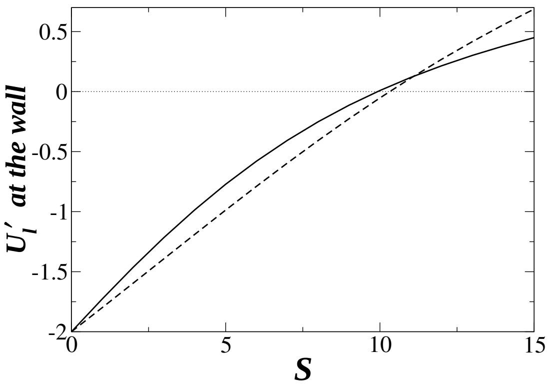

Figure 2.5: Comparison of U_l' at the wall for AJH with the Jeffery-Hamel flow. Solid line: AJH profiles, dashed line: Jeffery-Hamel profiles.

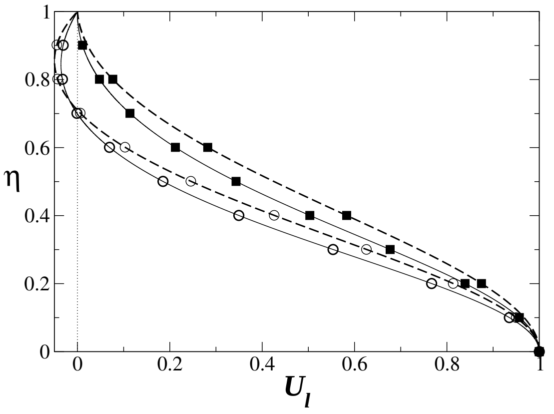

Figure 2.6: Comparison of axial velocity profiles for AJH flow through a diverging pipe with the Jeffery-Hamel profiles for the flow in a diverging channel. Solid lines: AJH profiles, dashed lines: Jeffery-Hamel profiles, squares: $S = 10$ and circles: $S = 15$.

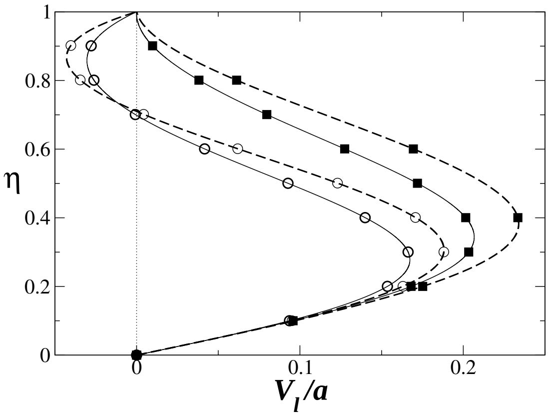

Figure 2.7: Comparison of radial velocity profiles (scaled by the wall slope, a) of AJH flow with Jeffery-Hamel profiles. Solid lines: AJH profiles, dashed lines: Jeffery-Hamel profiles, squares: $S = 10$ and circles: $S = 15$.

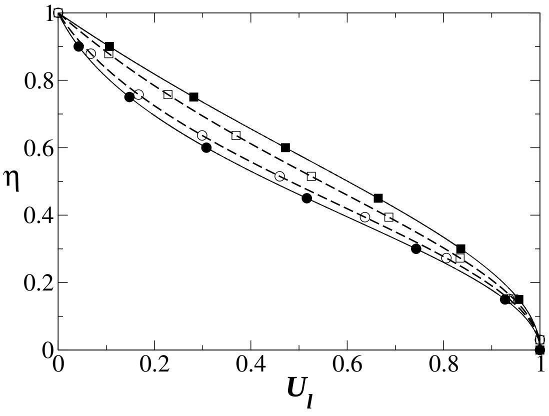

Figure 2.8: Comparison of numerically obtained axial velocity profiles (solid lines) at different axial locations (circles: $x = 22.9, S = 7.49$ and squares: $x = 46.4, S = 3.75$) with AJH profiles (dashed lines) at the same value of S.

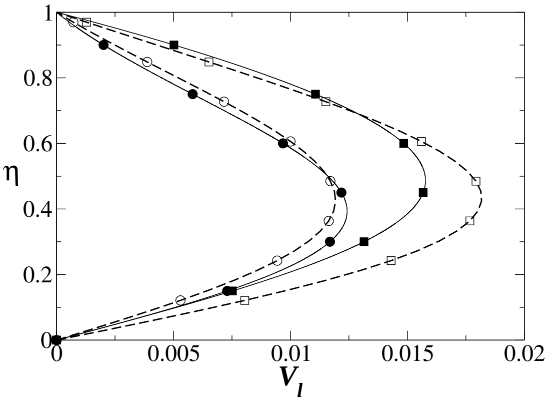

Figure 2.9: Comparison of numerically obtained radial velocity profiles (solid lines) at different axial locations (circles: $x = 22.9, S = 7.49$ and squares: $x = 46.4, S = 3.75$) with AJH profiles (dashed lines) at the same value of S.

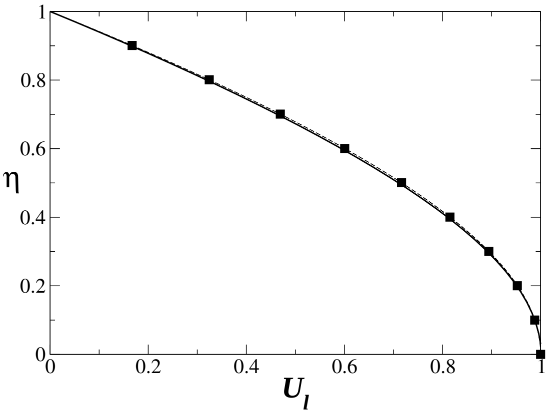

Figure 2.10: Comparison of numerically obtained axial velocity profile (solid line) at $x = 46.4$ and angle of divergence 1° with AJH profile (symbols and dashed line).

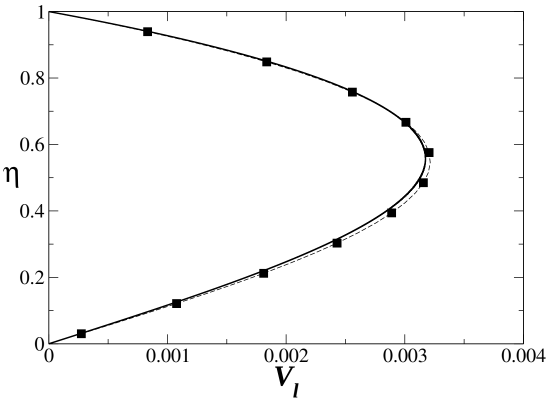

Figure 2.11: Comparison of numerically obtained radial velocity profile (solid line) at $x = 46.4$ and angle of divergence 1° with AJH profile (symbols and dashed line).

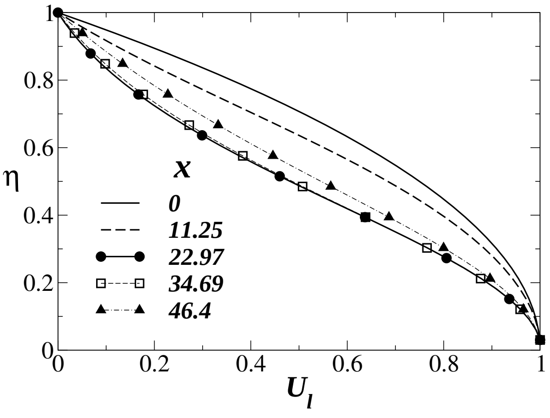

Figure 2.12: Axial velocity profiles computed numerically at different axial locations, $\mathrm{Re}_i = 150$, angle of divergence = 3°.

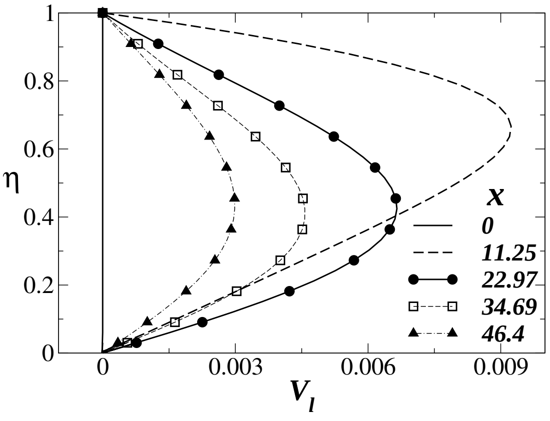

Figure 2.13: Radial velocity profiles computed numerically at different axial locations, $\mathrm{Re}_i = 150$, angle of divergence = 3°.

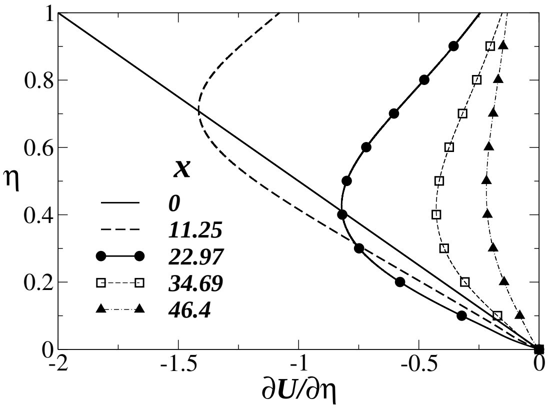

Figure 2.14: Gradient of U in the radial direction at different axial locations, $\mathrm{Re}_i = 150$, angle of divergence = 3°.

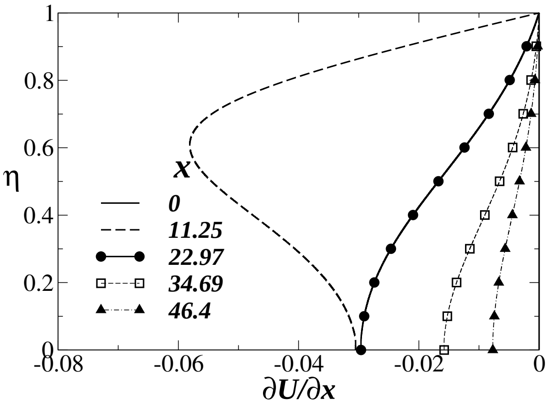

Figure 2.15: Gradient of U in the axial direction at different axial locations, $\mathrm{Re}_i = 150$, angle of divergence = 3°.

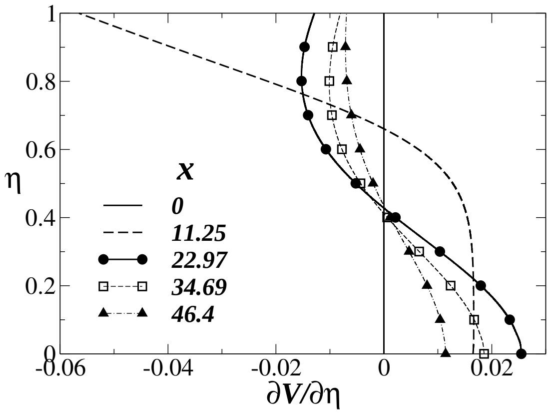

Figure 2.16: Gradient of V in the radial direction at different axial locations, $\mathrm{Re}_i = 150$, angle of divergence = 3°.

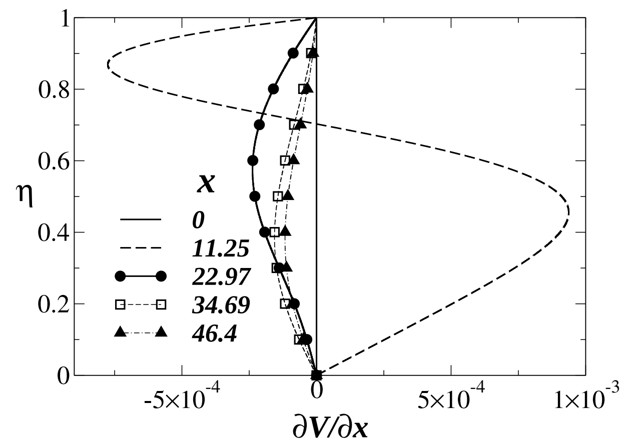

Figure 2.17: Gradient of V in the axial direction at different axial locations, $\mathrm{Re}_i = 150$, angle of divergence = 3°.

2.2 Non-parallel stability analysis

In this section first we describe the derivation of non-parallel stability equations for steady mean flows and discuss some issues generic to non-parallel flows. This analysis is valid for other studies considered in the thesis as well.

2.2.1 Derivation of three-dimensional stability equations for axisymmetric mean flow

In this section we derive non-parallel stability equations for the axisymmetric pipe. We begin with the dimensional continuity and Navier-Stokes equations in polar coordinates for incompressible laminar flows [see e.g. Shames (1992)]. Each flow quantity is then expressed as the sum of a steady mean and a time-dependent perturbation, such as

$$(U_{total})_d = U_d(x,r) + \hat{u_d}(x,r,\theta,t), \tag{2.19}$$

where the subscript d stands for a dimensional quantity. Flow quantities in the form (2.19) are substituted in the Navier-Stokes and continuity equations, the mean flow equation is subtracted, and nonlinear terms in the perturbations are neglected, to get

$$\frac{\partial \hat{u_d}}{\partial x_d} + \frac{1}{r_d}\frac{\partial \hat{w}_d}{\partial \theta_d} + \frac{\partial \hat{v}_d}{\partial r_d} + \frac{\hat{v}_d}{r_d} = 0, \tag{2.20}$$

$$\frac{\partial \hat{u}_d}{\partial t_d} + U_d\frac{\partial \hat{u}_d}{\partial x_d} + \hat{u}_d\frac{\partial U_d}{\partial x_d} + V_d\frac{\partial \hat{u}_d}{\partial r_d} + \hat{v}_d\frac{\partial U_d}{\partial r_d} = -\frac{1}{\rho}\frac{\partial \hat{p}_d}{\partial x_d} + \nu\left[\frac{\partial^2 \hat{u}_d}{\partial r_d^2} + \frac{1}{r_d}\frac{\partial \hat{u}_d}{\partial r_d} + \frac{1}{r_d^2}\frac{\partial^2 \hat{u}_d}{\partial \theta_d^2} + \frac{\partial^2 \hat{u}_d}{\partial x_d^2}\right], \tag{2.21}$$

$$\frac{\partial \hat{v}_d}{\partial t_d} + V_d\frac{\partial \hat{v}_d}{\partial r_d} + \hat{v}_d\frac{\partial V_d}{\partial r_d} - U_d\frac{\partial \hat{v}_d}{\partial x_d} + \hat{u}_d\frac{\partial U_d}{\partial r_d} = -\frac{1}{\rho}\frac{\partial p_d}{\partial r_d} + \nu\left[\frac{\partial^2 \hat{v}_d}{\partial r_d^2} + \frac{1}{r_d}\frac{\partial \hat{v}_d}{\partial r_d} - \frac{\hat{v}_d}{r_d^2} + \frac{1}{r_d^2}\frac{\partial^2 \hat{v}_d}{\partial \theta_d^2} - \frac{2}{r_d^2}\frac{\partial \hat{w}_d}{\partial \theta_d} + \frac{\partial^2 \hat{v}_d}{\partial x_d^2}\right], \tag{2.22}$$

$$\frac{\partial \hat{w}_d}{\partial t_d} + V_d \frac{\partial \hat{w}_d}{\partial r_d} - \frac{V_d \hat{w}_d}{r_d} + U_d \frac{\partial \hat{w}_d}{\partial x_d} = -\frac{1}{\rho r_d}\frac{\partial \hat{p}_d}{\partial \theta_d} + \nu \left[\frac{\partial^2 \hat{w}_d}{\partial r_d^2} + \frac{1}{r_d}\frac{\partial \hat{w}_d}{\partial r_d} - \frac{\hat{w}_d}{r_d^2} + \frac{1}{r_d^2}\frac{\partial^2 \hat{w}_d}{\partial \theta_d^2} + \frac{2}{r_d^2}\frac{\partial \hat{v}_d}{\partial \theta_d} + \frac{\partial^2 \hat{w}_d}{\partial x_d^2} \right]. \tag{2.23}$$

To non-dimensionalise the above equations, we use the local radius, $R(x)$ and the local centerline velocity, $U_c(x)$ at a given x as scales. These scales are chosen (unlike in the computation of mean flow) because they separate the effects of slope and Reynolds number and we can easily distinguish the order of magnitude of each term. The non-dimensional parameters are thus defined as

$$dx = \frac{dx_d}{R},\ \eta = \frac{r_d}{R},\ U_d = U_c U,\ V_d = U_c V,\ t_d = t\frac{R}{U_c},\ \hat{u}_d = U_c \hat{u},\ \hat{v}_d = U_c \hat{v},\ \hat{w}_d = U_c \hat{w},\ \hat{p}_d = \rho U_c^2 \hat{p}.$$

Since the flow under consideration varies significantly in the axial direction, a normal mode form may be used only in time and in the azimuthal coordinate θ. In the axial coordinate, the perturbation may be expressed as a rapidly varying wave-like part scaled by a relatively slowly varying function [see e.g. Bertolotti *et al.* (1992); Govindarajan & Narasimha (1995*a*)], such as

$$[\hat{u}, \hat{v}, \hat{w}, \hat{p}] = \mathrm{Real}\left\{ [u(x,\eta), v(x,\eta), w(x,\eta), p(x,\eta)] \exp\left[\mathrm{i}\left(\int \alpha(x)\mathrm{d}x + n\theta - \omega_d t_d \right) \right] \right\}, \tag{2.24}$$

where $\hat{u}$, $\hat{v}$ and $\hat{w}$ are the axial, radial and the azimuthal velocity perturbations respectively, $\hat{p}$ is the pressure perturbation, $\alpha(x)$ is a local axial wavenumber, n is the number of waves in the azimuthal direction, and ω is the disturbance frequency. The continuity equation is now

$$\frac{U_c'}{U_c}u + \frac{\partial u}{\partial x} + \mathrm{i}\alpha u - a\eta\frac{\partial u}{\partial \eta} + \frac{\mathrm{i}n}{\eta}w + \frac{\partial v}{\partial \eta} + \frac{v}{\eta} = 0. \tag{2.25}$$

The Navier-Stokes equations are written as

$$-\mathrm{i}\omega u + 2U\frac{U_c'}{U_c}u + U\left[\frac{\partial u}{\partial x} + \mathrm{i}\alpha u - ar\frac{\partial u}{\partial \eta}\right] + u\left[\frac{\partial U}{\partial x} - a\eta\frac{\partial U}{\partial \eta}\right] + V\frac{\partial u}{\partial \eta} + v\frac{\partial U}{\partial \eta} = -2\frac{U_c'}{U_c}p - \frac{\partial p}{\partial x} - \mathrm{i}\alpha p +$$

$$a\eta\frac{\partial p}{\partial \eta} + \frac{1}{\mathrm{Re}}\Big[- a\frac{U_c'}{U_c}u - a\frac{\partial u}{\partial x} - a\mathrm{i}\alpha u + 3a^2\eta\frac{\partial u}{\partial \eta} + \frac{U_c''}{U_c}u + 2\frac{U_c'}{U_c}\frac{\partial u}{\partial x} + 2\mathrm{i}\alpha\frac{U_c'}{U_c}u + \frac{\partial^2 u}{\partial x^2} + 2i\alpha\frac{\partial u}{\partial x} -$$

$$\alpha^2 u + \mathrm{i}\alpha' u - 2a\eta\frac{U_c'}{U_c}\frac{\partial u}{\partial \eta} - 2a\eta\frac{\partial^2 u}{\partial x \partial \eta} - 2a\eta\mathrm{i}\alpha\frac{\partial u}{\partial \eta} + a^2 r^2\frac{\partial^2 u}{\partial \eta^2} + \frac{1}{\eta}\frac{\partial u}{\partial \eta} - \frac{n^2}{\eta^2}u + \frac{\partial^2 u}{\partial \eta^2}\Big], \tag{2.26}$$

$$-\mathrm{i}\omega v + V\frac{\partial v}{\partial \eta} + v\frac{\partial V}{\partial \eta} + U\left[\frac{U_c'}{U_c}v + \frac{\partial v}{\partial x} + \mathrm{i}\alpha v - a\eta\frac{\partial v}{\partial \eta}\right] + v\left[\frac{U_c'}{U_c}V + \frac{\partial V}{\partial x} - ar\frac{\partial V}{\partial \eta}\right] = -\frac{\partial p}{\partial \eta} +$$

$$\frac{1}{\mathrm{Re}}\Big[\frac{\partial^2 v}{\partial \eta^2} + \frac{1}{\eta}\frac{\partial v}{\partial \eta} - \frac{v}{\eta^2} - \frac{n^2}{\eta^2}v - \frac{2\mathrm{i}n}{r^2}w - a\frac{U_c'}{U_c}v - a\frac{\partial v}{\partial x} - \mathrm{i}\alpha a v + 3a^2 r\frac{\partial v}{\partial \eta} + \frac{U_c''}{U_c}v + 2\frac{U_c'}{U_c}\frac{\partial v}{\partial x} + 2\mathrm{i}\alpha\frac{U_c'}{U_c}v +$$

$$\frac{\partial^2 v}{\partial x^2} + 2\mathrm{i}\alpha\frac{\partial v}{\partial x} - \alpha^2 v + \mathrm{i}\alpha' v - 2a\eta\frac{U_c'}{U_c}\frac{\partial v}{\partial \eta} - 2a\eta\frac{\partial^2 v}{\partial x \partial \eta} - 2a\eta\mathrm{i}\alpha\frac{\partial v}{\partial \eta} + a^2\eta^2\frac{\partial v^2}{\partial \eta^2}\Big] \tag{2.27}$$

$$-\mathrm{i}\omega w + V\frac{\partial w}{\partial \eta} - \frac{Vw}{\eta} + U\Big[\frac{U_c'}{U_c}w + \frac{\partial w}{\partial x} + \mathrm{i}\alpha w - ar\frac{\partial w}{\partial \eta}\Big] = -\frac{\mathrm{i}n}{\eta}p + \frac{1}{\mathrm{Re}}\Big[\frac{\partial^2 w}{\partial \eta^2} + \frac{1}{\eta}\frac{\partial w}{\partial \eta} - \frac{w}{\eta^2} - \frac{n^2}{\eta^2}w +$$

$$\frac{2\mathrm{i}n}{\eta^2}v - a\frac{U_c'}{U_c}w - a\frac{\partial w}{\partial x} - \mathrm{i}\alpha a w + 3a^2\eta\frac{\partial w}{\partial \eta} + \frac{U_c''}{U_c}w + 2\frac{U_c'}{U_c}\left(\frac{\partial w}{\partial x} + \mathrm{i}\alpha w\right) + \frac{\partial^2 w}{\partial x^2} + 2\mathrm{i}\alpha\frac{\partial w}{\partial x} - \alpha^2 w +$$

$$\mathrm{i}\alpha' w - 2a\eta\frac{U_c'}{U_c}\frac{\partial w}{\partial \eta} - 2a\eta\frac{\partial^2 w}{\partial x \partial \eta} - 2a\eta\mathrm{i}\alpha\frac{\partial w}{\partial \eta} + a^2\eta^2\frac{\partial^2 w}{\partial \eta^2}\Big]. \tag{2.28}$$

Taking the derivative of (2.25) with respect to η and substituting the resulting expression for $\partial^2 v/\partial\eta^2$ in equation (2.27), we obtain

$$-\mathrm{i}\omega v + V\frac{\partial v}{\partial \eta} + v\frac{\partial V}{\partial \eta} + U\Big[\frac{U_c'}{U_c}v + \frac{\partial v}{\partial x} + \mathrm{i}\alpha v - a\eta\frac{\partial v}{\partial \eta}\Big] + u\Big[\frac{U_c'}{U_c}V + \frac{\partial V}{\partial x} - ar\frac{\partial V}{\partial \eta}\Big] + \frac{\partial p}{\partial \eta} + \frac{1}{\mathrm{Re}}\Big[\frac{n^2}{\eta^2}v + \frac{2\mathrm{i}n}{\eta^2}w +$$

$$a\frac{U_c'}{U_c}v + a\frac{\partial v}{\partial x} + \mathrm{i}\alpha a v - 3a^2 r\frac{\partial v}{\partial \eta} - \frac{U_c''}{U_c}v - 2\frac{U_c'}{U_c}\frac{\partial v}{\partial x} - 2\mathrm{i}\alpha\frac{U_c'}{U_c}v - \frac{\partial^2 v}{\partial x^2} - 2\mathrm{i}\alpha\frac{\partial v}{\partial x} + \alpha^2 v - \mathrm{i}\alpha' v + 2a\eta\frac{U_c'}{U_c}\frac{\partial v}{\partial \eta} +$$

$$2ar\frac{\partial^2 v}{\partial x \partial r} + 2a\eta\mathrm{i}\alpha\frac{\partial v}{\partial \eta} - a^2\eta^2\frac{\partial v^2}{\partial \eta^2} + \frac{U_c'}{U_c}\frac{\partial u}{\partial \eta} + \frac{\partial^2 u}{\partial x \partial \eta} + \mathrm{i}\alpha\frac{\partial u}{\partial \eta} - a\frac{\partial u}{\partial \eta} - a\eta\frac{\partial^2 u}{\partial \eta^2} - \frac{\mathrm{i}n}{\eta^2}w + \frac{\mathrm{i}n}{\eta}\frac{\partial w}{\partial \eta}\Big] = 0. \tag{2.29}$$

where $a\,(\equiv dR(x)/dx_d)$ is the slope of the pipe and $U_c' = dU_c/dx$. The above equations have many terms that arise from the fact that flow is developing in the streamwise direction. Terms containing U_c'/U_c, V, $\partial U/\partial x$, and $\partial V/\partial x$ arise due to the axial variation of the mean flow. Terms containing $\partial u/\partial x$ and α' appear due to the non-parallel nature of the disturbances. The extra terms containing a arise due to the non-dimensionalisation chosen, for example

$$\frac{\partial \hat{u}_d}{\partial x_d} = \frac{1}{R}\left[U_c'\hat{u} + U_c\frac{\partial \hat{u}}{\partial x} - arU_c\frac{\partial \hat{u}}{\partial \eta}\right], \tag{2.30}$$

Since axial variations are slow and the Reynolds number is large, a consistent approximation is to retain all terms up to $O(a)$ and $O\left(\mathrm{Re}^{-1}\right)$ and neglect higher order effects [see e.g. Govindarajan & Narasimha (1997, 2005)]. The result is a set of partial differential equations for the perturbation velocities and pressure, each of first order in x and up to second order in η, which amounts to a seventh order system in r. They are

$$-i\omega u + U\left[2\frac{U_c'}{U_c}u + \frac{\partial u}{\partial x} + i\alpha u - a\eta\frac{\partial u}{\partial \eta}\right] + u\left[\frac{\partial U}{\partial x} - a\eta\frac{\partial U}{\partial \eta}\right] + V\frac{\partial u}{\partial \eta} + v\frac{\partial U}{\partial \eta} = -2\frac{U_c'}{U_c}p - \frac{\partial p}{\partial x} - i\alpha p +$$

$$a\eta\frac{\partial p}{\partial \eta} + \frac{1}{Re}\left[-\alpha^2 u + \frac{1}{\eta}\frac{\partial u}{\partial \eta} - \frac{n^2}{\eta^2}u + \frac{\partial^2 u}{\partial \eta^2}\right], \tag{2.31}$$

$$-i\omega v + V\frac{\partial v}{\partial \eta} + v\frac{\partial V}{\partial \eta} + U\left[\frac{U_c'}{U_c}v + \frac{\partial v}{\partial x} + i\alpha v - ar\frac{\partial v}{\partial \eta}\right] = -\frac{\partial p}{\partial \eta} + \frac{1}{Re}\left[\frac{\partial^2 v}{\partial \eta^2} + \frac{1}{\eta}\frac{\partial v}{\partial \eta} - \frac{\left(1+n^2\right)}{\eta^2}v - \frac{2in}{\eta^2}w\right] \tag{2.32}$$

$$-i\omega w + V\frac{\partial w}{\partial \eta} - \frac{Vw}{\eta} + U\left[\frac{U_c'}{U_c}w + \frac{\partial w}{\partial x} + i\alpha w - ar\frac{\partial w}{\partial \eta}\right] = -\frac{in}{\eta}p + \frac{1}{Re}\Big[\frac{\partial^2 w}{\partial \eta^2} + \frac{1}{\eta}\frac{\partial w}{\partial \eta} - \frac{\left(1+n^2\right)}{\eta^2}w +$$

$$\frac{2in}{\eta^2}v - \alpha^2 w\Big], \tag{2.33}$$

$$-i\omega v + V\frac{\partial v}{\partial \eta} + v\frac{\partial V}{\partial \eta} + U\left[\frac{U_c'}{U_c}v + \frac{\partial v}{\partial x} + i\alpha v - ar\frac{\partial v}{\partial \eta}\right] = -\frac{\partial p}{\partial \eta} + \frac{1}{\mathrm{Re}}\left[-\frac{n^2}{\eta^2}v - \frac{in}{\eta^2}w - \alpha^2 v - i\alpha\frac{\partial u}{\partial \eta} - \frac{in}{\eta}\frac{\partial w}{\partial \eta}\right] \tag{2.34}$$

Equations (2.31) to (2.34) may be rewritten in the form [Sahu & Govindarajan (2005)]

$$\mathcal{H}\phi(x,\eta) + \mathcal{G}\frac{\partial\phi(x,\eta)}{\partial x} = \omega\mathcal{B}\phi(x,\eta). \tag{2.35}$$

Here $\phi = [u, v, w, p]$, $\omega = \omega_d R/U_c$ and the non-zero elements of the 4×4 matrix operators $\mathcal{H}$, $\mathcal{G}$ and $\mathcal{B}$ are given by

$$h_{11} = U\left[2\frac{U_c'}{U_c} + \mathrm{i}\alpha - a\eta\frac{\partial}{\partial\eta}\right] + \frac{\partial U}{\partial x} - a\eta\frac{\partial U}{\partial\eta} + V\frac{\partial}{\partial\eta} + \frac{1}{\mathrm{Re}}\left[\alpha^2 + \frac{n^2}{\eta^2} - \frac{1}{\eta}\frac{\partial}{\partial\eta} - \frac{\partial^2}{\partial\eta^2}\right], h_{12} = \frac{\partial U}{\partial\eta},$$

$$h_{14} = \left(2\frac{U_c'}{U_c} + \mathrm{i}\alpha - a\eta\frac{\partial}{\partial\eta}\right),\ \ h_{22} = V\frac{\partial}{\partial\eta} + \frac{\partial V}{\partial\eta} + U\left[\frac{U_c'}{U_c} + \mathrm{i}\alpha - a\eta\frac{\partial}{\partial\eta}\right] - \frac{1}{\mathrm{Re}}\left[\frac{\partial^2}{\partial\eta^2} + \frac{1}{\eta}\frac{\partial}{\partial\eta} - \frac{(1+n^2)}{\eta^2} - \alpha^2\right],$$

$$h_{23} = \frac{2}{\mathrm{Re}}\frac{\mathrm{i}n}{\eta^2},\ \ h_{24} = \frac{\partial}{\partial\eta},\ \ h_{32} = -\frac{2}{\mathrm{Re}}\frac{\mathrm{i}n}{\eta^2},$$

$$h_{33} = V\frac{\partial}{\partial\eta} - \frac{V}{\eta} + U\left[\frac{U_c'}{U_c} + \mathrm{i}\alpha - a\eta\frac{\partial}{\partial\eta}\right] - \frac{1}{\mathrm{Re}}\left[\frac{\partial^2}{\partial\eta^2} + \frac{1}{\eta}\frac{\partial}{\partial\eta} - \frac{(1+n^2)}{\eta^2} - \alpha^2\right],\ \ h_{34} = \frac{in}{\eta},\ \ h_{41} = \frac{\mathrm{i}\alpha}{\mathrm{Re}}\frac{\partial}{\partial\eta},$$

$$h_{42} = V\frac{\partial}{\partial\eta} + \frac{\partial V}{\partial\eta} + U\left(\frac{U_c'}{U_c} + \mathrm{i}\alpha - a\eta\frac{\partial}{\partial\eta}\right) + \frac{1}{\mathrm{Re}}\left(\frac{n^2}{\eta^2} + \alpha^2\right),\ \ h_{43} = \frac{\mathrm{i}n}{\mathrm{Re}}\left(\frac{1}{\eta^2} + \frac{1}{\eta}\frac{\partial}{\partial\eta}\right),\ \ h_{44} = \frac{\partial}{\partial\eta};$$

$$g_{11} = g_{22} = g_{33} = g_{42} = U,\ \ g_{14} = 1,\ \text{ and }\ b_{11} = b_{22} = b_{33} = b_{42} = \mathrm{i}.$$

In equation (2.35), we confirm that if we set a, U_c' and $\partial\phi/\partial x$ to zero, we get the stability equations of Gill (1973) and Lessen *et al.* (1968) for the parallel (fully developed) flow through a straight pipe. Secondly, the stability equations for developing flow in the entry region of a straight pipe are obtained simply by setting the angle of divergence to zero in equation (2.35). The boundary conditions emerge from requiring that all quantities vary continuously with r at the centerline [Batchelor & Gill (1962)], and obey no-slip at the wall.

$$u = v = w = p = 0, \qquad \text{at } \eta = 0,\ \text{for } n \neq 1, \tag{2.36}$$

$$u = p = 0, \quad v + \mathrm{i}w = 0, \qquad \text{at } \eta = 0,\ \text{for } n = 1, \tag{2.37}$$

$$u = v = w = 0, \qquad \text{at } \eta = 1. \tag{2.38}$$

The no-slip boundary condition at the wall is relaxed for microflows. In that case, the modified set of boundary conditions at the wall are

$$u + Kn\left(\frac{\partial u}{\partial\eta}\right) = v - au = w = 0, \qquad \text{at} \quad \eta = 1, \tag{2.39}$$

Note that for $n = 1$, we have only six boundary conditions for a seventh order system. We therefore generate an extra boundary condition by differentiating the continuity equation with respect to r, and using the fact that $u(x, 0) = 0$, to get

$$2\frac{\partial v}{\partial\eta} + \mathrm{i}n\frac{\partial w}{\partial\eta} = 0 \qquad \text{at } \eta = 0,\ \text{for } n = 1. \tag{2.40}$$

Equation (2.35) may be solved as an eigenvalue problem of larger size [Balachandar & Govindarajan, unpublished] as described below. The streamwise derivative in equation (2.35) couples neighboring axial locations in the flow-field to one another. Consider two streamwise locations 1 and 2 separated by an incremental distance, *i.e.*, $x_2 = x_1 + \Delta x$. We may write

$$\frac{\partial \phi}{\partial x} = \frac{(\phi_2 - \phi_1)}{\Delta x} + O(\Delta x), \tag{2.41}$$

where the subscripts 1 and 2 denote the values at x_1 and x_2 respectively. Since the dimensional frequency ω_d remains constant, ω_1 and ω_2 are related as follows

$$\kappa \equiv \frac{\omega_2}{\omega_1} = [1 + a\Delta x]\frac{U_{c1}}{U_{c2}}. \tag{2.42}$$

To first order in Δx we may therefore express equation (2.35) as

$$\begin{bmatrix} \mathcal{H}_1 - \mathcal{G}_1/\Delta x & \mathcal{G}_1/\Delta x \\ -\mathcal{G}_2/\Delta x & \mathcal{H}_2 + \mathcal{G}_2/\Delta x \end{bmatrix} \begin{bmatrix} \phi_1 \\ \phi_2 \end{bmatrix} = \omega_1 \begin{bmatrix} \mathcal{B}_1 & 0 \\ 0 & \kappa\mathcal{B}_2 \end{bmatrix} \begin{bmatrix} \phi_1 \\ \phi_2 \end{bmatrix}. \tag{2.43}$$

The partial differential equation (2.35) is thus expressed as an eigenvalue problem of twice the size of the corresponding Orr-Sommerfeld problem. (Higher-order approximations to the streamwise derivative could be considered instead of (2.41) and the resulting eigensystem would be of correspondingly large size.)

In order to obtain the correct dependence of the system on the axial coordinate, the problem needs to be solved by trial and error. This is because the apportionment in (2.24) between the x-dependences of α and the eigenfunction is arbitrary. There are many ways of performing this apportionment [Bertolotti *et al.* (1992)], and so long as all rapid changes are included in α there is no difference in the prediction of the growth of any physical quantity. We have checked that this is the case for the present flow as well.

The procedure we follow is as follows. First the homegeneous part of equation (2.35) is solved at x_1 by assuming a guess value of the streamwise wavenumber α_1. The exercise is repeated at x_2 to obtain an α_2 giving the same dimensional frequency (ω_d). The axial variation of the wavenumber, $\mathrm{d}\alpha/\mathrm{d}x$ is thus obtained from α_1 and α_2. By taking the homogeneous part of (2.35), the largest term that we have neglected is of $O(R^{-2/3})$ in the critical layer and higher order elsewhere [see e.g. Lin (1955); Govindarajan & Narasimha (1997)]. If we make the reasonable assumption that $\mathrm{d}\alpha/\mathrm{d}x \sim O\left(\mathrm{Re}^{-1}\right)$, we may approximate $\mathrm{d}\alpha/\mathrm{d}x$ by the value obtained by solving the homogeneous problem, since

$$\frac{\mathrm{d}\alpha}{\mathrm{d}x} = \left.\frac{\mathrm{d}\alpha}{\mathrm{d}x}\right|_h + O\left(\mathrm{Re}^{-5/3}\right) \approx \left.\frac{\mathrm{d}\alpha}{\mathrm{d}x}\right|_h.$$

In subsequent iterations, $\mathrm{d}\alpha/\mathrm{d}x$ is maintained constant, since the correction due to the inhomogeneous terms on this quantity is of higher order. An alternative procedure, that of setting $\alpha_2 = \alpha_1$, gave disturbance growth rates that differed from those obtained here only in the fifth decimal place. Then the eigenvalue problem [equation (2.43)] is solved by a spectral collocation method [Canuto *et al.* (1987)]. The eigenvalue ω_1 is obtained as a complex quantity. The complex streamwise wavenumber, α_1 is iterated until ω_1 assumes the desired real value ($= \omega_d R/U_c$) at x_1. This procedure is the same in principle as the parabolized stability equation solutions of Bertolotti *et al.* (1992), for example. The regrouping in the form of an eigenvalue problem is done only to make it convenient to obtain a local solution.

The numerical mean flow is interpolated to obtain profiles at neighbouring x-locations, with $\Delta x = 0.05$. Profiles obtained from computations using 512 grid points as well as 1024 grid points have been checked to give eigenvalues correct up to 4 decimal places. Halving or doubling the Δx has even less of an effect on the eigenvalue. The procedure is validated by solving the non-parallel stability problem for Falkner-Skan velocity profiles of boundary layers. For a wide range of pressure gradients and disturbance frequencies, the results matched exceedingly well with standard non-parallel results.

We compute the growth of disturbances followed streamwise at a constant value of the non-dimensional radius r. At a given x, the growth rate g of the dimensional disturbance kinetic energy, $\hat{E}_d = 1/2(\hat{u}_d^2 + \hat{v}_d^2 + \hat{w}_d^2)$, for example, is given by

$$g = \frac{1}{\hat{E}_d}\frac{\partial \hat{E}_d}{\partial x_d} = -2\alpha_i + \frac{1}{E_d}\frac{\partial E_d}{\partial x_d}\Big|_r, \tag{2.44}$$

where $E_d = 1/4(u_d u_d{}^* + v_d v_d{}^* + w_d w_d{}^*)$, the star denotes a complex conjugate. The growth factor for this quantity is thus

$$\frac{E_d}{E_{cr}} = \exp\left[\int_{x_{cr}}^{x} g(x_d)\mathrm{d}x_d\right] \tag{2.45}$$

where the subscript cr stands for the critical location, at which $g = 0$. The dimensional frequency ω_d is calculated at a location at x_0 where the disturbance kinetic energy starts growing and then kept constant downstream, i.e. $\omega_d = \omega_0 U/R$, ω_0 is the non-dimensional frequency at x_0. From equation (2.44) we see that a disturbance may amplify at one r and decay at another. Secondly, one disturbance quantity could be amplifying while others decay. This is an interesting property of spatially developing flow, requiring that the monitoring location be set very carefully in an experiment. We are now equipped with all the stability equations needed. Before solving them completely it is of interest to study the stability behaviour in the inviscid limit (Re $\to \infty$).

2.3 Inviscid stability analysis

The analysis is worthwhile, since fully-developed pipe flow is linearly stable at any Reynolds number. For two-dimensional flow, necessary conditions for instability in the inviscid limit have been derived by Rayleigh (1880*b*) and Fjortoft (1950). Rayleigh (1880*b*) states that it is necessary to have a point of inflection in the velocity profile for the flow to be unstable. Fjortoft (1950) theorem says that if a point of inflection exists, it is further necessary that $U''(U - U_{pi}) \leq 0$ somewhere in the profile, where U_{pi} is the velocity at the point of inflection. The inviscid stability criterion for axial flow between rotating cylinders is given in Chandrasekhar (1981). Similar criteria for centrifugal instabilities is given in Billant & Gallaire (2005). Several other similar studies exist, e.g, for compressible flows. Shankar & Kumaran (2000) derived the inviscid stability criterion for flow in a flexible tube, with the rigid case included as the limiting one. For the present derivation, we start with the stability equations [given in (2.25) and (2.31)-(2.33)] in cylindrical co-ordinate system, in the limit Re $\to \infty$ and $a \to 0$, which reduce to the parallel flow equations [Davey & Drazin (1969); Lessen *et al.* (1968)].

$$-\mathrm{i}\alpha c u + U\mathrm{i}\alpha u + vU' = -p\mathrm{i}\alpha, \tag{2.46}$$

$$-\mathrm{i}\alpha c v + U\mathrm{i}\alpha v = -p', \tag{2.47}$$

$$-\mathrm{i}\alpha c w + U\mathrm{i}\alpha w = -\frac{1}{\eta}\mathrm{i}np, \tag{2.48}$$

$$\text{and} \qquad \mathrm{i}\alpha u + v' + \frac{v}{\eta} + \frac{1}{\eta}\mathrm{i}nw = 0r, \tag{2.49}$$

where $c(=\beta/\alpha)$ is the phase speed of the disturbance. Eliminating azimuthal velocity (w) and pressure (p) from the above equations, we get

$$(U-c)\left[\mathrm{i}\alpha u+\frac{\alpha^2\eta^2}{n^2}\left(\mathrm{i}\alpha u+v'+\frac{v}{\eta}\right)\right]+vU'=0. \tag{2.50}$$

$$(U-c)\left(\mathrm{i}\alpha u'+\alpha^2 v\right)+U'\mathrm{i}\alpha u+v'U'+vU''=0. \tag{2.51}$$

Differentiating equation (2.50) with respect to η and then subtracting equation (2.51) from the resulting equation, we obtain

$$(U-c)\left[\frac{\mathrm{i}\alpha\eta}{n^2}u'+\frac{2\mathrm{i}\alpha}{n^2}u+\frac{3}{n^2}v'+\frac{\eta}{n^2}v''+\frac{v}{\eta}\left(\frac{1}{n^2}-1\right)\right]+U'\left[\frac{\mathrm{i}\alpha\eta}{n^2}u+\frac{\eta}{n^2}v'+\frac{1}{n^2}v\right]=0. \tag{2.52}$$

Now using equations (2.50) and (2.51), to eliminate streamwise velocity (u) and its derivative u', we obtain

$$(U-c)\left[v''+\frac{\left(3n^2+\alpha^2\eta^2\right)}{(\alpha^2\eta^2+n^2)}\frac{v'}{\eta}-\frac{\left(\alpha^2\eta^2+n^2+2\right)}{(\alpha^2\eta^2+n^2)}\alpha^2 v+(1-n^2)\frac{v}{\eta^2}\right]-\left[U''-\frac{\left(\alpha^2\eta^2-n^2\right)}{\eta(\alpha^2\eta^2+n^2)}U'\right]v=0. \tag{2.53}$$

We define a function $f(\eta)$ such that

$$\frac{f'}{f}=\left[\frac{3n^2+\alpha^2\eta^2}{\eta(\alpha^2\eta^2+n^2)}\right], \tag{2.54}$$

On multiplying equation (2.53) with $f(\eta)v^*$ and integrating across the pipe from $\eta=0$ to $\eta=1$, we get

$$\int_0^1 (fv')'v^* d\eta-\int_0^1 f\left[\frac{\alpha^2\eta^2+n^2+2}{\alpha^2\eta^2+n^2}\right]\alpha^2|v|^2 d\eta+\int_0^1 (1-n^2)\frac{|v|^2}{\eta^2}dr=$$

$$\int_0^1 f\left[U''-\frac{\alpha^2\eta^2-n^2}{\eta(\alpha^2\eta^2+n^2)}U'\right]\frac{|v|^2}{|U-c|^2}(U-c)^* d\eta, \tag{2.55}$$

v and v^* are zero at the wall ($\eta=1$) and $v'=0$ at the centerline ($\eta=0$). Intergating the first term in equation (2.55) and using the boundary conditions, we get for the first term in equation (2.55)

$$\int_0^1 (fv')'v^* d\eta=fv^*v'\Big|_0^1-\int_0^1 f|v'|^2 d\eta=-\int_0^1 f|v'|^2 d\eta, \tag{2.56}$$

Since f is always positive [from equation (2.54)], the first and second term in the equation (2.55) are real and negative. For any $n \geq 1$ the third term is also zero or negative. For $n=0$, combining the second and third terms in equation (2.55), we get

$$-\int_0^1 f\left[\frac{\alpha^2\eta^2+n^2+2}{\alpha^2\eta^2+n^2}\right]\alpha^2|v|^2 d\eta+\int_0^1 f(1-n^2)\frac{|v|^2}{\eta^2}d\eta=-\int_0^1 f\frac{|v|^2}{\eta^2}(1+\alpha^2\eta^2)d\eta. \tag{2.57}$$

Again this is a negative quantity. Hence for any n, the left hand side of equation (2.55) is real and negative and we may write the imaginary part of the equation (2.55) as

$$c_i\int_0^1 f\left[U''-\frac{(\alpha^2\eta^2-n^2)}{\eta(\alpha^2\eta^2+n^2)}U'\right]\frac{|v|^2}{|U-c|^2}d\eta=0, \tag{2.58}$$

Where c_i is the imaginary part of the phase speed, c. For flow to be unstable, $c_i > 0$. This implies that for unstable flow, we must have

$$\int_0^1 f\left[U'' - \frac{(\alpha^2\eta^2 - n^2)}{\eta(\alpha^2\eta^2 + n^2)}U'\right]\frac{|v|^2}{|U-c|^2}d\eta = 0. \tag{2.59}$$

For this to hold, we must have

$$I \equiv U'' - \frac{(\alpha^2\eta^2 - n^2)}{\eta(\alpha^2\eta^2 + n^2)}U' \tag{2.60}$$

changing sign somewhere between $\eta = 0$ and $\eta = 1$. Hence a necessary condition for instability of pipe flow is that the quantity $I = 0$ somewhere in the domain. If we set $\eta \to \infty$ in the above equation, we recover Rayleigh's criterion for two-dimensional flow. Now consider a flow where I goes through a zero somewhere in the profile. The real part of the equation (2.55) is given by

$$\int_0^1 f(U - c_r)\left[U'' - \frac{(\alpha^2\eta^2 - n^2)}{\eta(\alpha^2\eta^2 + n^2)}U'\right]\frac{|v|^2}{|U-c|^2}d\eta \leq 0. \tag{2.61}$$

Multipling equation (2.59) with $(c_r - U_s)$, we get

$$\int_0^1 f(c_r - U_s)\left[U'' - \frac{(\alpha^2\eta^2 - n^2)}{\eta(\alpha^2\eta^2 + n^2)}U'\right]\frac{|v|^2}{|U-c|^2}d\eta = 0, \tag{2.62}$$

where U_s is the velocity at the radial location where $I = 0$. Now adding equations (2.61) and (2.62), we have

$$\int_0^1 f(U - U_s)\left[U'' - \frac{(\alpha^2\eta^2 - n^2)}{\eta(\alpha^2\eta^2 + n^2)}U'\right]\frac{|v|^2}{|U-c|^2}d\eta \leq 0. \tag{2.63}$$

Hence, at least in some part of the domain from 0 to R, we must have

$$(U - U_s)\left[U'' - \frac{(\alpha^2\eta^2 - n^2)}{\eta(\alpha^2\eta^2 + n^2)}U'\right] \leq 0. \tag{2.64}$$

This gives an additional necessary condition of instability for pipe flows. As discussed above the two-dimensional counterpart of the above criterion is the Fjortoft's theorem. It can be shown analytically, as follows, that flow through a pipe of any non-zero wall divergence satisfies the necessary conditions of inviscid instability.

As derived in § 2.1.2, the mean flow for small divergence obeys the axisymmetric Jeffery-Hamel equation. The velocity profile deviates from the parabolic profile by a function $\epsilon(\eta)$, which may be taken to be small everywhere when S is small. Substituting

$$U = 1 - \eta^2 + \epsilon(\eta), \tag{2.65}$$

in equation (2.13) and linearising (retaining only first order terms in ϵ and S), we get

$$\epsilon''' + \frac{\epsilon''}{\eta} - \frac{\epsilon'}{\eta^2} = 8S\eta\left(1 - \eta^2\right). \tag{2.66}$$

This equation may be solved to give

$$\epsilon = \frac{S}{36}\left(-7 + 9\eta^4 - 2\eta^6\right). \tag{2.67}$$

which satisfies the no-slip boundary condition at the wall, and the no shear condition at the centreline. This expression is compared to the ϵ obtained by solving the AJH equation in figure 2.18. It can be seen that the expression is good for $S < 0.1$ or so.

The axisymmetric Rayleigh condition for instability [equation (2.60)] states that

$$I \equiv \left[U'' - \frac{K}{\eta}U'\right], \tag{2.68}$$

must change sign somewhere in the domain, where

$$K = \left(1 - n^2/\alpha^2\eta^2\right)/\left(1 + n^2/\alpha^2\eta^2\right). \tag{2.69}$$

As seen above, K can take on any value between -1 and 1, corresponding to the limits $n/\alpha \to \infty$ and $n/\alpha \to 0$ respectively. For small S, using equation (2.67), we have

$$I = 2(-1 + K) + (3 - K)S\eta^2 + \frac{(K-5)}{3}S\eta^4, \tag{2.70}$$

which lies between the limits

$$I_1 = -4 + 2S\left(2 - \eta^2\right) \quad \text{and} \tag{2.71}$$

$$I_2 = 2S\eta^2\left(1 - \frac{2}{3}\eta^2\right). \tag{2.72}$$

For a straight pipe ($S = 0$), $I_1 = -4$, $I_2 = 0$, so the flow is stable to any linear perturbation at infinite Reynolds number. On the other hand for any non-zero but small S it can be seen that I_1 is always negative and I_2 is always positive but small.

We therefore test if some small but non-zero value δ of the ratio n^2/α^2 will satisfy the necessary condition. We restrict ourselves to a portion $\eta > \eta_s$ of the pipe sufficiently far from the centreline, such that $\eta_s \gg n/\alpha$. Here, from equation (2.69),

$$K \approx 1 - \frac{2\delta}{\eta^2},$$

and

$$I = \frac{\eta^4}{2}\left[1 - \frac{2}{3}\eta^2\right] - \frac{\delta}{S}. \tag{2.73}$$

For $\delta/S < 1/6$, I goes through a zero at η_i, given by

$$\frac{\delta}{S} = \frac{\eta_i^4}{2}\left[1 - \frac{2}{3}\eta_i^2\right]. \tag{2.74}$$

Incidentally, from the sign of $dI/d\eta$ we can see that I is a monotonically increasing function of η.

Further, from equations (2.65) and (2.67), we have

$$U - U_s = (\eta_i^2 - \eta^2) + \frac{S}{4}(\eta_i^4 - \eta^4) - \frac{S}{18}(\eta_i^6 - \eta^6) \tag{2.75}$$

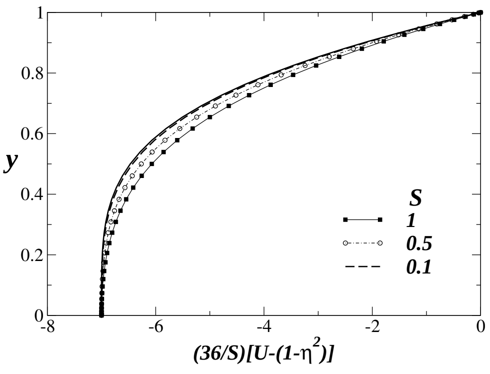

Figure 2.18: The comparison of ϵ [equation (2.67)] with the deviation of AJH profile from the parabolic profile for different S (the variation of $36\epsilon/S$ is shown by the solid line without any symbol).

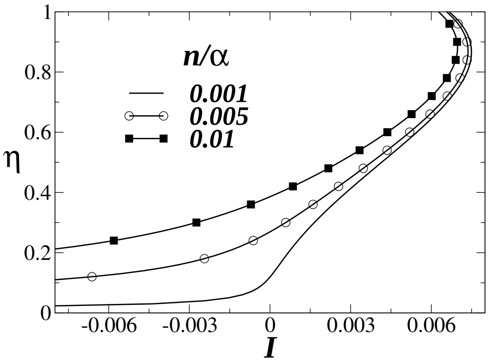

Figure 2.19: Variation of I for different n/α.

for small S, so

$$I < 0 \text{ and } (U - U_s) > 0 \text{ for } \eta < \eta_i \quad \text{and}$$

$$I > 0 \text{ and } (U - U_s) < 0 \text{ for } \eta > \eta_i.$$

Thus $I(U - U_s)$ is negative everywhere for $\eta > \eta_s$in the domain and this satisfies the axisymmetric Fjortoft criterion which is another necessary condition for instability.

On the other hand, for a two-dimensional diverging channel for small S,

$$I \equiv -2 + S\eta^2(2 - \eta^2), \tag{2.76}$$

does not change sign. We thus have an interesting contrast where the channel is inviscidly stable but the pipe is not.

2.4 Results of the stability analysis

For flow through a straight pipe, we compare our eigenspectrum with that of Meseguer & Trefethen (2003); Schmid & Henningson (2001). Every eigenvalue matches up to the 10^{th} decimal place. The eigenspectrum for axisymmetric ($n = 0$) and non-axisymmetric ($n = 1$) disturbances are given in figures 2.20 and 2.21 respectively. As mentioned above, the non-parallel equations and solution procedure are checked by solving for boundary layer flow at various pressure gradients.

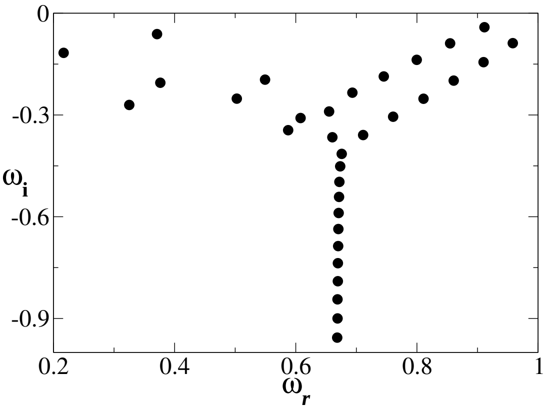

Figure 2.20: Eigenspectrum for swirl mode ($n = 1$), Re = 3000, flow through a straight pipe.

In the range Re > 1000 and $a < 1°$ the results from a non-parallel analysis are found to be the same as those obtained by assuming the flow to be parallel [neglecting non-parallel terms in the stability equation (2.35)]. Also in this regime, the similarity solutions giving the AJH profiles are very close to numerically obtained mean flow. Figure 2.22 shows the stability boundary in this regime in terms of the critical Reynolds number for linear instability as a function of the angle of divergence. At any small (but non-zero) divergence angle, we find a *finite* Reynolds number for linear instability. It can be seen that a power-law relationship is obeyed. The best fit of the data gives $\text{Re}_{cr} = 11.2a^{-0.98}$, which is practically indistinguishable from $\text{Re}_{cr} = 10/a$. The critical Reynolds number thus varies as the inverse of the divergence angle. The inverse relationship arises because an inviscid mechanism is operational at very high Reynolds numbers and so stability depends only on the basic flow. The basic flow in turn depends only on the parameter S [equation (2.13)] which is a product of Re and a. We thus find that there is a limiting velocity profile corresponding to $S = 10$, and flows where S is greater than 10 are linearly unstable. Incidentally at $S \approx 10$ the AJH flow separates, so the occurrance of linear instability is intuitive.

The necessary condition was satisfied for very small n/α. Given that n can take only integer values,

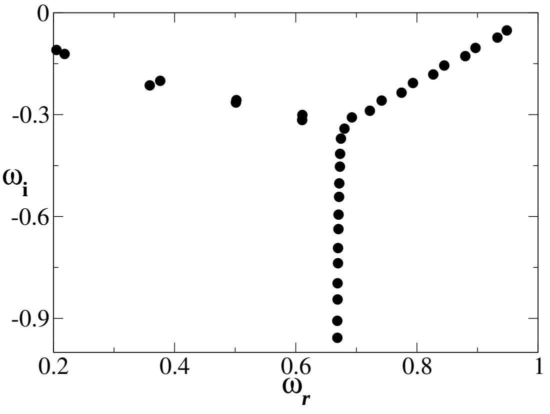

Figure 2.21: Same as figure 2.20 but for axisymmetric mode ($n = 0$).

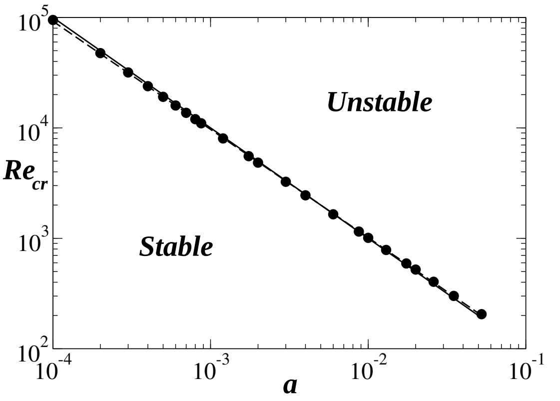

Figure 2.22: Variation of the critical Reynolds number with the tangent a of the divergence angle, at small angles of divergence. Symbols: stability analysis; dashed line: best fit; solid line: $\mathrm{Re}_{cr} = 10/a$.

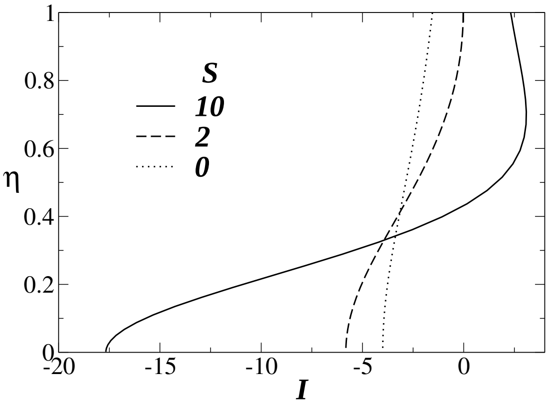

Figure 2.23: The inviscid instability function I for the swirl ($n = 1$) mode for different values of S. $S = 0$ represents the flow in a straight pipe.

the limit corresponds to extremely small wave lenght disturbances. In viscous flows, these wavelengths are not found to be dominant. We therefore consider a realistic $\alpha = 1.26$ which corresponds to critical instability. The variation of I for the non-axisymmetric swirl mode ($n = 1$) and axisymmetric ($n = 0$) modes with the radial coordinate are seen in figures 2.23 and 2.24. It can be seen that for swirl mode I undergoes a sign change for $S > 2$, whereas it is positive everywhere for the axisymmetric mode for all S upto 10. This implies that the swirl mode is inviscidly unstable but the axisymmetric mode is stable for attached flow in a diverging pipe. It is useful to note that the least stable mode in a straight pipe is the swirl mode ($n = 1$) [Burridge & Drazin (1969); Corcos & Sellars (1959)]. This feature is maintained in diverging pipes too.

We now examine the behaviour at higher levels of divergence. For the geometry shown in figure 2.1, a non-parallel spatial stability analysis [equation (2.43)] is performed on the numerically obtained profiles. All the results presented here are for Re = 150 at the inlet. Typical plots of the eigenfunctions u, v, w and their axial variations are shown in figures 2.25 to 2.26.

The growth rate of the disturbance depends on how far the monitoring location is from the centerline, and what is the quantity being monitored. An examination of equation (2.44) shows that the second term on the right hand side determines the r-dependence, and comes from the flow quantity under con-

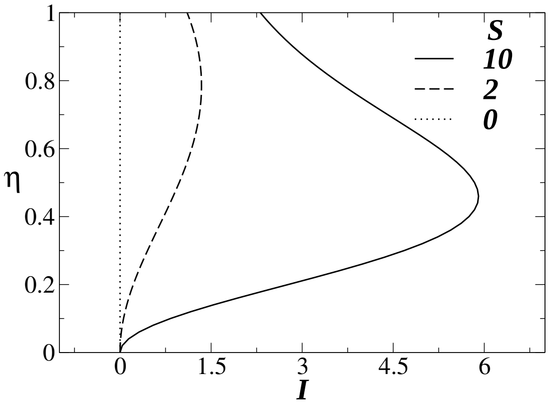

Figure 2.24: Same as figure 2.23 but for axisymmetric mode ($n = 0$).

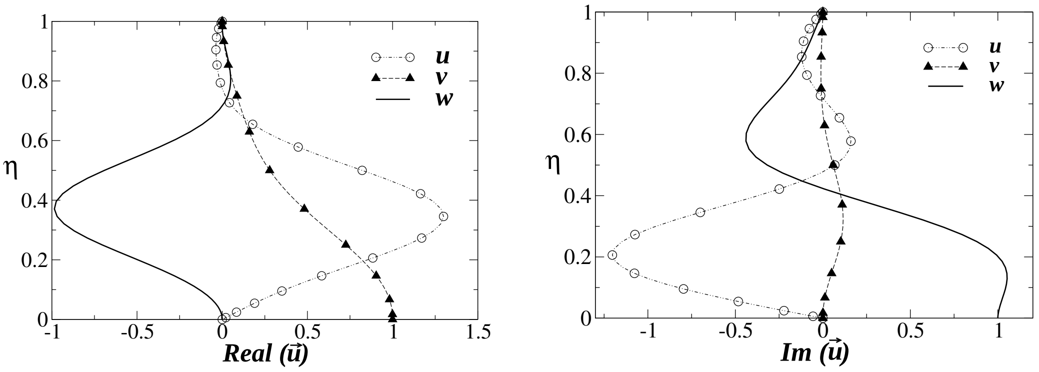

Figure 2.25: (a) Real (b) imaginary part of eigenfunction $\vec{u} = [u, v, w]$ for $Re_i = 150, \beta_d = 0.31$ and $n = 1$ at $x_d/R_i = 28.1$.

sideration. The amplitude of disturbance kinetic energy [equation (2.45)] of the swirl ($n = 1$) mode for different radial lacations are plotted in figures 2.27 to 2.30. Here ω_0 is the non-dimensional frequency at the neutral location. The corresponding growth of disturbance kinetic energy for axisymmetric mode ($n = 0$) are shown in figures 2.36 to 2.34. It can be seen that disturbance kinetic energy is growing everywhere in the pipe for both the swirl and axisymmetric modes, but the amplification is more for the swirl mode. The amplitude of the disturbance kinetic energy averaged across the pipe for non-axisymmetric and axisymmetric disturbances are shown in figures 2.35 and 2.36 respectively. The amplitude of the disturbance kinetic energy is decaying for smaller ω_0. The maximum growth of the disturbance kinetic energy for different n are plotted in figure 2.37. It can be seen that non-axisymmetric ($n = 1$) mode is the more unstable one.

The main results in this study are that (a) the critical Reynolds number for linear instability of flow in a diverging pipe is finite at any divergence and (b) the critical Reynolds number is surprisingly low even for small angles of divergence. For small divergence, instability is determined by the parameter $S(x)$ describing the mean profile, the mechanism is inviscid. As $a \to 0$, the flow is unstable to the swirl mode for $S > 10$, so the critical Reynolds number approaches infinity as $1/a$. The disturbance growth at low Reynolds numbers indicates that a different route to turbulence from that in a straight pipe is likely. The swirl mode is found to be most unstable one. At divergences as low as 1°, the effect of flow non-parallelism is already large, so a non-parallel analysis is essential.

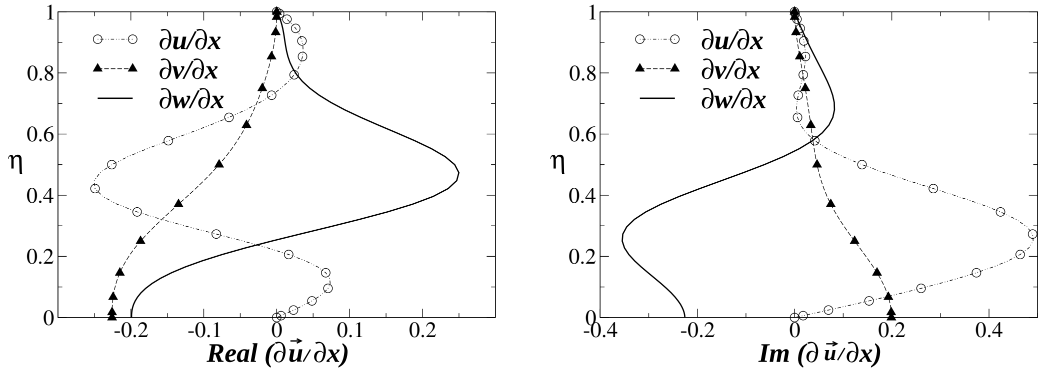

Figure 2.26: Gradient of (a) real (b) imaginary part of eigenfunction $\vec{u} = [u, v, w]$ in axial direction for $Re_i = 150, \beta_d = 0.31$ and $n = 1$ at $x_d/R_i = 28.1$.

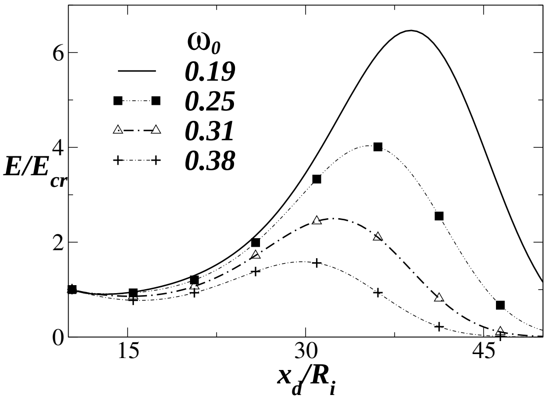

Figure 2.27: Amplification of disturbance kinetic energy for non-axisymmetric ($n = 1$) mode at $\eta = 0.08$ for typical disturbance frequencies, Re = 150.

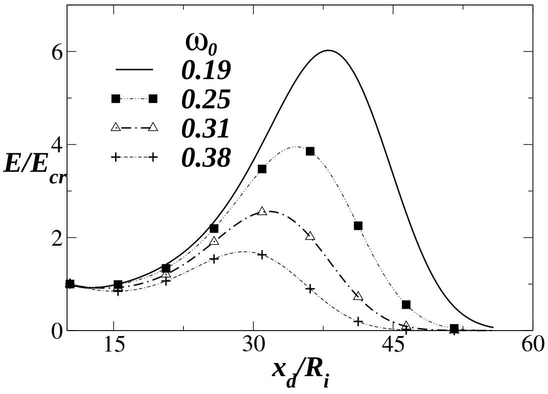

Figure 2.28: Same as figure 2.27 but for $\eta = 0.25$.

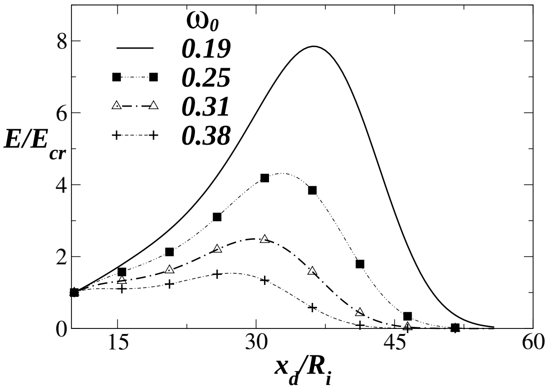

Figure 2.29: Same as figure 2.27 but for η = 0.75.

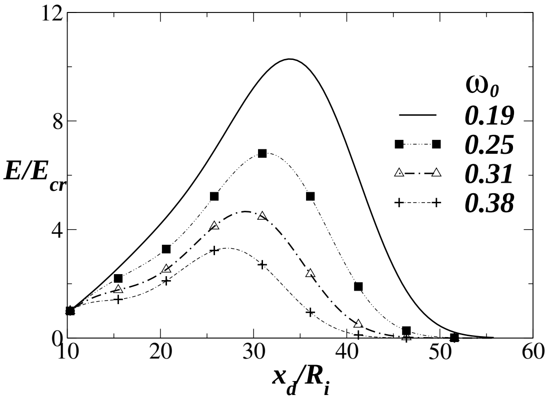

Figure 2.30: Same as figure 2.27 but for η = 0.9.

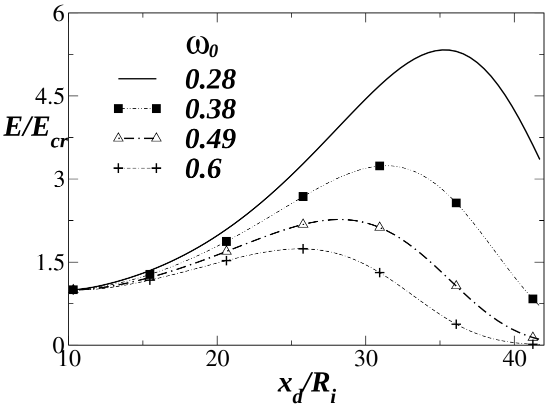

Figure 2.31: Amplification of disturbance kinetic energy for axisymmetric (n = 0) mode at η = 0.08 for typical disturbance frequencies, Re = 150.

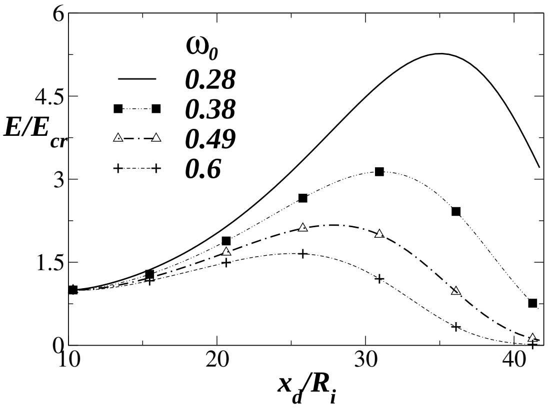

Figure 2.32: Same as figure 2.31 but for η = 0.25.

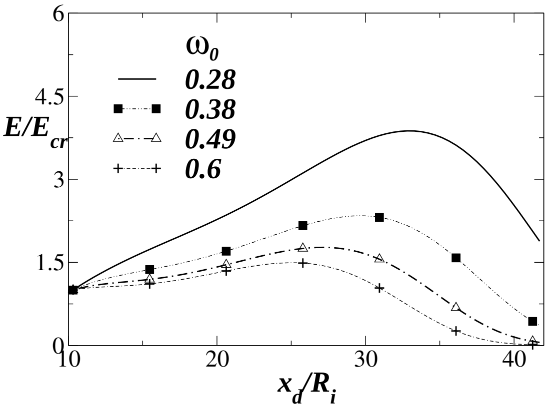

Figure 2.33: Same as figure 2.31 but for η = 0.75.

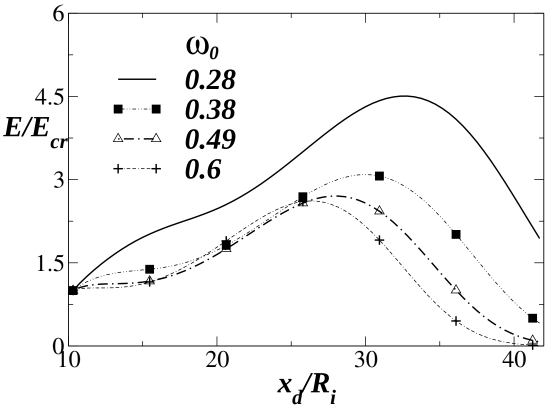

Figure 2.34: Same as figure 2.31 but for η = 0.9.

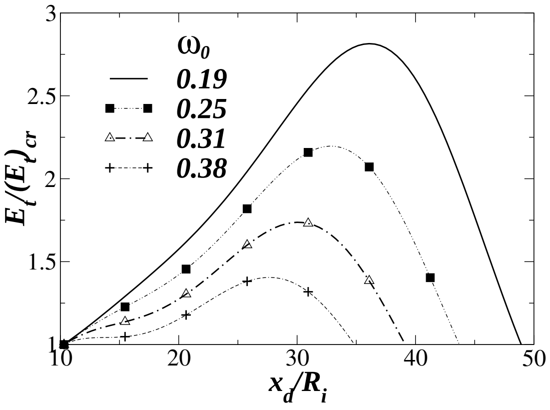

Figure 2.35: Amplification of disturbance kinetic energy averaged across the pipe for non-axisymmetric ($n = 1$) mode for typical disturbance frequencies, Re = 150.

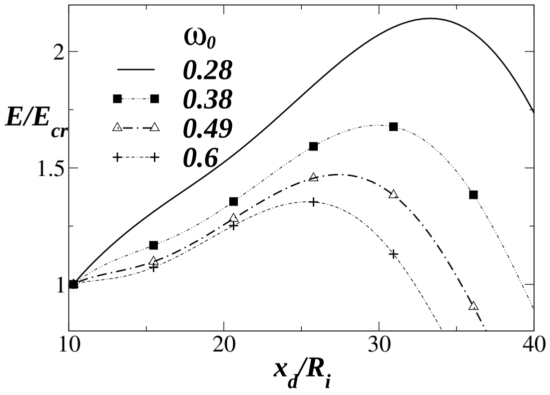

Figure 2.36: Same as figure 2.35 but for axisymmetric ($n = 0$) mode.

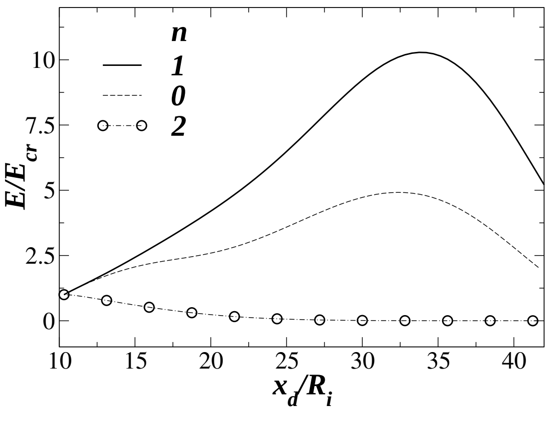

Figure 2.37: Maximum amplification of disturbance kinetic energy for different azimuthal wave number n.

CHAPTER 3

Flow through converging-diverging pipes

In this chapter, we discuss a derivative problem, that of flow through a pipe of constant average radius with symmetrically and asymmetrically serrated walls. A schematic of the pipe is shown in figure 3.1. Flow through these geometries could be closer to the real-life situations, especially in small-scale flow [of diameters of the order of millimeters] through rough pipes, than a divergence which continues for ever. Therefore the insight gained here is of potential practical interest. It is well known from earlier studies that local divergence and convergence can drastically effect instability behaviour [Eagles (1965, 1972); Eagles & Weissman (1975)]. The objective here is to study the effect of asymmetry in the boundary. We have studied three type of flows (i) flow through a pipe having symmetric convergence and divergence, (ii) flow from right to left, and (iii) left to right of an asymmetrically converging-diverging pipe. The computational domain for symmetric and asymmetric pipes are shown in figures 3.2(a) and (b) respectively.

3.1 Mean flow

The mean flow is computed by solving the axisymmetric Navier-Stokes equations as described in § 2.1.1. The centerline velocity U_E and the radius R_E of the pipe at the smallest cross-section are used as velocity and length scales respectively. The corresponding Reynolds number Re_E is defined as $U_E R_E/\nu$. The boundary conditions at the centerline are $\Psi = \Omega = V = \partial U/\partial \eta = 0$. No-slip and impermeable boundary conditions are imposed at the wall. A periodic boundary condition is implimented in the axial direction.

The axial and radial velocity profiles scaled with the local centerline velocity (U_c/U_E) for the symmetric and asymetric pipe, U_l and V_l, at different axial locations are shown in figures 3.3 to 3.8. The Reynolds number is 100. It is immediately evident that the profiles are different in each case. In particular, it can be seen in figures 3.9 to 3.11 that the flow from left to right appears more inflectional than flow through the same pipe from right to left and the symmetric pipe, so we expect the former to be more unstable. Secondly, in the inviscid limit, the quantity I [equation (2.60)] has to change sign for the flow to be unstable at $\mathrm{Re} \to \infty$. Because of the fact that both U' and U'' are negative, I is always negative near the centerline. This means that if I at the wall is negative as well, the flow is inviscidly stable. We have plotted I at the wall in figure 3.12 as a function of x. It can be seen that I changes sign somewhere in the domain when the flow is from left to right, whereas it is fully negative when the flow is from right to left in the geometry figure 3.2(b). I for flow through the symmetric converging-diverging pipe [figure 3.2(a)] lies in between. Therefore when the flow is from left to right in the geometry shown in figure 3.2(b), a necessary condition for inviscid instability is satisfied.

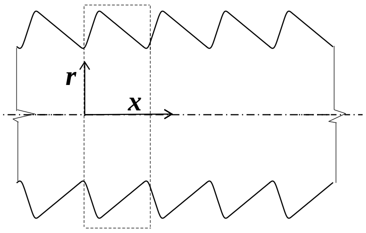

Figure 3.1: Schematic digaram of the pipe (computational domain is shown by dotted line).

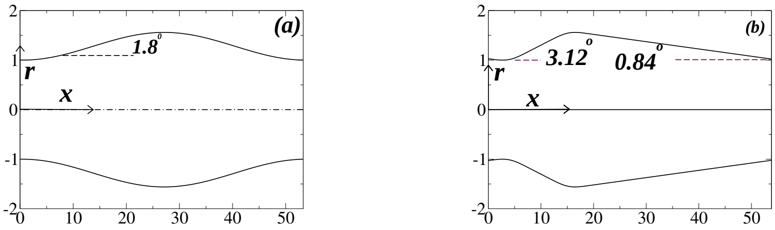

Figure 3.2: Computational domain (a) symmetric boundary (divergence angle and convergence angle are the same and equal to 1.8°), (b) asymmetric boundary (divergence angle = 3.12° and convergence angle = 0.84°.

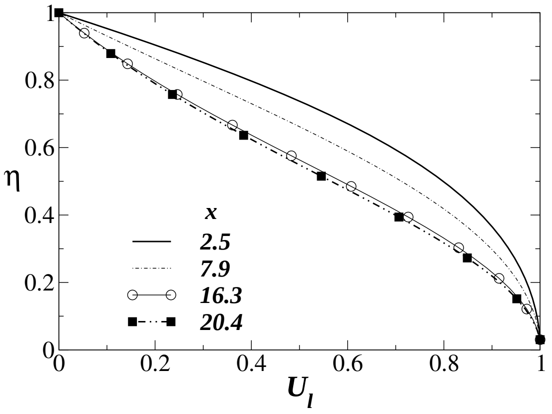

Figure 3.3: Axial velocity profiles at different axial locations in the symmetric pipe shown in figure 3.2(a), Re_E = 100.

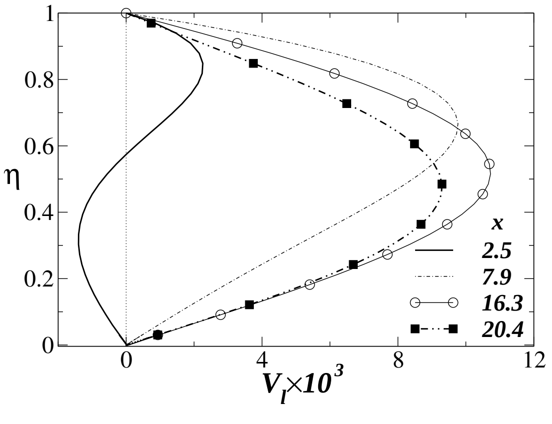

Figure 3.4: Radial velocity profiles at different axial locations in the symmetric pipe shown in figure 3.2(a), Re_E = 100.

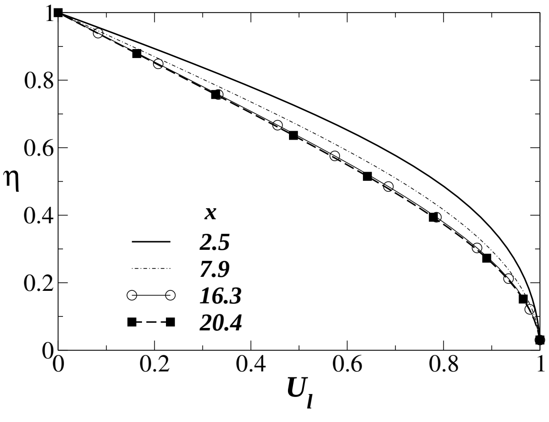

Figure 3.5: Axial velocity profiles at different axial locations for the flow from right to left in the asymmetric pipe shown in figure 3.2(b), $\mathrm{Re}_E = 100$.

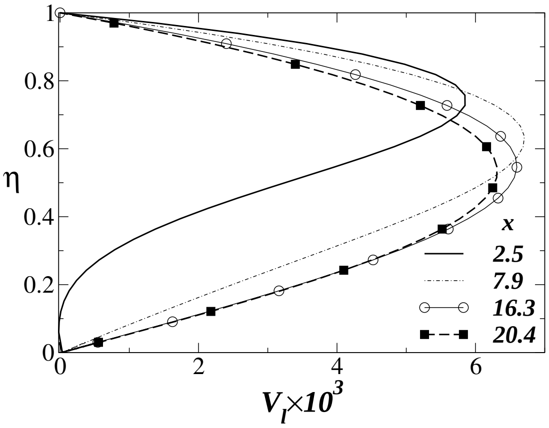

Figure 3.6: Radial velocity profiles at different axial locations for the flow from right to left in the asymmetric pipe shown in figure 3.2(b), $\mathrm{Re}_E = 100$.

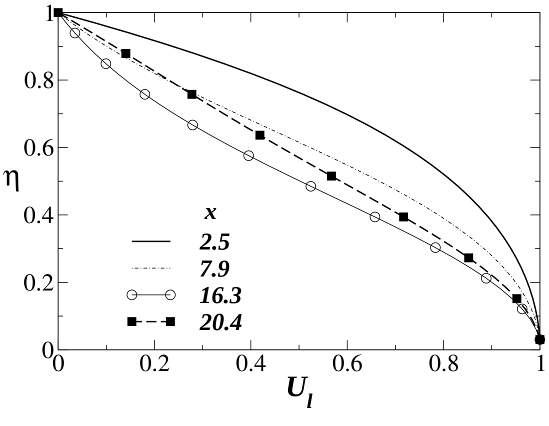

Figure 3.7: Axial velocity profiles at different axial locations for the flow from left to right in the asymmetric pipe shown in figure 3.2(b), $\mathrm{Re}_E = 100$.

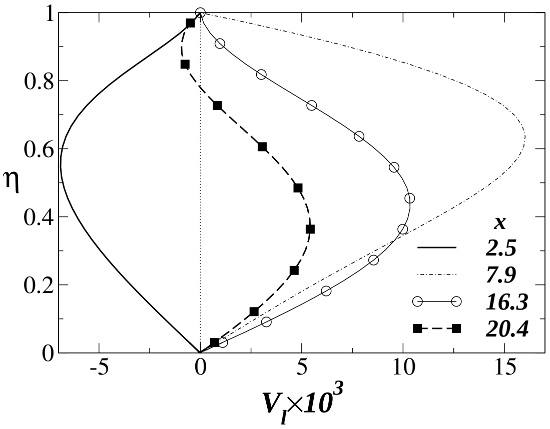

Figure 3.8: Radial velocity profiles at different axial locations for the flow from left to right in the asymmetric pipe shown in figure 3.2(b), $\mathrm{Re}_E = 100$.

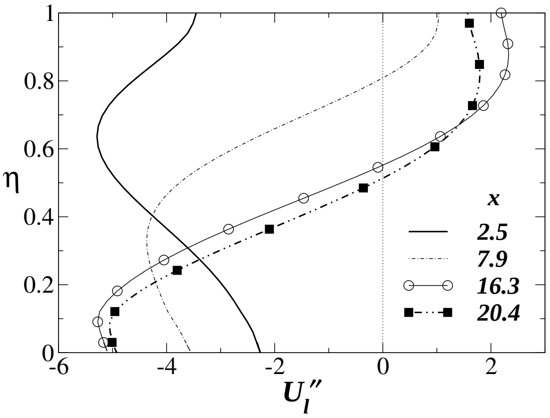

Figure 3.9: $\partial^2 U/\partial\eta^2$ at different axial locations in the symmetric pipe shown in figure 3.2(a), $\mathrm{Re}_E = 100$.

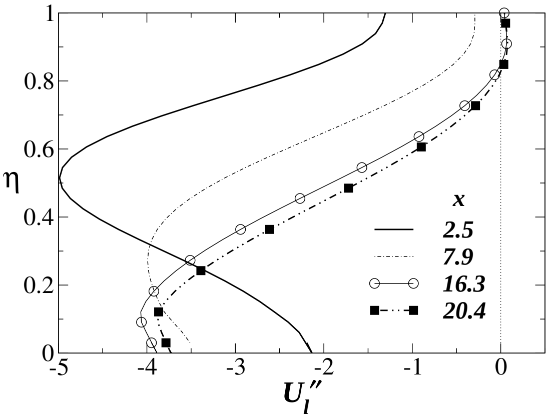

Figure 3.10: $\partial^2 U/\partial\eta^2$ at different axial locations for the flow from right to left in the asymmetric pipe shown in figure 3.2(b), $\mathrm{Re}_E = 100$.

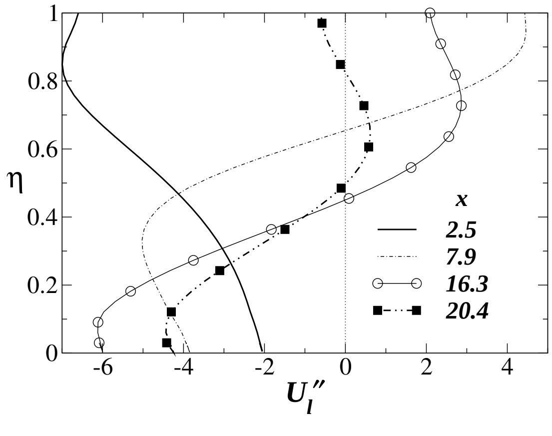

Figure 3.11: $\partial^2 U/\partial\eta^2$ at different axial locations for the flow from left to right in the asymmetric pipe shown in figure 3.2(b), $\mathrm{Re}_E = 100$.

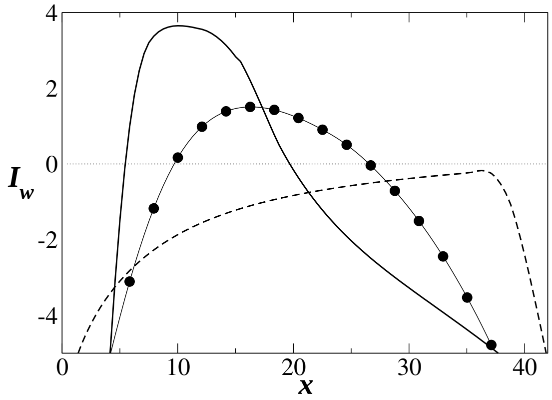

Figure 3.12: Variation of inviscid stability function I at the wall for the swirl mode ($n = 1$). Solidline: flow is from left to right ($\omega_d = 0.25$); dashed line: flow is from right to left in the figure (3.2b) ($\omega_d = 0.21$); circles: flow in the symmetric boundary figure (3.2a) ($\omega_d = 0.18$).

3.2 Results of the stability analysis

The stability analysis is same as that for flow through the diverging pipe as in discussed in chapter 2. The amplitude of the disturbance kinetic energy scaled by the mean kinetic energy, $E_m = 1/2(U^2 + V^2)$ at $r = 0.08$ for the flow from left to right and right to left in the asymmetric pipe [figure 3.2(b)] are shown in figures 3.13 and 3.14 respectively. The Reynolds number is 100. Figure 3.15 shows the same quantity for the flow through the symmetric pipe [shown in figure 3.2(a)]. It can be seen that amplitude of the disturbance kinetic energy amplifies when the flow is from left to right whereas it decays when the flow is from right to left in the asymmetric pipe [shown in figure 3.2(b)]. The result for flow through the symmetric pipe lies between the two. The growth of the disturbance kinetic energy is different at different radial locations (not shown). This becomes evident when one looks at the amplification of the disturbance kinetic energy averaged across the pipes, shown in figure 3.16. For flow from left to right in the asymmetric pipe, the disturbance kinetic energy grows everywhere, but maximum near the core region.

In summary, the instability behaviour can be changed dramatically by reversing the direction of flow. For a very small divergence the flow is already linearly unstable at 100. For a larger angle of

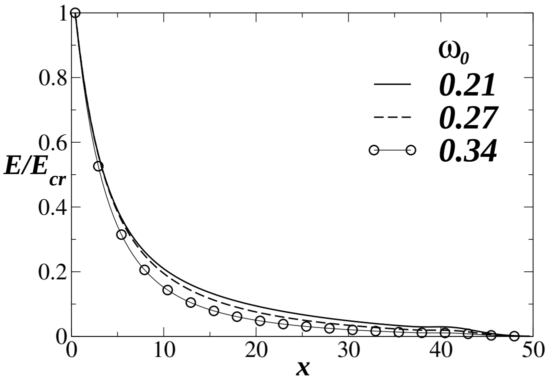

Figure 3.13: Amplification of disturbance kinetic energy at $r = 0.08$ for Re = 100 and $n = 1$ for typical disturbance frequencies when the flow is from left to right shown in figure (3.2b).

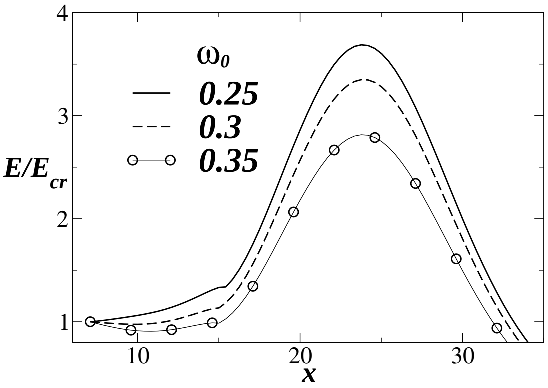

Figure 3.14: Amplification of disturbance kinetic energy $r = 0.08$ for Re = 100 and $n = 1$ for typical disturbance frequencies when the flow is from right to left shown in figure (3.2b).

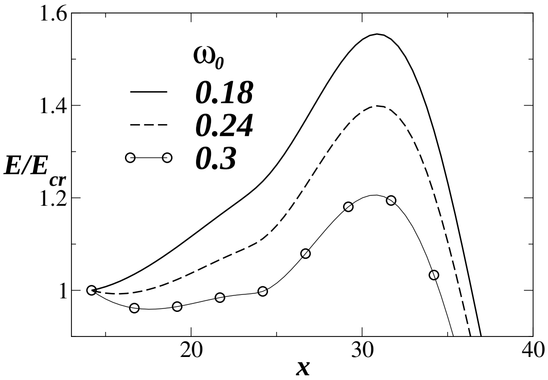

Figure 3.15: Amplification of disturbance kinetic energy $r = 0.08$ for Re = 100 and $n = 1$ for typical disturbance frequencies for the flow in the symmetric boundary shown in figure (3.2a).

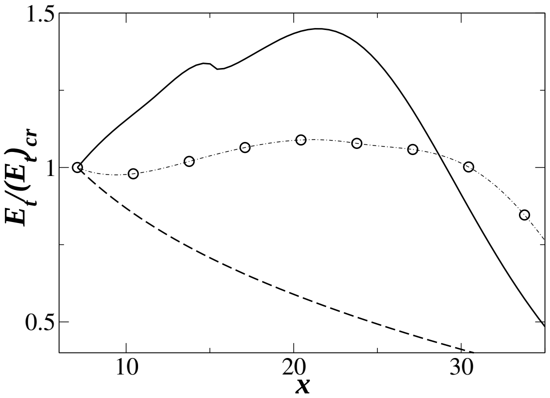

Figure 3.16: Amplification of disturbance kinetic energy average across the pipe for Re $= 100$ and $n = 1$ [solid line: flow is from left to right ($\omega_d = 0.25$), circles: flow is from right to left ($\omega_d = 0.21$) in geometry shown the figure (3.2b) and dashed line: flow in the geometry shown in figure (3.2a) ($\omega_d = 0.18$).]

divergence the instability Reynolds number could be much lower.

The linear mechanism may thus be important in small-scale flows. In a small-scale pipe [having a diameter of millimeters], the local irregularities on the boundary could be sufficient to make the flow unstable at low Reynolds number. Since wall irregularities are of the same order as the diameter of the pipe, they could act as local divergences and allow disturbances to grow.

CHAPTER 4

Small-scale flows: the influence of wall slip

At various points in the thesis, we talk about small-scale flows but we have not included any features of small-scale flows in the study. Here we make a minor foray into this regime, by considering the effect of wall slip. The dynamics of fluids and their interaction with surfaces in small-scale flows are very different from those of large scale. It is known that even in case of simple liquids, the no-slip boundary condition is not justified on a microscopic level. Therefore velocity slip at the wall can have an effect in microfluidics and small-scale flows. Slip is characterised by the Knudsen number, Kn. In gases, Knudsen number, Kn_{gas} is related to the Reynolds and Mach number [Karniadakis & Beskok (2002)] as follows.

$$Kn_{gas} = \frac{\lambda}{H} = \left(\frac{\gamma\pi}{2}\right)^{1/2} \frac{M}{\mathrm{Re}}, \tag{4.1}$$

where λ is mean free path between molecular collisons, γ is ratio of specific heat and M is the Mach number. We consider the flow of liquids here, and the Knudsen number is taken simply to be

$$Kn = l_s/H, \tag{4.2}$$

where l_s is the slip length. Note that the Knudsen number as used here is merely a non-dimensional number derived from the given quantity of slip existing in a flow. It does not represent the physics involving the cause of the slip. It has been demostrated recently that it is possible to have significant slip velocity at the wall even at large scale having strongly hydrophobic surfaces [Watanabe & Mizunuma (1998); Watanabe & Udagawa (1999)]. The present study is applicable for such cases. We consider flows for which the Knudsen number is small enough that second order effects may be neglected, and the Navier-Stokes equations with Maxwell's slip boundary condition (discussed in § 1.2) describe the flows.

It is known that the slip velocity on hydrophobic surfaces results in a significant drag reduction in micro-channel flows [Choi *et al.* (2003); Tretheway & Meinhart (2002)]. Secondly in small-scale flows local divergences/convergences of the wall are common. Motivated by the fact that a small divergence of the wall can cause the critical Reynolds number for linear instability to plumet [Eagles (1965, 1972); Eagles & Weissman (1975)], we examine velocity slip at a diverging wall. Our investigation could be carried further to become relevant in the study of arterial flows because of the hydrophobic nature of blood and the non-uniform boundary of the arteries. In this chapter we discuss the influence of slip on the flow through a diverging channel/pipe.

4.0.1 Mean flow

Flow through divergent/convergent geometries

The computational method is the same as described in chapter 3 except for the relaxation of the no-slip boundary condition, and the imposition of Maxwell's slip boundary condition (1.1) instead, at the wall.

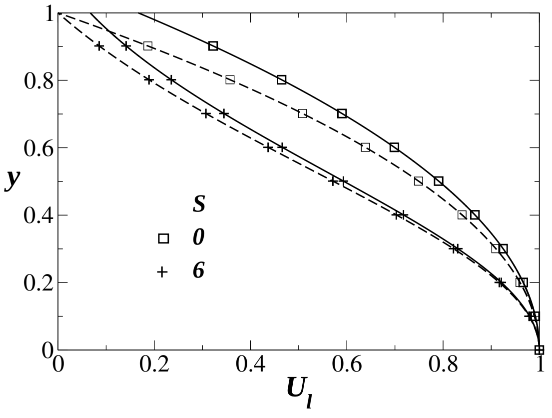

Figure 4.1: Axial velocity for the flow through a diverging channel at various values of the divergence parameter S. Solid line: $Kn = 0.1$, dashed line: no-slip.

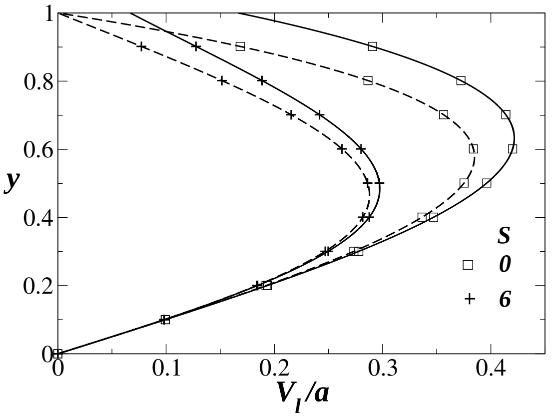

Figure 4.2: Normal velocity for the flow through a diverging channel at various values of the divergence parameter S. Solid line: $Kn = 0.1$, dashed line: no slip.

As before $U_l = 1$, $U_l' = 0$ at the centerline. For flow through a diverging pipe and a channel, equations (2.13) and (2.13) respectively are solved by a fourth order Runge-Kutta method. Note that V_l, being normal to the centreline, will not be zero at the wall when there is a finite amount of slip (U_s).

The effect of slip at different S on the axial and normal components of the velocity for diverging channel and pipe are shown in figures 4.1 to 4.4. It can be seen that slip decreases with S at a given Knudsen number. This is an artiface of the way we have defined the Kn. The gradient of the velocity ($\partial U_l/\partial\eta$) at the wall decreases with S and goes through zero at separation.

Although no stability results are presented for flow through a converging-diverging pipe, the comparison of axial and radial velocity profiles for slip ($Kn = 0.1$) and no-slip ($Kn = 0$) flows for the flow from left to right in the asymmetric pipe [shown in figure 3.2(b)] are shown in figures 4.5 and 4.6 respectively. The Reynolds number, based on the centerline velocity and the radius at the smallest cross-section is 100.

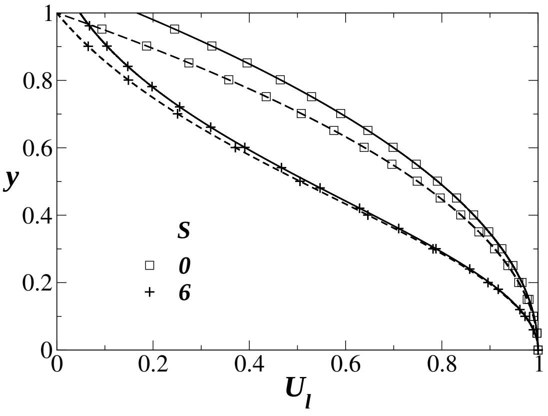

Figure 4.3: Comparison of axial velocity profiles for the flow through a axisymmetric diverging pipe, solid line: $Kn = 0.1$, dashed line: $Kn = 0$.

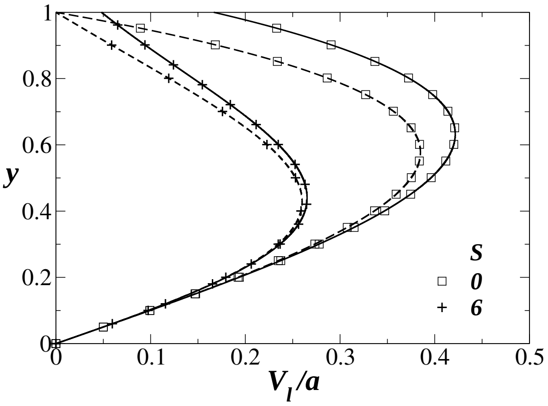

Figure 4.4: Comparison of normal velocity profiles for the flow through a axisymmetric diverging pipe, solid line: $Kn = 0.1$, dashed line: $Kn = 0$.

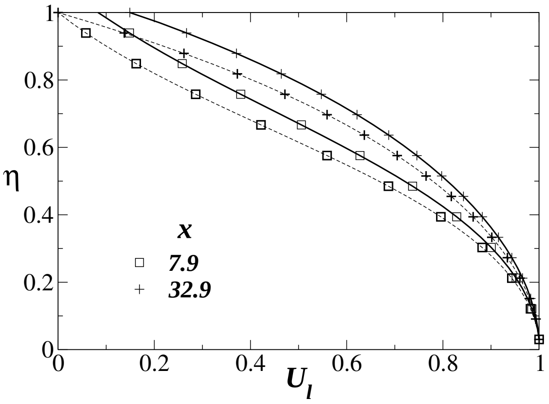

Figure 4.5: Axial velocity profiles at two different locations for the flow from left to right in the asymmetric pipe [shown in figure 3.2(b)], $\mathrm{Re}_E = 100$, solid line: $Kn = 0.1$, dashed line: no-slip ($Kn = 0$).

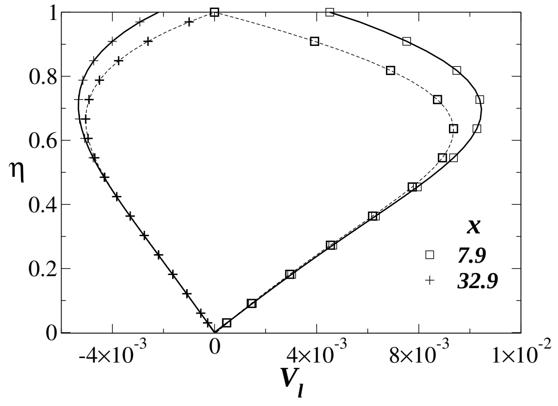

Figure 4.6: Radial velocity profiles at two different locations for the flow from left to right in the asymmetric pipe [shown in figure 3.2(b)], $\mathrm{Re}_E = 100$, solid line: $Kn = 0.1$, dashed line: no-slip ($Kn = 0$).

4.1 Three-dimensional stability equations for divergent channel flow

In § 2.2 we have formulated the non-parallel stability equations for an axisymmetric pipe. Here we derive non-parallel stability equations for two-dimensional flows (where the basic flow does not vary in the spanwise direction). The approach here is same as described in § 2.2.1. All quantities are non-dimensionalised using the half-channel width $H(x)$ and the centreline velocity $U_c(x)$. Again the relationship $\mathrm{d}x_d = H\mathrm{d}x$ is used. As before, we consider small divergence angles and Reynolds numbers much larger than 1, so streamwise variations in the basic flow are slow. A consistent non-parallel approximation as before is to retain all terms up to $O(a)$ and $O\left(\mathrm{Re}^{-1}\right)$ and to neglect terms of higher order in either of these. As usual, each flow quantity is expressed as the sum of a steady mean and a time-dependent perturbation, such as

$$u = U(y) + \hat{u}(x, y, z, t), \tag{4.3}$$

with

$$[\hat{u}] = \mathrm{Real}\left\{u(x, y)\exp\left[\mathrm{i}\left(\int \alpha(x)\mathrm{d}x + \beta z - \omega t\right)\right]\right\}, \tag{4.4}$$

such that $\partial u/\partial x \sim O\left(\mathrm{Re}^{-1}\right)$. The streamwise and spanwise wavenumbers are α and β respectively and ω is the disturbance frequency. The equations for linear stablity now are

$$-au + \frac{\partial u}{\partial x} + \mathrm{i}\alpha u - ay\frac{\partial u}{\partial y} + \frac{\partial v}{\partial y} + \mathrm{i}\beta w = 0, \tag{4.5}$$

$$-\mathrm{i}\omega u + U\left[\frac{\partial u}{\partial x} + (\mathrm{i}\alpha - 2a)\,u\right] + (v - ayu)\,U' = (2a - \mathrm{i}\alpha)\,p - \frac{\partial p}{\partial x} + ay\frac{\partial p}{\partial y} + \frac{1}{\mathrm{Re}}\left[\frac{\partial^2 u}{\partial y^2} - \left(\alpha^2 + \beta^2\right)u\right], \tag{4.6}$$

$$-\mathrm{i}\omega v + U\left[\frac{\partial v}{\partial x} + \mathrm{i}\alpha v\right] + ayU'v = -\frac{\partial p}{\partial y} + \frac{1}{\mathrm{Re}}\left[\frac{\partial^2 v}{\partial y^2} - \left(\alpha^2 + \beta^2\right)v\right], \tag{4.7}$$

$$-\mathrm{i}\omega w + U\left[\frac{\partial w}{\partial x} + \mathrm{i}\alpha w\right] = -\mathrm{i}\beta p + \frac{1}{\mathrm{Re}}\left[\frac{\partial^2 w}{\partial y^2} - \left(\alpha^2 + \beta^2\right)w\right]. \tag{4.8}$$

The no-slip boundary conditions are

$$u = v = w = 0 \quad \text{at} \quad y = \pm 1. \tag{4.9}$$

For slip flow the boundary conditions are

$$u \pm Kn\frac{\partial u}{\partial y} = v \mp au = w \pm Kn\frac{\partial w}{\partial y} = 0 \quad \text{at} \quad y = \pm 1, \tag{4.10}$$

with finite pressure at the walls for both no-slip and slip case. Setting $n/r = \beta$, neglecting terms containing $1/r$ and replacing r by y in the non-parallel stability equations (2.25) and (2.31)-(2.33) for axisymmetric pipe we arrive at the stability equations (4.5 - 4.8) for a diverging channel. In the latter, if we set a, and all the streamwise derivative terms to zero, we obtain the Orr-Sommerfeld and Squire equations for parallel flow [see e.g. Drazin & Reid (1981)].

The solution method is as before. We always find that the even mode in v is much more unstable than the odd mode. When appropriate, this fact is used to speed up the computations by considering only a half-channel. To validate our solution method further, we solve the channel flow problem from equations (4.5) - (4.8) without slip by the approach of Govindarajan & Narasimha (2005). The results agree very well. In that approach, the lowest-order stability problem correct to $O(\mathrm{Re}^{-1/2})$, comprising ordinary differential equations in y is derived. This is solved first as an eigenvalue problem, exactly as one would solve the Orr-Sommerfeld equation. Higher order effects are obtained up to the desired order of accuracy by exploiting the properties of adjoint differential operators. The disturbance amplitude is expressible in terms of an ordinary differential equation in x, whose coefficients contain the lowest-order eigenfunctions. The method of Govindarajan & Narasimha (2005) is not applicable for slip flows.

4.2 Results of the stability analysis

4.2.1 Flows through diverging channel

We first examine whether wall slip has an effect on the Rayleigh (1880*a*) inviscid stability measure U'' (discussed in § 2.3). In a divergent channel, U'' at the centreline remains negative, and for small divergences, is close to the value in a plane channel of -2. The dependence of U'' at the wall on S is shown in figure 4.7. If this quantity is positive, it follows that Rayleigh's criterion is satisfied. In the absence of slip, the profile is inflexional beyond $S = 2.95$, whereas with slip for $Kn = 0.1$, the profile is inflexional for $S \geq 2.5$. The difference is too small to predict the direction of the effect of slip. This indicates that when the profile is near-inflexional, the divergence could be more important for stability than changes in the wall boundary conditions. If this expectation is realised, there will be no large stabilization due to wall-slip, unlike in a plane channel.

Only two-dimensional perturbations, being the least stable, are presented in this section on linear instability. For a plane channel ($\theta = 0$), the present solutions match well with Lauga & Cossu (2005) as seen in figure 4.8. It is seen that the critical Reynolds number increases sharply with increase in the Knudsen number. The boundaries of neutral stability at various Knudsen number for angles of divergence $\theta = 0.1°$ and $1°$ are shown in figures 4.9 and 4.10 respectively. Here the neutral Reynolds number is defined as that for the disturbance kinetic energy integrated across the channel. At the lower level of divergence, slip is seen to stabilise the flow, but much less than it would in a plane channel. At the

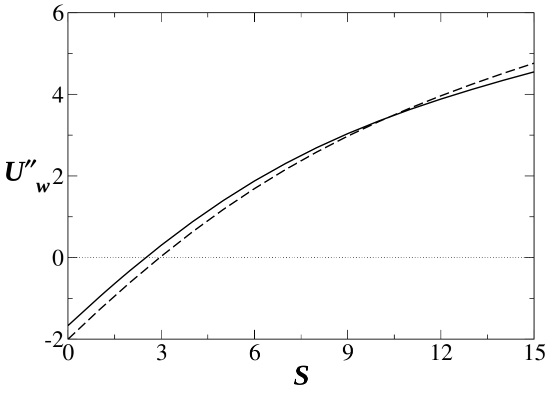

Figure 4.7: Variation of U'' at the wall for different S (solid line: $Kn = 0.1$ and dashed line: $Kn = 0$).

larger divergence, increasing the Knudsen number has a small destablising effect. The effect of slip and divergence is summarised in the plot of the critical Reynolds number Re_{cr} versus Kn in figure 4.11. To highlight the result, we plot the ratio $\mathrm{Re}_{cr}/\mathrm{Re}_0$ Vs Kn, where Re_0 is the critical Reynolds number for the no-slip ($Kn = 0$) case. As the angle of divergence increases, the effect of slip is progressively reversed, from being hugely stabilising to mildly destabilising. It is to be noted that due to our definition of Kn, the wall slip for a profile close to separation is negligible. In other words, we prescribe smaller and smaller wall slip velocity for increasing divergence. If we maintain the slip velocity constant as the divergence increases, the destabilisation would be much higher.

Figure 4.12 shows the cross-over in terms of the critical Reynolds number. At a Knudsen number of 0.1, Re_{cr} varies with wall slope approximately as a power law, with an exponent of -0.8. This means that the parameter S at which the flow is neutrally stable increases slowly with the wall slope, roughly as $S \sim a^{0.2}$. It is worth noting that as S increases, the slope of the velocity profile at the wall decreases, so a given Knudsen number corresponds to smaller slip velocities at higher divergences. The results from the Orr-Sommerfeld equation applied to the Jeffery-Hamel profiles are shown in figure 4.13. It may be concluded that for wall divergences below a degree, flow non-parallelism acts only through the basic profile and the explicit non-parallel terms are negligible. This has been checked to be true for the entire spectrum of eigenvalues for a variety of conditions. Beyond this angle, explicit non-parallel effects are noticeable but not large. This finding is in contrast to what is seen in pipe flows, where the non-parallel terms have a large destabilising effect [see § 2.4]. At the largest divergences shown, i.e., for $a \sim 0.2$, the flow is mildly separated at the critical Reynolds number. Any firm statements at these angles of divergence would require a non-parallel stability analysis correct to a higher order of accuracy in a and $O\left(\mathrm{Re}^{-1}\right)$ than considered here. We only show Orr-Sommerfeld results as a qualitative indicator that nothing special happens when one encounters a mildly separated profile.

Transient growth of linearly stable eigenmodes

The study of transient growth presented in this subsubsection is done in collaboration with my colleague Dr. A. Sameen. In contrast to the least stable linear eigenmode, the maximum transient growth of disturbance kinetic energy is shown here to depend primarily on the Reynolds number of the flow and not on the slope of the walls. The introduction of velocity slip at the walls has a very small effect in the presence of divergence as well, similar to the findings for a plane channel of Lauga & Cossu (2005) and Min & Kim (2005). We restrict ourselves to extremely small wall solpes where there is a negligible effect

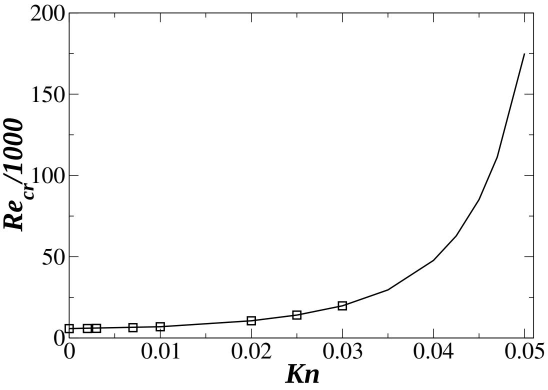

Figure 4.8: Variation with velocity slip at the wall of the critical Reynolds number Re_{cr} for linear instability in a plane channel. Line: present study, symbols: Lauga & Cossu (2005).

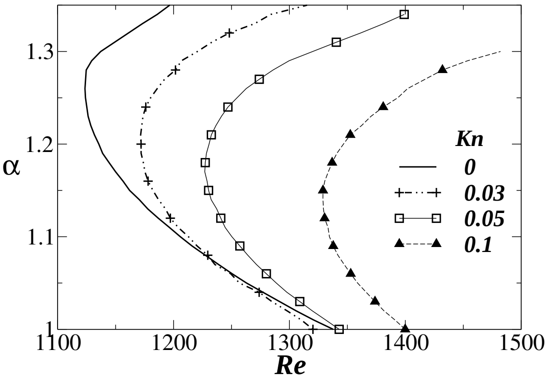

Figure 4.9: Neutral stability curve for different values of Kn, angle of divergence = 0.1°.

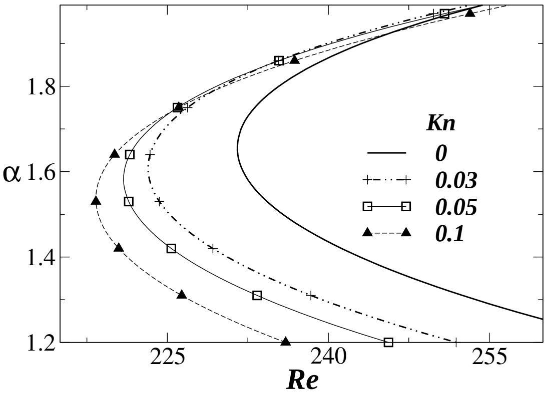

Figure 4.10: Neutral stability curve for different values of Kn, angle of divergence = 1.0°.

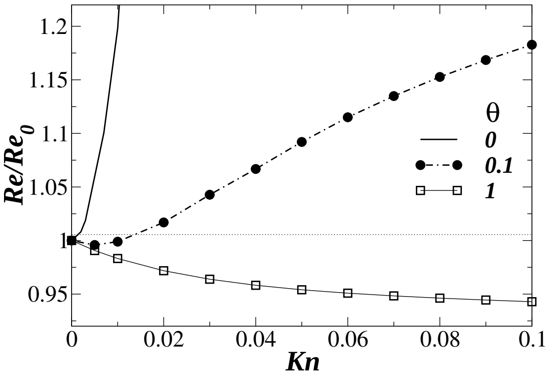

Figure 4.11: Re/Re$_0$ Vs Kn for different angle of divergence (θ).

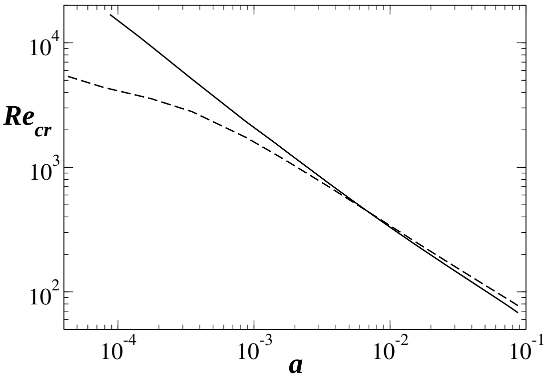

Figure 4.12: Variation of the critical Reynolds number, Re$_{cr}$ with wall divergence, solid line: $Kn = 0.1$, dashed line: $Kn = 0$.

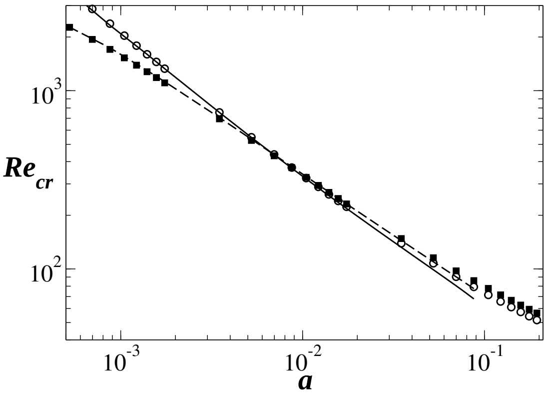

Figure 4.13: A portion of figure 4.12 is magnified, with the corresponding results from the Orr-Sommerfeld equation shown in symbols.

of the non-parallel terms on the stability. We therefore use eigenvalues and eigenfunctions from the Orr-Sommerfeld and Squire equations with slip boundary conditions. In other words, non-parallel effects are neglected in transient growth computations. If $\Lambda = diag\{\omega_1, \omega_2, ...\omega_N\}$ is constructed out of the N least stable eigenvalues of this system, and κ is similarly constructed from the expansion coefficients of the corresponding eigenfunctions, the resulting disturbance kinetic energy, $g(t)$, may be written as [Schmid & Henningson (2001)]

$$g(t) = \frac{||\kappa(t)||_E^2}{||\kappa(0)||_E^2} = \frac{||e^{-\mathrm{i}\Lambda t}\kappa(0)||_E^2}{||\kappa(0)||_E^2}. \tag{4.11}$$

Maximising $g(t)$ for all possible initial conditions $\kappa(0)$, we define

$$G(t) \equiv \max_{\kappa\neq 0} g(t). \tag{4.12}$$

In a linearly stable situation, the quantity $G(t)$ increases initially, and after attaining a maximum G_{max}, decays to zero as $t \to \infty$. For given values of Re, α, β and θ, G_{max} is thus the maximum possible factor over which the initial disturbance kinetic energy can grow algebraically. Our computations of $G(t)$ for a plane channel at Reynolds numbers of 1000 and 1500 (appropriately scaled) at different Knudsen numbers are, as mentioned above, in excellent agreement with Min & Kim (2005) and Lauga & Cossu (2005) respectively.

The contours of constant G_{max} for a range of α and β are plotted in figures 4.16 (a) and (b) for a Reynolds number of 200 and wall slopes of 0.005 and 0.02. It is seen that velocity slip has only a marginal effect, as does the slope. We now define a Reynolds number $\mathrm{Re}_{0.95}$ equal to 95% of the linear instability-critical Reynolds number Re_{cr}. The algebraic amplification of disturbances obtained at this Reynolds number is a fair measure of the maximum possible, since exponential growth may take over at higher Reynolds numbers. The Reynolds number of 200 at which the contours are shown is about two-fifths of Re_{cr} at $a = 0.005$, while at $a = 0.02$, $\mathrm{Re}_{0.95} = 200$. The maximum algebraic growth obtained just before linear instability serves only to amplify the initial perturbation by an order of magnitude. This is in contrast to a plane channel, where the factor is about 200 even at one-sixth of Re_{cr} [Schmid & Henningson (2001)]. The results are qualitatively the same over a range of Re and θ.

In all cases in this Knudsen number range, the largest transient growth is obtained for streamwise independent disturbances ($\alpha = 0$) of spanwise wavenumber β close to 2, so the remaining results are presented at these wavenumbers. Figure 4.17 shows the G_{max} at Reynolds numbers of 150 and 300. The slope at which the flow becomes linearly unstable (to two-dimensional perturbations) is shown by the vertical line in each case. Beyond this point the dominance of exponential Vs. transient growth depends on their relative magnitude. To see when the former is seen to swamp the latter, we choose a sample divergence angle of 1° for which the linear instability critical Reynolds is about 230. In figures 4.14 and 4.15 we have plotted $G(t)$ Vs. time at Reynolds number just above the critical Reynolds number and double of the Re_{cr} respectively. It can be seen that as expected, at a Reynolds number close to critical, the linear mode is very slowly growing, so transient growth could be called the winner. However, at Reynolds number of 460, the exponential growth clearly dominates. The switch-over therefore occurs at some intermediate Reynolds number, but we have chosen $0.95R_{cr}$ as representative.

In the relevant range, transient growth is (i) small, and (ii) relatively insensitive to wall divergence, unlike the dominant linear mode, which is hugely destabilised. The small destabilising effect of slip on transient growth is summarised in figure 4.18. We may conclude that algebraic growth mechanism may not be such a major player in diverging channels, whether with or without slip. In figure 4.19, it is seen that the transient growth obtainable just below Re_{cr} drops sharply with wall divergence, and is very small

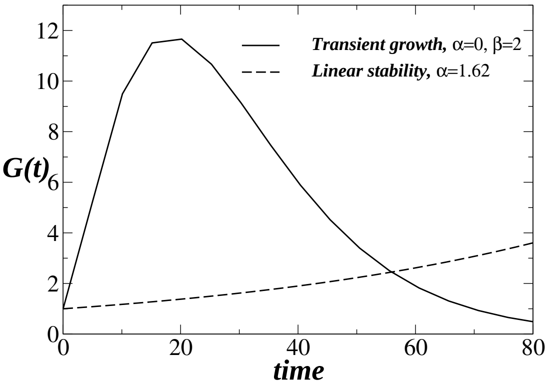

Figure 4.14: G_{max} vs time at Reynolds number just above critical Reynolds number. Angle of divergence = 1°.

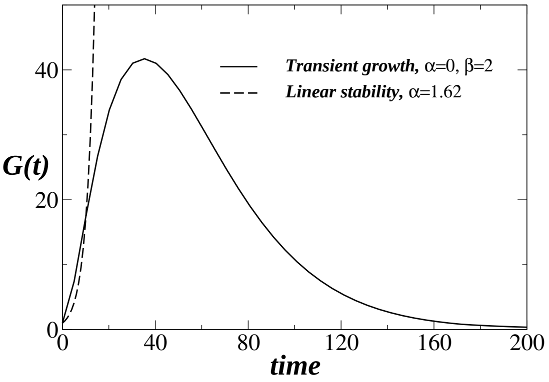

Figure 4.15: G_{max} vs time at Reynolds number double of the critical Reynolds number. Angle of divergence = 1°.

even for modest divergence. This result is compared to the maximum transient growth in a plane channel in figure 4.20. Note that the dashed lines in this figure consist of points from figure 4.19 obtained at various levels of wall divergence, each at its $\mathrm{Re}_{0.95}$. At values of wall divergence below 2 degrees or so, the two lines without slip are almost indistinguishable, showing that G_{max} is primarily dependent on the Reynolds number and not on the slope. Scaling arguments at small α show [see e.g. Schmid & Henningson (2001)] that G_{max} should vary as Re^2. This has been shown to hold true for a variety of flows such as for plane Poiseuille, plane Couette, flow in circular pipes and Blasius boundary layers, with different constants of proportionality. The relationship is seen here to hold in the case of divergent flows as well, with $G_{max} \sim f(Kn)\mathrm{Re}^2$ where $f(Kn)$ is a weak function of Kn. At higher divergences, where the velocity profile is close to separation at the wall, there is a clear deviation from the power law. This could be of theoretical interest, and merits further investigation.

The result that transient growth is dependent only on the Reynolds number and not on the wall divergence may be explained partially as follows. For the streamwise-independent modes ($\alpha = 0$) the Orr-Sommerfeld and Squire equations reduce to

$$\frac{1}{\mathrm{Re}}\left(\frac{d^4v}{dy^4} - 2\beta^2\frac{d^2v}{dy^2} + \beta^4 v\right) = \omega_i\left(\frac{d^2v}{dy^2} - \beta^2 v\right), \tag{4.13}$$

$$\eta\omega_i + \frac{1}{\mathrm{Re}}\left(\beta^2\eta - \frac{d^2\eta}{dy^2}\right) = -\mathrm{i}\beta U' v. \tag{4.14}$$

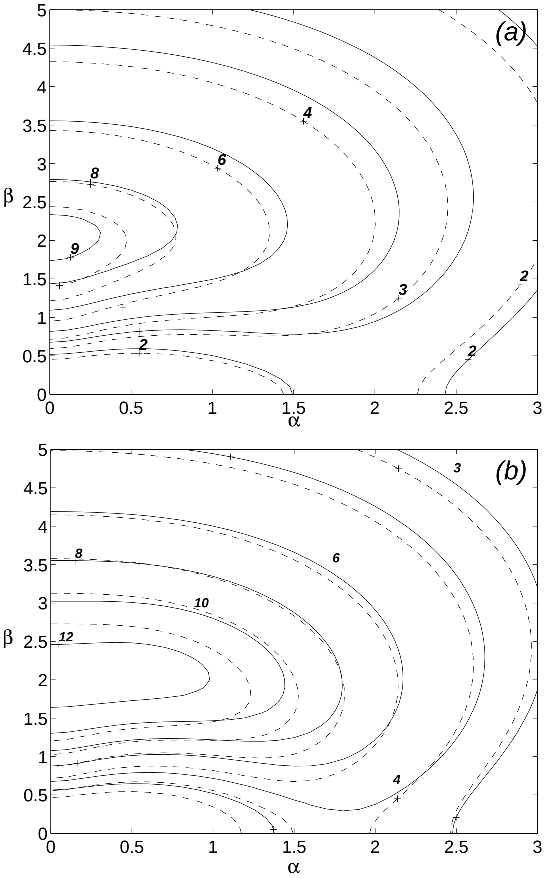

Figure 4.16: The contour of G_{max} for Re = 200 without slip (solid lines) and at $Kn = 0.1$ (dashed lines) for (a) $a = 0.005$, and (b) $a = 0.02$. At the latter wall divergence, a Reynolds number of 200 is 95% of the critical Reynolds number for linear instability.

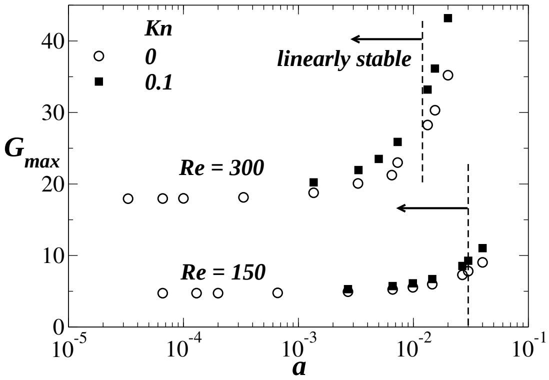

Figure 4.17: The maximum transient growth of disturbance kinetic energy at $\alpha = 0, \beta = 2.0$ as a function of slope. The vertical lines show the divergence beyond which the flow is linearly unstable at each Reynolds number.

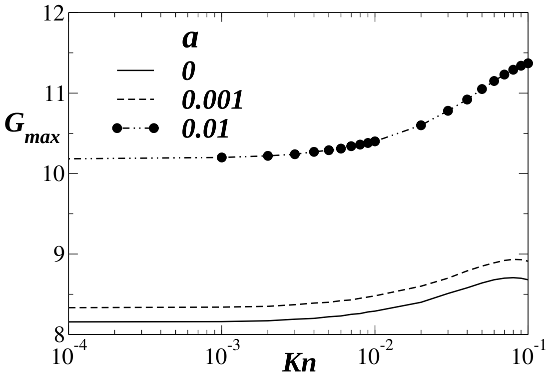

Figure 4.18: The maximum transient growth of disturbance kinetic energy at $\alpha = 0$, $\beta = 2.0$ as a function of Knudsen number. The Reynolds number is 200.

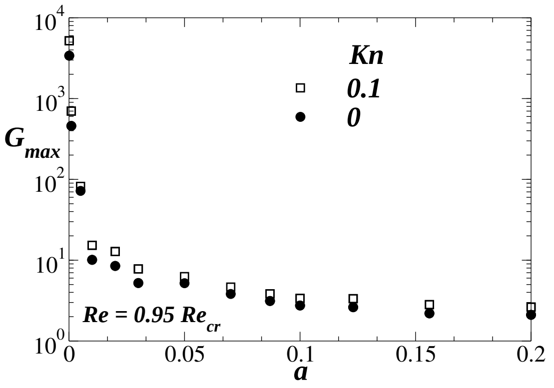

Figure 4.19: G_{max} at $\alpha = 0$ and $\beta = 2$, as a function of wall divergence at $\mathrm{Re}_{0.95}$. The point at the lowest slope ($a = 10^{-4}$) is obtained at a Reynolds number of $\mathrm{Re}_{0.95} = 4282$, while at $a = 0.2$, $\mathrm{Re}_{0.95} = 56.6$. The solid line is for a plane channel without slip. The long dashes are the quantity plotted against $\mathrm{Re}_{0.95}$. The coincidence of the two lines over most of the range shows that unlike linear instability, the transient growth is not affected by wall slope. The power law behaviour is seen to hold for slip flow as well.

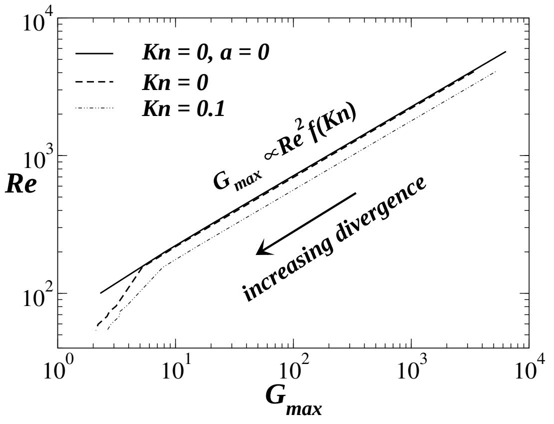

Figure 4.20: G_{max} at $\alpha = 0$ and $\beta = 2$, as a function of Reynolds number. The solid line is for a plane channel without slip. The coincidence of the two lines over most of the range shows that unlike linear instability, the transient growth is not affected by wall slope. The power law behaviour is seen to hold for slip flow as well.

$\hat{\eta}$ is the y component of disturbance vorticity whose amplitude η is defined as in equation (4.4), and $\omega = i\omega_i$, since $\omega_r = 0$ now. Note that Henningson & Schmid (1994) v is independent of the velocity profile, and its growth rate exponent scales inversely as Re. The vorticity η is "slave" to v, (incidentally is out of phase with it) for $\alpha = 0$. Thus, although η does depend on the velocity profile, the transient growth is unaffected. The presence of slip gives rise to a small destabilisation. For $Kn > 0.1$ we find that the nature of stabilisation is different, but since the slip model is no longer appropriate here, this range is being approached in a different study.

4.2.2 Flows through diverging pipe

The boundaries of neutral stability at various Knudsen number for angles of divergence $\theta = 0.1°$ and 1° are shown in figures 4.21 and 4.22 respectively. As non-axisymmetric swirl ($n = 1$) mode is most unstable for pipe flow, we consider the swirl ($n = 1$) mode in this section.

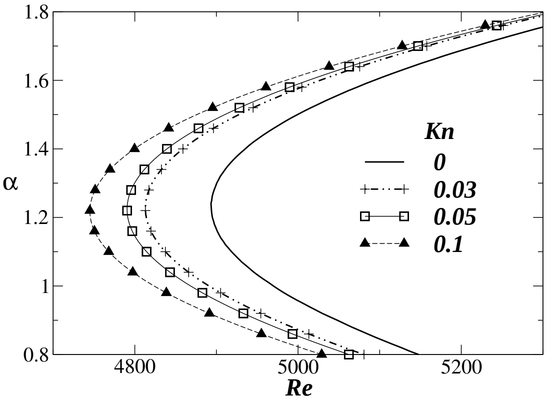

Figure 4.21: Neutral stability curves for the flow through a diverging pipe for different values of *Kn*, angle of divergence = 0.1°.

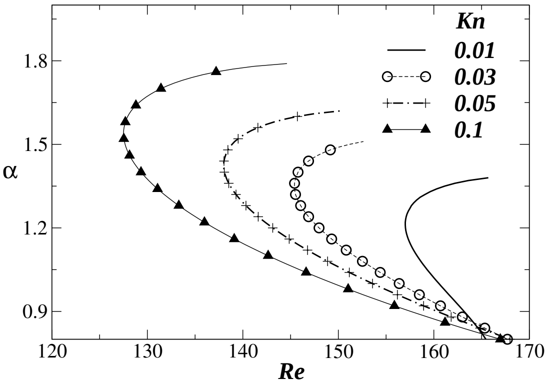

Figure 4.22: Neutral stability curves for the flow through a diverging pipe different values of *Kn*, angle of divergence = 1°.

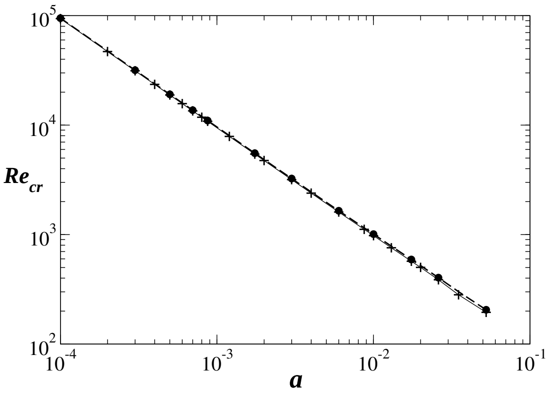

Figure 4.23: Variation of the critical Reynolds number for the flow through a diverging pipe, Re_{cr} with slope (a) of the wall (plus: $Kn = 0.1$, circles: $Kn = 0$).

CHAPTER 5

Developing flow in the entry region of a pipe

The laminar velocity profile through a circular pipe is parabolic once the flow is fully developed. However, as discussed in chapter 1, the distance l_e required to reach this fully-developed state can be very long [Ekman (1910); Reshotko (1958); Wygnanski & Champagne (1973)], and scales linearly with the Reynolds number Re, roughly as $l_e/R \sim \mathrm{Re}/20$, where R is the pipe radius. Therefore high Reynolds number laminar flow through a pipe of limited length may never reach a parabolic state. Thus, the entry region could play an important role in the transition to turbulence in a circular pipe. Although many researchers have worked on this problem, there is significant discrepancy among the results, as discussed in chapter 1. In all these studies, the basic flow is taken in an approximate form, usually of boundary-layer type. In the present study, the axisymmetric Navier-Stokes equations are solved in an accurate manner using a parallel machine (as described in § 2.1.1). In the next section we discuss the mean flow in the entry region of a pipe.

5.1 Mean flow

The flow studied here is through a straight pipe (shown in figure 1.2) with a uniform axial velocity U_i at the inlet. A large enough length of pipe is considered for the Neumann condition to be applicable at the outlet, where the profile is checked to be parabolic. The boundary conditions are $\Psi = \Omega = V = \partial U/\partial r = 0$ at the centreline ($r = 0$), and $U = V = 0$ at the wall ($r = 1$).

Sample axial and radial velocity profiles at different axial locations for $\mathrm{Re}_i = 5000$ are shown in figures 5.1 and 5.2 respectively. The centreline velocity at the exit is exactly twice that at the inlet, which indicates that the flow is fully developed. The shape factor H (defined by displacement thickness over momentum thickness) is shown in the figure 5.3 for $\mathrm{Re}_i = 5000$ and $\mathrm{Re}_i = 3000$. The displacement and momentum thickness are defined as follows

$$\int_0^R \left(1 - \frac{U}{U_c}\right) r dr, \quad \text{and} \quad \int_0^R \frac{U}{U_c}\left(1 - \frac{U}{U_c}\right) r dr,$$

respectively. It can be seen that in the upstream region the shape factor is similar to that of a decelerating boundary layer on a two-dimensional surface. Downstream $H > 2.59$, which resembles an accelerating two-dimensional boundary layer. By analogy, this would lead us to expect instability in the upstream region, rather than downstream. Although this is the case in the present study, the instability arises outside the boundary layer region. It can be seen in figure 5.2 that unlike in boundary-layer flow, the radial velocity V does not attain a constant value outside the wall region, this feature of entry flow is important in its instability.

We compare the present mean flow results of the developing flow in the entry region in a pipe with that of the earlier studies (discussed in § 1.1.4). The comparison of present velocity profiles with Blasius flow for Re = 5000 at $x = 73.2$ is shown in figure 5.4. Then the present velocity profiles are compared

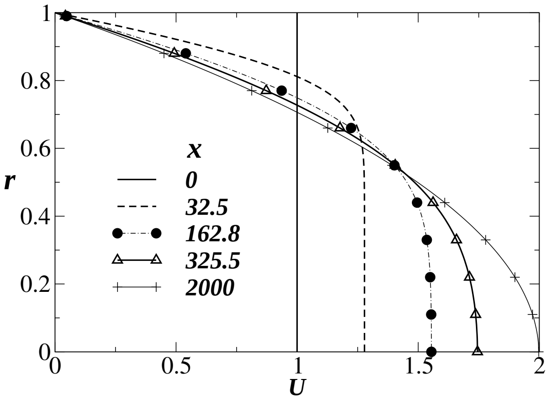

Figure 5.1: Axial velocity profiles at different axial locations for $\text{Re}_i = 5000$.

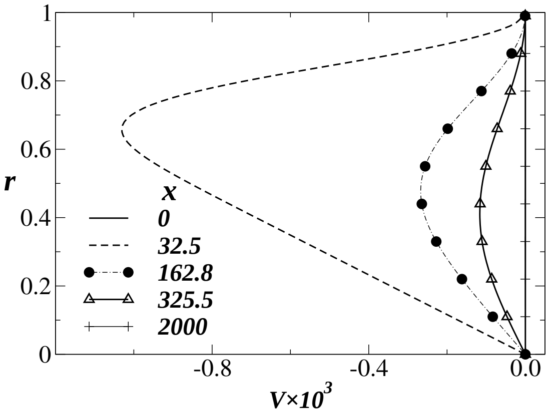

Figure 5.2: Radial velocity profiles at different axial locations for $\text{Re}_i = 5000$.

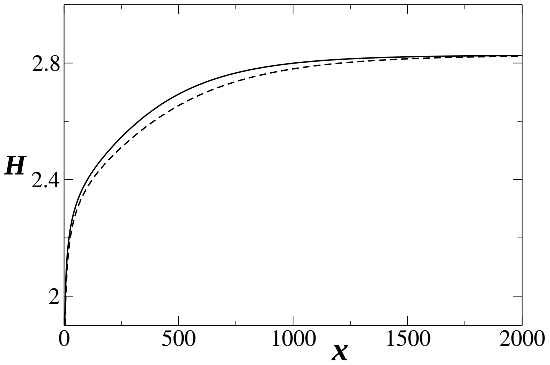

Figure 5.3: Shape factor in the developing region, solid line: $\text{Re}_i = 5000$, dashed line: $\text{Re}_i = 3000$.

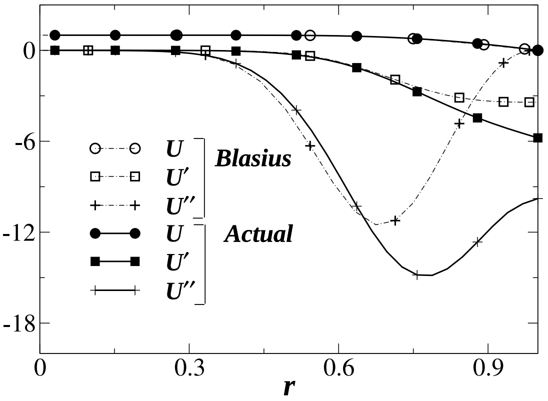

Figure 5.4: Comparison of axial velocity profile and its derivatives (from Navier-Stokes solutions) with Blasius flow for Re = 5000 at x = 73.2.

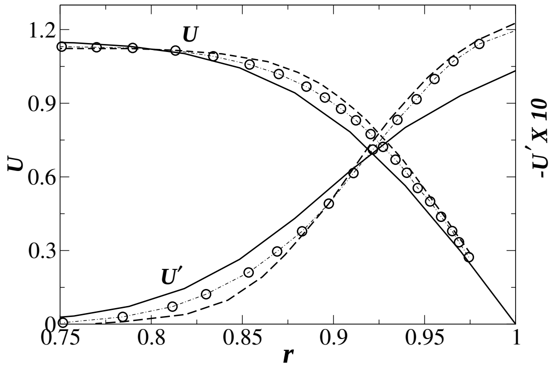

Figure 5.5: Developing flow velocity profile and its gradient in a pipe for Re = 5000 at x = 7.32. Circles: Sparrow profile, dashed line: Hornbeck profile, solid line: present method.

with the Sparrow and Hornbeck profiles in figures 5.5 and 5.6 at two different axial locations x = 7.32 and x = 30.8 respectively. It can be seen that exact solution is considerably different from all the approximate profiles used in earlier studies. Duck (2005); Williams (2001) used mean flow of Mohanty & Asthana (1979). This profile is somewhat better than the others, but its second derivative is still very different from the exact solution. The comparison of the centerline velocity of Mohanty & Asthana (1979) with that of present study is shown in figure 5.7. These differences too will be seen to be important in the present instability.

5.2 Results of the stability analysis

As discussed in § 2.2, the equations for stability of the developing flow in the entry region of a straight pipe are obtained by setting the angle of divergence to zero in equations (2.31) to (2.34). These are solved as described in chapter 2. While the least stable mode for fully-developed flow is the helical (n = 1) mode, the axisymmetric (n = 0) mode is found to be the most unstable in the case of developing flow, consistent with earlier work [Garg (1981); Sarpkaya (1975)]. In order to first estimate how much effect a more accurate basic flow has on the result, we conduct a parallel flow stability analysis (to compare with the earlier results, by neglecting non-parallel terms in the stability equations). The growth of the axisymmetric mode is shown in figure 5.8. Unlike in the earlier studies, the flow is found to be

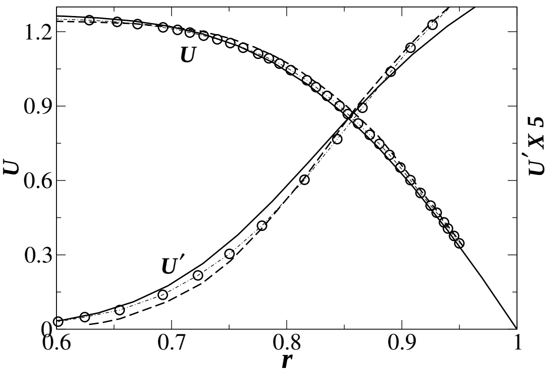

Figure 5.6: Developing flow velocity profile and its gradient in a pipe for Re = 5000 at $x = 30.8$. Circles: Sparrow profile, dashed line: Hornbeck profile, solid line: present method.

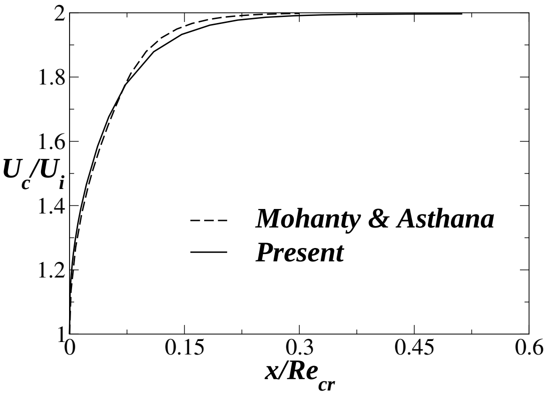

Figure 5.7: Comparison of axial variation of the centerline velocity by Mohanty & Asthana (1979) with that of present.

unstable even at a Reynolds number of 2000. The disturbance amplification, however, is very small even at Re = 5000.

We now include non-parallel effects. As seen in figure 5.8, for a given inlet Reynolds number, the flow is expected to be linearly unstable within a certain axial extent. Too far upstream, the effective Reynolds number is too low for instability, and too far downstream, the flow is fully developed and thus linearly stable. The amplitude of the disturbance kinetic energy given by equation (2.45) at $r = 0.08$ and $r = 0.25$ for the axisymmetric mode are shown in figures 5.9 and 5.10 respectively. The Reynolds number is 5000. It is found that the amplitude of the disturbance kinetic energy decays for $r > 0.6$, and that the maximum growth of the disturbance kinetic energy is close to the centerline. In other words, an experiment where the probe was positioned within $0 < r < 0.6$ would measure exponential growth of disturbances of the right frequency, while probes placed closer to the wall would register a stable flow. The disturbance kinetic energy integrated across the pipe decays at these Reynolds numbers.

For comparing with the experiments of Sarpkaya (1975), we note that Sarpkaya measured the variation of the amplitude of the axial disturbance velocity, while our stability analysis deals with individual eigenmodes. Since the former gives the integrated effect of the latter over all modes, and since only a small range of wavenumbers is unstable at the Reynolds numbers considered, we expect the experiment to display a significantly lower level of instability than predicted by the stability analysis. Secondly, it

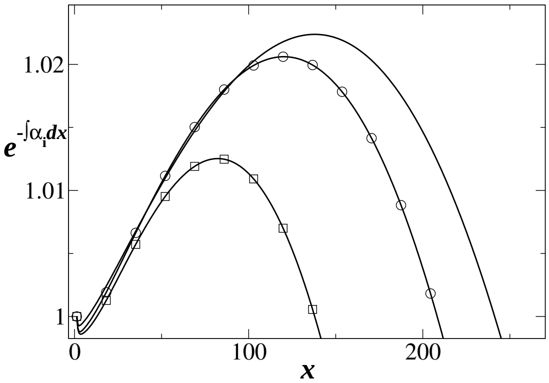

Figure 5.8: Amplification of the disturbance $\left(\exp-\left[\int \alpha_i dx\right]\right)$ by parallel stability analysis for $\omega_d = 0.5$. Solid line: Re = 5000, circles: Re = 4000, squares: Re = 3000.

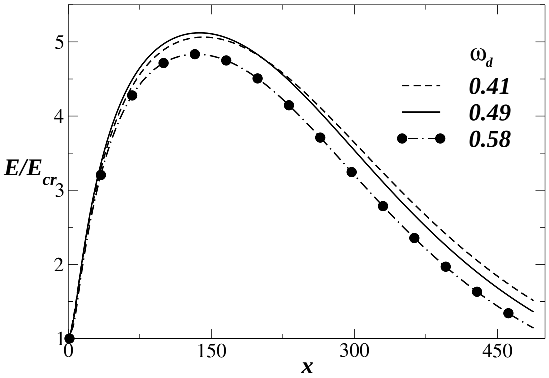

Figure 5.9: Amplification of the disturbance kinetic energy for the axisymmetric ($n = 0$) mode for typical disturbance frequencies for Re = 5000 at $r = 0.08$.

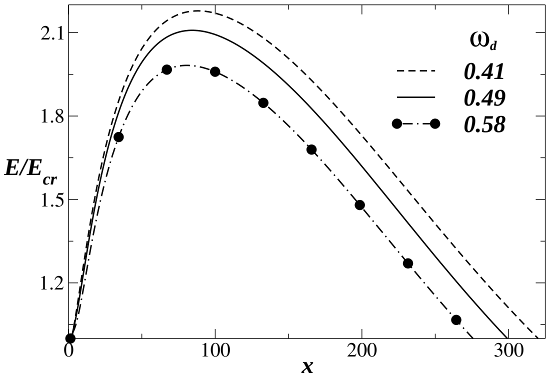

Figure 5.10: Same as figure 5.9, but for $r = 0.25$.

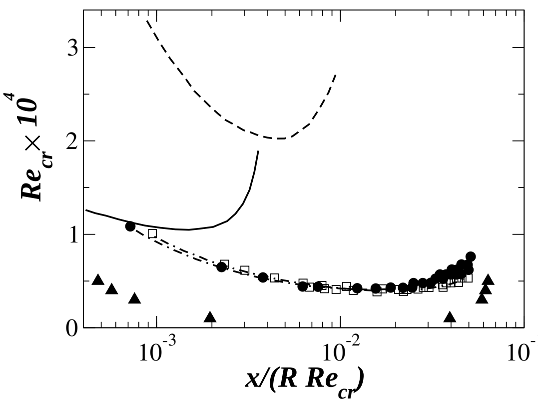

Figure 5.11: Axial variation of the critical Reynolds number. Filled triangles: present non-parallel study ($n = 0$ mode) at $r = 0.25$. Filled circles and open squares: experimental results of Sarpkaya (1975) for axisymmetric and non-axisymmetric disturbances respectively. The theoretical results of Huang & Chen (1974) and Tatsumi (1952) for axisymmetric disturbances are shown by the dashed and solid lines respectively.

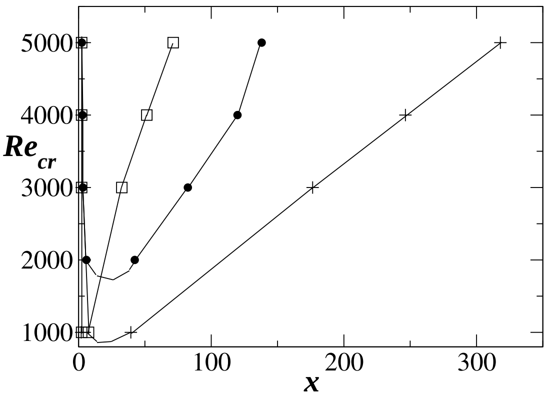

Figure 5.12: Axial variation of the critical Reynolds number ($n = 0$ mode). Filled circles: parallel stability analysis, open squares and plus symbol: non-parallel results at $r = 0.5$ and $r = 0.25$ respectively. The lines are shown to guide the eye.

was seen above that stability is a function of the radial location at which the growth rates are monitored, and in the experiment it is not mentioned what this location is. Figure 5.11 shows the comparison of the zero growth curve obtained from the present non-parallel analysis at $r = 0.25$ with that of the experiment. The qualitative behaviour is the same, and as expected, the region of instability obtained experimentally is smaller. Note that at a Reynolds number of 1000, there is already a significant axial extent over which disturbance growth is obtained. The growth rates, however, are extremely small, and would be difficult to see in an experiment. It is evident from the same figure that the critical Reynolds numbers predicted by earlier theoretical studies are unrealistically high.

The regions of instability at two radial locations are shown in figure 5.12, the result from a parallel stability analysis is shown for reference. Surprisingly, disturbance growth is much higher closer to the centreline rather than at the wall. This indicates that the radial velocity in the core is an important destabilising factor. An experiment which takes account of the radial location, and in which the Fourier modes of the instability are obtained is called for, to check the present predictions in greater detail.

To summarise, flow in the entry region of a pipe is linearly unstable at a Reynolds number as low as 1000, in qualitative agreement with experiment, but further experiments are required. Disturbance growth is highest in the core region. We have made no approximation in solving for the mean flow and have performed a complete non-parallel analysis correct to $O\left(\mathrm{Re}^{-1}\right)$.

CHAPTER 6

Other studies

6.1 Pulsatile flow through a straight pipe

The studies described in this chapter are still in the preliminary stage. The mean flow is computed and stability equations for sinusodally varying flows are given. The main point of the study is to estimate the effect of asymmetries, in the form of departures from sinusoidal. The instability of such a flow will be studied in future. Pulsatile flow through a pipe has been a topic of interest [Bertram & Pedley (1983)] because of its relevance to the blood flow through arteries. Arterial flow is of course very complicated but we study only one aspect, namely the pulsatile nature of the flow. The geometry is a straight rigid-walled pipe. Fedele *et al.* (2005) considered a pulsatile flow through a pipe by imposing periodic pressure gradient at the inlet. They have used an analytical velocity profile in the stability analysis. Here we have undertaken a similar study. The boundary conditions at the centreline are $\psi = \Omega = V = \partial U/\partial r = 0$. No-slip and impermeable boundary conditions are imposed at the wall, *i.e,* $U = 0$ and $V = 0$. At the exit the Neumann boundary condition ($\partial\psi/\partial x = 0$) is used. We prescribe an inlet axial velocity given by $U_i = (1 - r^2)\,[A + Bcos\,(2\pi/T)\,t]$, where T is the time period of the oscillation of the inlet velocity. We solve the Navier-Stokes equation directly using a full-multigrid algorithm on a parallel machine [Venkatesh *et al.* (2005)] to get the periodic basic flow. The velocity at each point is

$$U\,(x, r, t) = \bar{U}\,(x, r) + u_p\,(x, r, t)\,, \quad \text{and} \quad V\,(x, r, t) = \bar{V}\,(x, r) + v_p\,(x, r, t)\,, \tag{6.1}$$

where $\bar{U}\,(x, r)$ and $\bar{V}\,(x, r)$ are time averaged velocities in the x and r direction respectively, and $u_p\,(x, r, t)$ and $v_p\,(x, r, t)$ are the corresponding unsteady parts of the velocity.

The axial and radial velocity profiles for the inlet velocity $U_i = (1 - r^2)\,[0.85 + 0.15cos\,(2\pi/10)\,t]$ at different times are shown in figures 6.1 and 6.2 respectively. The unsteady part of the velocity $u_p(r, t)$ and $v_p(r, t)$ are shown as functions of time in figures 6.3 and 6.4. The Reynolds number is 800 based on the maximum of U_i. The axial location $x = 94$ far away from the inlet is chosen where there is no further axial variation in the flow.

We then prescribe an asymmetric inlet flow given by

$$U_i = (1 - r^2)(A + Bh), \tag{6.2}$$

where h is of the form $sin(a + bt)$ in one half and $sin(c + dt)$ in the other half of the cycle. Here we have taken $a = 0$, $b = 2$, $c = 3\pi/4$ and $d = 0.5$. The axial and radial velocity profiles for the asymmetric inlet flow are shown in figures 6.5 to 6.8. At any radial location, the flow is sinusoidal, but there is a phase lag between one radial location and another. This lag is negligible up to about half the distance to the wall from the centreline, but becomes more pronounced towards the wall, as can be seen in figures 6.3 and 6.4, and also in figure 6.5. Other simulations we have carried out show the same feature. This observation suggests that a full numerical simulation is necessary to obtain the periodic base flow, and merits further understanding. The time averaged axial and radial velocity profiles at $x = 94$ for both the

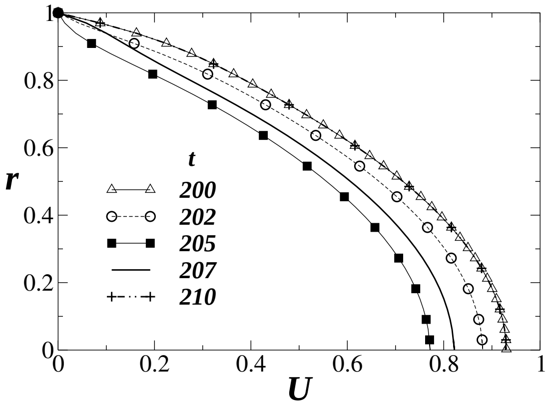

Figure 6.1: Axial velocity profiles for $U_i = (1 - r^2)\,[0.85 + 0.15cos\,(2\pi/10)\,t]$ at different times ($x = 94$ and Re = 800).

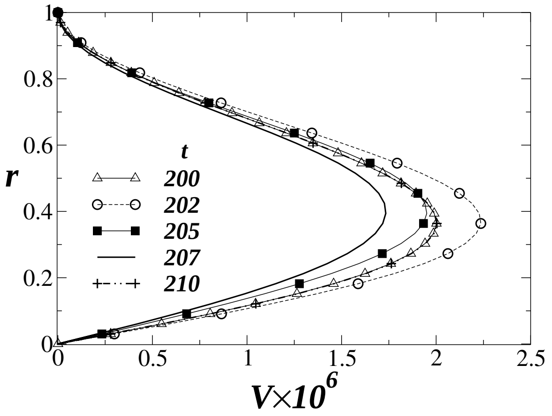

Figure 6.2: Radial velocity profiles for the same case as figure 6.1.

symmetric and asymmetric cases are shown in figures 6.9 and 6.10 respectively.

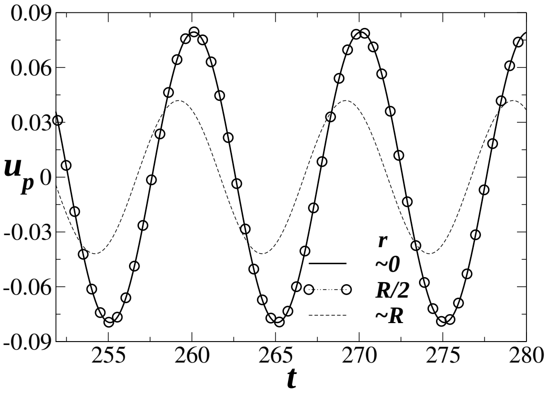

Figure 6.3: $u_p(r, t)$ Vs time at different radial locations for the same case as figure 6.1.

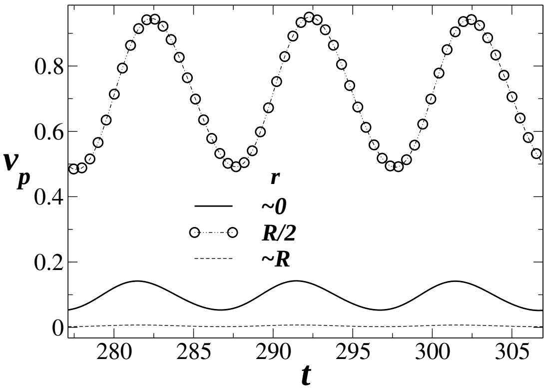

Figure 6.4: $v_p(r, t)$ Vs time at different radial locations for for the same case as figure 6.1.

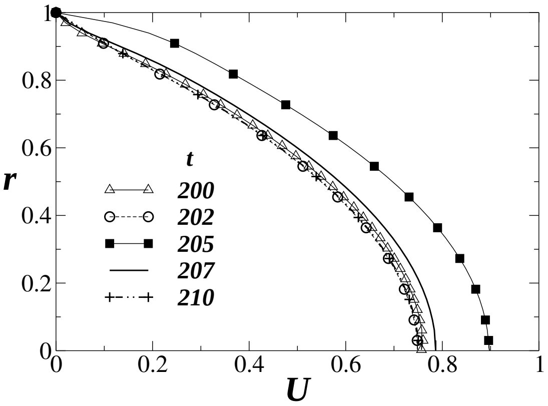

Figure 6.5: Axial velocity profiles for different time at $x = 94$, Re = 800 (asymmetric inlet profile).

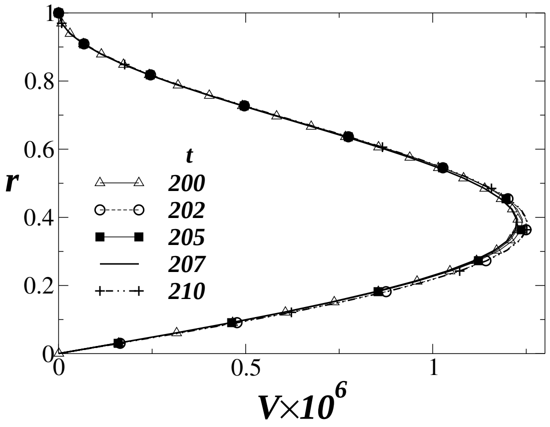

Figure 6.6: Radial velocity profiles for the same case as figure 6.5.

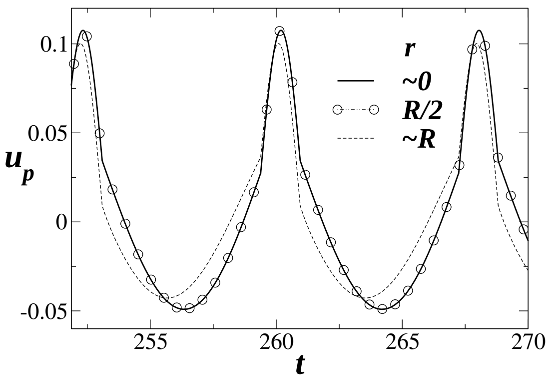

Figure 6.7: $u_p(r,t)$ Vs time at different radial locations for the same case as figure 6.5.

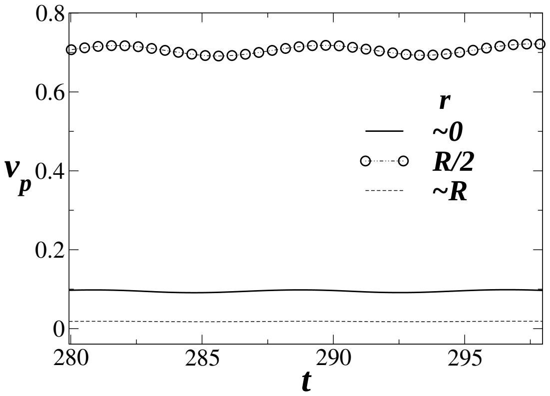

Figure 6.8: $v_p(r,t)$ Vs time for the same case as figure 6.5.

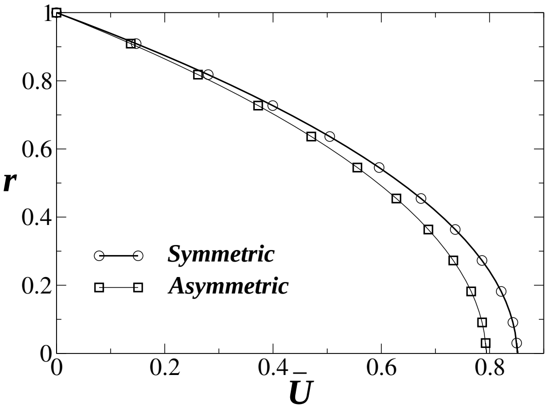

Figure 6.9: Time averaged axial velocity profiles at x = 94.

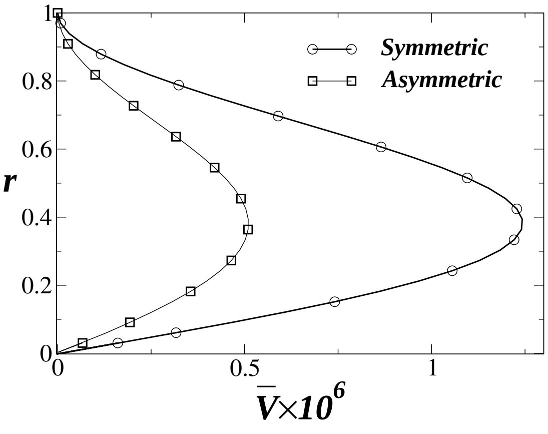

Figure 6.10: Time averaged radial velocity profiles at x = 94.

6.2 Floquet stability equations for pulsatile flow

Floquet theory is a linear theory of stability for flow which is a periodic function of time [Iooss & Joseph (1989)]. The basic flow at each point consists of a steady and time dependent part [equation (6.1)]. We add disturbances $[\hat{u}, \hat{v}, \hat{w}, \hat{p}]$ into the flow. In a normal mode form velocity perturbations appear in pairs, for example, the streamwise velocity component may be written as

$$\hat{u}\,(x, r, \theta, t) = \mathrm{Real}\left[u_1(r)e^{\mathrm{i}(\alpha_1 x + n_1\theta - \Omega_1 t)} + u_2(r)e^{\mathrm{i}(\alpha_2 x + n_2\theta - \Omega_2 t)}\right], \qquad (6.3)$$

The other components of velocity and the disturbance pressure may be expressed similarly. From the plots of u_p and v_p shown in figures 6.3, 6.4, 6.7 and 6.8 one can find the unsteady part of basic flow in the form

$$u_p\,(r, t) = \mathrm{Real}\left[A(r)e^{\mathrm{i}\Omega t}\right]. \qquad (6.4)$$

Adding the disturbances of equation (6.3) to the basic flow (6.1), substituting the sum into the Navier-Stokes equations, subtracting the basic flow and linearising the resulting equations we get four disturbance equations. Averaging these equations over a large period of time with $\alpha_1 = \alpha_2 = \alpha$, $n_1 = n_2 = n$ and $\Omega = \Omega_1 - \Omega_2$, we get

$$\mathrm{i}\alpha U_m u_1 + U_m' v_1 + \mathrm{i}\alpha p_1 - \frac{1}{\mathrm{Re}}\left[u_1'' + \frac{u_1'}{r} - \frac{n^2}{r^2}u_1 - \alpha^2 u_1\right] + \frac{A}{2}\mathrm{i}\alpha u_2 + \frac{A'}{2}v_2 = \mathrm{i}\Omega_1 u_1, \qquad (6.5)$$

$$\mathrm{i}\alpha U_m v_1 - \frac{1}{\mathrm{Re}}\left[v_1'' + \frac{v_1'}{r} - \frac{\left(1+n^2\right)}{r^2}v_1 - \alpha^2 v_1\right] + \frac{2}{\mathrm{Re}}\frac{\mathrm{i}nw_1}{r^2} + p_1' + \frac{A}{2}\mathrm{i}\alpha v_2 = \mathrm{i}\Omega_1 v_1, \qquad (6.6)$$

$$-\frac{2}{\mathrm{Re}}\frac{\mathrm{i}nv_1}{r^2} + i\alpha U_m w_1 - \frac{1}{\mathrm{Re}}\left[w_1'' + \frac{w_1'}{r} - \frac{\left(1+n^2\right)}{r^2}w_1 - \alpha^2 w_1\right] + \frac{\mathrm{i}np_1}{r} + \frac{A}{2}\mathrm{i}\alpha w_2 = \mathrm{i}\Omega_1 w_1, \qquad (6.7)$$

$$\frac{1}{\mathrm{Re}}\mathrm{i}\alpha u_1' + \mathrm{i}\alpha U_m v_1 + \frac{1}{\mathrm{Re}}\left[\alpha^2 v_1 + \frac{n^2}{r^2}v_1\right] + \frac{\mathrm{i}n}{\mathrm{Re}}\left[\frac{w_1}{r^2} + \frac{w_1'}{r}\right] + p_1' + \frac{A}{2}\mathrm{i}\alpha v_2 = \mathrm{i}\Omega_1 v_1, \qquad (6.8)$$

$$\frac{A}{2}\mathrm{i}\alpha u_1 + \frac{A'}{2}v_1 + \mathrm{i}\alpha U_m u_2 - \frac{1}{\mathrm{Re}}\left[u_2'' + \frac{u_2'}{r} - \frac{n^2}{r^2}u_2 - \alpha^2 u_2\right] + v_2 U_m' + \mathrm{i}\alpha p_2 = \mathrm{i}(\Omega_1 - \Omega)u_2, \qquad (6.9)$$

$$\frac{A}{2}\mathrm{i}\alpha v_1 + \mathrm{i}\alpha U_m v_2 - \frac{1}{\mathrm{Re}}\left[v_2'' + \frac{v_2'}{r} - \frac{\left(1+n^2\right)}{r^2}v_2 - \alpha^2 v_2\right] + \frac{2}{\mathrm{Re}}\frac{\mathrm{i}nw_2}{r^2} + p_2' = \mathrm{i}(\Omega_1 - \Omega)v_2, \qquad (6.10)$$

$$\frac{A}{2}\mathrm{i}\alpha w_1 - \frac{2}{\mathrm{Re}}\frac{\mathrm{i}nv_2}{r^2} + \mathrm{i}\alpha U_m w_2 - \frac{1}{\mathrm{Re}}\left[w_2'' + \frac{w_2'}{r} - \frac{\left(1+n^2\right)}{r^2}w_2 - \alpha^2 w_2\right] + \frac{\mathrm{i}np_2}{r} = \mathrm{i}(\Omega_1 - \Omega)v_2, \qquad (6.11)$$

$$\frac{A}{2}\mathrm{i}\alpha v_1 + \frac{1}{\mathrm{Re}}\mathrm{i}\alpha u_2' + \mathrm{i}\alpha U_m v_2 + \frac{1}{\mathrm{Re}}\left[\alpha^2 v_2 + \frac{n^2}{r^2}v_2\right] + \frac{\mathrm{i}n}{\mathrm{Re}}\left[\frac{w_2}{r^2} + \frac{w_2'}{r}\right] + p_2' = \mathrm{i}(\Omega_1 - \Omega)v_2. \qquad (6.12)$$

None of the other modes survives the averaging process. Above equations in matrix form is

$$\begin{bmatrix} a_{11} & a_{12} & \cdots & a_{18} \\ \vdots & \vdots & \ddots & \vdots \\ a_{81} & a_{82} & \cdots & a_{88} \end{bmatrix} \begin{bmatrix} u_1 \\ v_1 \\ w_1 \\ p_1 \\ u_2 \\ v_2 \\ w_2 \\ p_2 \end{bmatrix} = \omega_1 \begin{bmatrix} b_{11} & b_{12} & \cdots & b_{18} \\ \vdots & \vdots & \ddots & \vdots \\ b_{81} & b_{82} & \cdots & b_{88} \end{bmatrix} \begin{bmatrix} u_1 \\ v_1 \\ w_1 \\ p_1 \\ u_2 \\ v_2 \\ w_2 \\ p_2 \end{bmatrix} \tag{6.13}$$

where

$a11 = L - 1/(r^2 \times \mathrm{Re})$, $a12 = U_m'$, $a13 = 0$, $a14 = \mathrm{i}\alpha$, $a15 = (\mathrm{i} \times \alpha \times A(r))/2$, $a16 = A'(r)/2$, $a17 = 0$, $a18 = 0$,

$a21 = 0$, $a22 = L$, $a23 = (2 \times \mathrm{i} \times n)/(r^2 \times \mathrm{Re})$, $a24 = D$, $a25 = 0$, $a26 = (\mathrm{i} \times \alpha \times A(r)/2)$, $a27 = 0$, $a28 = 0$,

$a31 = 0$, $a32 = -(2 \times \mathrm{i} \times n)/(r^2 \times \mathrm{Re})$, $a33 = L$, $a34 = (\mathrm{i} \times n)/r$, $a35 = 0$, $a36 = 0$, $a37 = (\mathrm{i} \times \alpha \times A(r))/2$, $a38 = 0$,

$a41 = \mathrm{i} \times \alpha \times D$, $a42 = ((\mathrm{i} \times \alpha \times \mathrm{Re} \times U_m) + n^2/r^2 + \alpha^2)$, $a43 = \mathrm{i} \times n \times (1/r^2 + D/r)$, $a44 = \mathrm{Re} \times D$, $a45 = 0$, $a46 = (\mathrm{i} \times \alpha \times \mathrm{Re} \times A(r)/2)$, $a47 = 0$, $a48 = 0$,

$a51 = (\mathrm{i} \times \alpha \times A(r)/2)$, $a52 = A'(r)/2$, $a53 = 0$, $a54 = 0$, $a55 = L - 1/(r^2 \times \mathrm{Re}) + \mathrm{i} \times \Omega$, $a56 = U_m'$, $a57 = 0$, $a58 = \mathrm{i}\alpha$,

$a61 = 0$, $a62 = (\mathrm{i} \times \alpha \times A(r)/2)$, $a63 = 0$, $a64 = 0$, $a65 = 0$, $a66 = L + \mathrm{i} \times \Omega$, $a67 = (2 \times \mathrm{i} \times n)/(r^2 \times \mathrm{Re})$, $a68 = D$,

$a71 = 0$, $a72 = 0$, $a73 = (\mathrm{i} \times \alpha \times A(r)/2)$, $a74 = 0$, $a75 = 0$, $a76 = -(2 \times \mathrm{i} \times n)/(r^2 \times \mathrm{Re})$, $a77 = L + \mathrm{i} \times \Omega$, $a78 = (\mathrm{i} \times n)/r$,

$a81 = 0$, $a62 = (\mathrm{i} \times \alpha \times \mathrm{Re} \times A(r)/2)$, $a83 = 0$, $a84 = 0$, $a85 = \mathrm{i} \times \alpha \times D$, $a86 = ((\mathrm{i} \times \alpha \times \mathrm{Re} \times U_m) + n^2/r^2 + \alpha^2) + \mathrm{i} \times \mathrm{Re} \times \Omega$, $a87 = \mathrm{i} \times n \times (1/r^2 + D/r)$, $a88 = \mathrm{Re} \times D$.

The operator L and D are defined as follows

$$L = \mathrm{i}\alpha U_m - \frac{1}{\mathrm{Re}}\left[D^2 + D/r - (1 + n^2)/r^2 - \alpha^2\right], \quad D = \partial/\partial r, \quad \text{and} \quad D^2 = \partial^2/\partial r^2.$$

In equation (6.13), we confirm that if we set A to zero, we get the parallel stability equations of Gill (1973); Lessen *et al.* (1968).

The Floquet stability analysis is not valid for asymmetric time periodic flows given in equation (6.2). At present we do not have substantial results to include in the thesis. In future, we are planning to complete this work in our group.

6.3 Flow separation in divergent channel/pipe

At higher angles of divergence and at high Reynolds number flow separation occurs in diverging channels and pipes. In this section we study the separation in channels and pipes for angle of divergence from 0° to 60°. The 0° and 90° cases have been studied ingreat detail, but we did not find any studies of separation as a function of angle of divergence. We solve the Navier-Stokes equations as discussed in § 2.1.1 and use the parallelised solver Venkatesh *et al.* (2005) for this study. A pipe and channel having an aspect ratio (defined by the ratio of smallest radius to biggest radius) of 0.5 are considered here at Re = 150. A schematic diagram for divergent pipe of aspect ratio 0.5 is shown in figure 6.11. For different angles of divergence, the separation and reattachment points for the flow through diverging pipes and channels are shown in figures 6.12 and 6.13 respectively. It can be seen that for both the flows through the diverging pipe and the channel, separation and reattachment occur almost at the same locations. The axial velocity profiles for flow through diverging pipe and channel are shown in in figures 6.14 and 6.15 respectively. In future, we are planning to conduct full non-parallel stability analysis e.g. global stability analysis of such flows without the approximations made in this thesis.

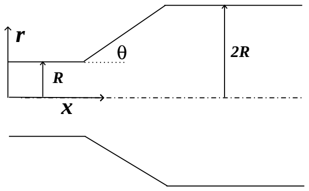

Figure 6.11: Schematic diagram of the divergent pipe having an aspect ratio of 0.5, not to scale.

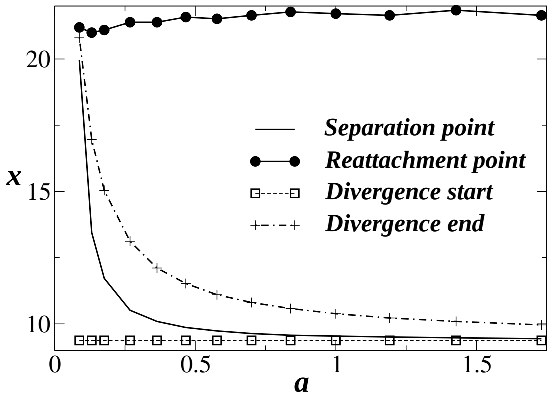

Figure 6.12: Separation and reattachment point in diverging pipe. Aspect ratio of the diverging pipe =0.5, Re = 150. The point where the diverging portion starts and ends are shown as a guideline.

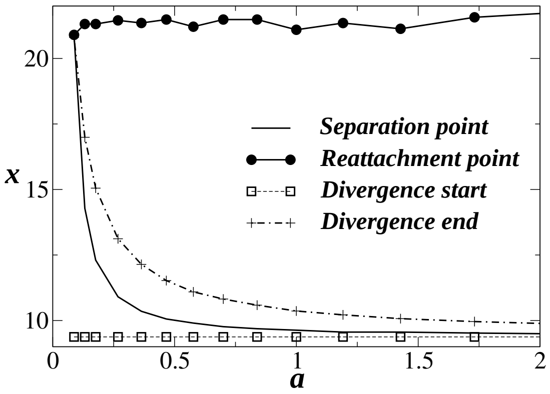

Figure 6.13: Same as figure 6.12 but for diverging channel.

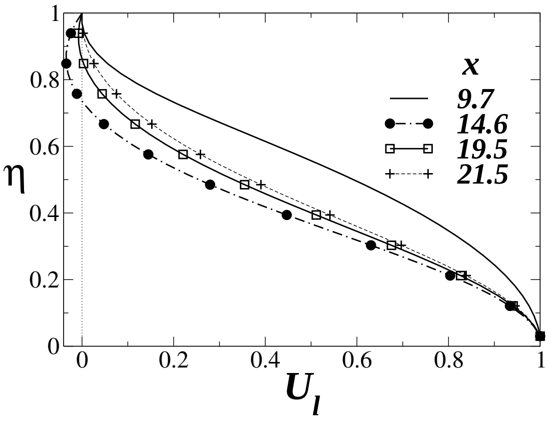

Figure 6.14: Axial velocity profiles for different axial locations. Aspect ratio of the pipe =1:2, Re = 150.

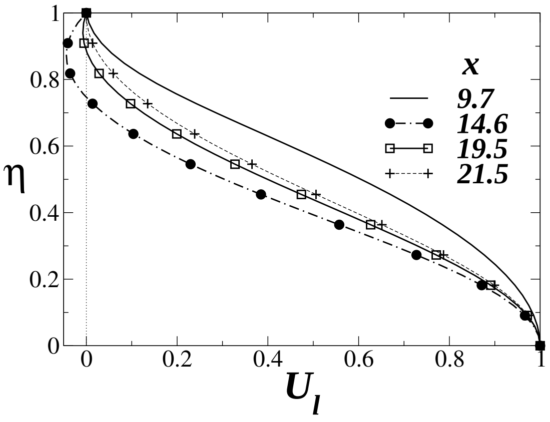

Figure 6.15: Same as figure 6.14 but for diverging channel.

CHAPTER 7

Conclusions

Fully developed laminar flow (Hagen-Poiseuille flow) through a straight pipe is linearly stable at any Reynolds number, Re. In this case, nonlinear and/or transient growth mechanisms drive the transition to turbulence. However there are many variations from these conditions where linear instability can play a significant role in transition to turbulence. Some of these situations are addressed in this thesis. They are, flow through (i) a divergent pipe, (ii) a variety of diverging-converging pipes with constant average radius, (iii) diverging pipes/channels with velocity slip at the wall, and (iv) the entry region of a straight pipe. The instabilities of these spatially developing laminar flows is shown to be fundamentally different from flows that do not vary downstream. We have also studied separation in diverging channels and pipes.

It is not in general possible to derive analytical solutions for the laminar flows described above. We obtain the mean flow by solving the steady two-dimensional/axisymmetric Navier-Stokes equations exactly. For the accuracy desired, the computational time required for solving the elliptic equations is very large. A full-multigrid algorithm (FMG) is used to accelerate the convergence. The code is parallelised at the National Aerospace Laboratories, Bangalore. The FMG speeds up the solution by a factor of hundred as compared to many traditional algorithms, and the parallel code (using an eight processor machine) gives a superlinear speed-up of 11 times over a single processor. However at small angle of divergence a ($< 1^\circ$), the velocity profiles for a diverging pipe are obtained analytically by deriving an axisymmetric Jeffery-Hamel equation (AJH).

In a diverging pipe the critical Reynolds number for linear instability is finite at any divergence and the critical Reynolds number is surprisingly low even for small angles of divergence. The flow is shown to satisfy the necessary conditions for inviscid instability at any divergence. For small divergence, instability is determined by the parameter $S(x)$ describing the mean profile, the mechanism is inviscid, as angle of divergence, $a \to 0$, the flow is unstable to the swirl ($n = 1$) mode for $S > 10$, so the critical Reynolds number approaches infinity as $1/a$. At divergences as low as 1°, the effect of flow non-parallelism is already large, so a non-parallel analysis is essential. A non-parallel analysis yields linear instability to the swirl mode at surprisingly low Reynolds numbers, of about 150 for a divergence of 3°, which would suggest a role for such instabilities in the transition to turbulence.

We then study the effect of local asymmetric convergence/divergence on laminar flow through a pipe of constant *average* radius. The main finding is that the instability behaviour can be changed dramatically by reversing the direction of flow. Since the Reynolds numbers for these instabilities are low, exponential growth of disturbance is offered as a possible mechanism that could be operating in small-scale flows, due to the presence of wall roughness.

Fluid dynamics (and the role of the walls) at small-scale can be very different from that at large scales. We make a minor foray into this regime, by considering the effect of wall slip at Knudsen numbers less than 0.1. In a plane two-dimensional channel velocity slip at the wall dramatically stabilizes the linear mode but has very little effect on the algebraic transient growth of disturbances [Lauga & Cossu (2005)]. We show that even for small divergences of the channel wall, the transient algebraic growth remains an insignificant player. Linear instability on the other hand, as is well known, occurs at Reynolds number two orders of magnitude lower than in a plane channel. Slip has a small destabilising effect. We predict that a different route to chaos, via linear instability, could take place at small scales in the presence of divergence and hope to motivate experimental verification of this assertion.

The question of why slip has the counter-intuitive effect, although small, of destabilising the flow needs to be addressed in future. For example, in flow through a channel of width 100 μm, where wall roughness is of the order of 5% of the width will already, we predict, be unstable at Reynolds numbers of $50 - 100$. This translates to velocities of 0.5 to 1 m/s for water. So even a 10% decrease in the critical Reynolds number could have practical relevance to flows through micro-channels or between hydrophobic walls. For $Kn \rightarrow 0$ the results could provide pointers to larger-scale flows with local divergences, such as through arteries. We have considered only Jeffery-Hamel flows, representing channels which diverge indefinitely at a given angle, but our results are relevant to channels of arbitrary geometry with local divergences extending to a few channel widths. We have checked that numerical profiles obtained in such channels match closely with Jeffery-Hamel profiles. Restricting ourselves to situations where the inlet flow is relatively quiet, we have not touched upon the role of nonlinearity here, but there are several interesting questions, such as whether a nonlinear self-sustaining mechanism of the general class of Waleffe (1995) would be in operation or whether nonlinear travelling-wave solutions [Faisst & Eckhardt (2004); Hof *et al.* (2004)] will be observed.

At high Reynolds numbers, the entry region is long, and could play an important role in transition to turbulence. We have shown that flow in the entry region of a pipe is linearly unstable at a Reynolds number as low as 1000, in qualitative agreement with experiment. Disturbance growth is highest in the core region. This indicates that the radial velocity in the core is an important destabilising factor.

As a general rule, the mean flow in each of the aforementioned problems must be computed accurately and a complete non-parallel analysis is essential.

APPENDIX I

Multigrid Algorithm for Two-dimensional Poisson Equation

Two-dimensional Poisson equation is

$$\frac{\partial^2 u}{\partial x^2} + \frac{\partial^2 u}{\partial y^2} = -f(x, y), \tag{I.1}$$

which is an elliptic equation and it has to solve by an iterative procedure. In equation (I.1) the unknown solution $u(x, y)$ is determined by the given source term $f(x, y)$ in a closed region. Let's consider a square domain $0 \leq x, y \leq L$ with homogeneous Dirichlet boundary conditions $u = 0$ on the perimeter of the square. The equation is discretized on a grid with $N + 2$ lattice points, i.e, N interior points and two boundary points, in the x and y directions. At any interior point, the exact solution obeys

$$u_{i,j} = \left[u_{i+1,j} + u_{i-1,j} + u_{i,j+1} + u_{i,j-1} + h^2 f_{i,j}\right]. \tag{I.2}$$

The different grids employed are called multigrid levels, l. The number of interior lattice points in the x and y directions is then taken to be 2^l, so that $N = 2^l + 2$, and the lattice spacing $h = 1/(N - 1)$. N is chosen in this manner so that the downward multigrid iteration can construct a sequence of coarser lattices with

$$2^{l-1} \rightarrow 2^{l-2} \rightarrow .... \rightarrow 2^0 = 1 \tag{I.3}$$

interior points in the x and y directions.

Suppose that $u(x, y)$ is the approximate solution at any stage of the calculation, and $u_{exact}(x, y)$ is the solution which we are trying to find. The multigrid algorithm uses the following definitions:

1. The *correction* is the function which must be added to the approximate solution to give the exact solution, which is

$$v = u_{exact} - u. \tag{I.4}$$

The *residual* or *defect* is defined as

$$r = \nabla^2 u + f. \tag{I.5}$$

From the above expressions, it is can be shown that the *correction* and the *residual* are related by the following equation

$$\nabla^2 v = \left[\nabla^2 u_{exact} + f\right] - \left[\nabla^2 u + f\right] = -r. \tag{I.6}$$

This equation has exactly the same form as the Poisson equation with v playing the role of the unknown function and r playing the role of the known source function.

A Simple V-cycle algorithm

The simplest multigrid algorithm is based on a two-grid improvement scheme. Considering two grids:

(a) a fine grid with $N = 2^l + 2$ points in each direction, and

(b) a coarse grid with $N = 2^{l-1} + 2$ points.

It is needed to relate one grid to another, *i.e.*, given any function on the lattice, it is needed to

(c) restrict the function from fine → coarse, and

(d) prolongate or interpolate the function from coarse → fine.

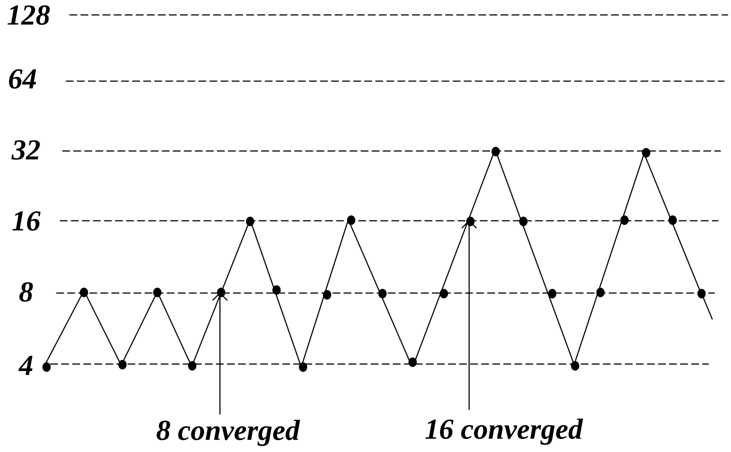

Figure I.1: Simple V-cycle in full-multigrid algorithm

B Multigrid algorithm

The multigrid algorithm consists of the following steps:

1. If $l = 0$ there is only one interior point, so solve exactly for

$$u_{1,1} = \left(u_{0,1} + u_{2,1} + u_{1,0} + u_{1,2} + h^2 f_{1,1}\right)/4.$$

2. Otherwise, calculate the current $N = 2^l + 2$.

3. Perform a few pre-smoothing iterations using a local algorithm such as Gauss-Seidel. The idea is to damp or reduce the short wavelength errors in the solution.

4. Estimate the *correction*, $v (= u_{exact} - u)$ as follows:

(a) Compute the *residual*

$$r_{i,j} = \frac{1}{h^2}\left[u_{i+1,j} + u_{i-1,j} + u_{i,j+1} + u_{i,j-1} - 4u_{i,j}\right] + f_{i,j}.$$

(b) Restrict the *residual* $r \rightarrow R$ to the coarser grid.

(c) Set the coarser grid *correction*, V to zero and improve it recursively.

(d) Interpolate the *correction* $(V - v)$ onto the finer grid.

5. Correct $u \rightarrow u + v$.

6. Perform a few post-smoothing Gauss-Seidel iterations and return the improved u to the next finer grid.

APPENDIX II

Chebyshev Spectral Collocation Method

A Chebyshev Expansions

The Chebyshev polynomials of the first kind are a set of orthogonal polynomials defined as the solutions to the Chebyshev differential equation and denoted $T_n(y)$. Chebyshev polynomials are defined in one of the following ways:

(1) Trignometric Function

$$T_n(y) = \cos(n\cos^{-1} y). \tag{II.1}$$

(2) Rodrigues' Formula

$$T_n(y) = \frac{(-1)^n 2^2 n!}{(2n)!}\sqrt{1-y^2}\frac{d^n}{dy^n}\Big[(1-y^2)^{n-1/2}\Big]. \tag{II.2}$$

(3) A Direct Formula

$$T_n(y) = \frac{1}{2}\Big[(y+\sqrt{1-y^2})^n + (y-\sqrt{1-y^2})^n\Big]. \tag{II.3}$$

(4) Solution of Sturm-Liouville

$$\frac{d}{dy}\Big(\sqrt{1-y^2}\frac{d}{dy}T_n(y)\Big) + \frac{n^2}{\sqrt{1-y^2}}T_n(y) = 0. \tag{II.4}$$

(5) Recurrence Relation

$$T_0(y) = 1, \quad T_1(y) = y, \quad T_{n+1}(y) = 2yT_n(y) - T_{n-1}(y). \tag{II.5}$$

The Chebyshev polynomials are orthogonal polynomials with respect to the weighting function $(1-y^2)^{1/2}$

$$\int_{-1}^{1}\frac{T_m(y)T_n(y)}{\sqrt{1-y^2}}dy = \begin{cases} \frac{1}{2}\pi\delta_{nm}, & \text{if } m \neq 0, \quad n \neq 0 \\ \pi, & \text{if } m = n = 0. \end{cases} \tag{II.6}$$

where δ_{nm} is the Kronecker delta. Chebyshev polynomials of the first kind satisfy the additional discrete identity

$$\sum_{k=1}^{m} T_i(y_k)T_j(y_k) = \begin{cases} \frac{1}{2}\pi\delta_{ij}, & \text{if } i \neq 0, \quad j \neq 0 \\ \pi, & \text{if } i = j = 0. \end{cases} \tag{II.7}$$

where y_k for $k = 1, ..., m$ are the m zeros of $T_m(y)$.

They also satisfy the recurrence relations

$$T_{n+1}(y) = 2yT_n(y) - T_{n-1}(x) \tag{II.8}$$

$$T_{n+1}(y) = yT_n(y) - \sqrt{(1-y^2)\left\{1 - [T_n(x)]^2\right\}} \tag{II.9}$$

Using Chebyshev polynomials a function $\phi(y)$ can be expanded as

$$\phi(y) = \sum_{n=0}^{N} a_n T_n(y) \tag{II.10}$$

Chebyshev-collocation method is accomplished by the specification of the collocation points chosen to be the Chebyshev Gauss-Lobatto points defined as

$$y_i = \cos(i\pi/N). \tag{II.11}$$

Chebyshev spectral methods are dealt in Canuto, Hussaini, Quarteroni & Zang (1987).

B Differentiation in Chebyshev Plane

The derivative of $\phi(y)$ is evaluated in two ways.

Method 1

The p^{th} derivative, $\phi_N^{(p)}(y_i)$ is

$$\phi_N^{(p)}(y_i) = \sum_{n=0}^{N} a_n T_n^{(p)}(y_i). \tag{II.12}$$

$T_n^{(p)}(y_i)$ is evaluated from the recurrence relation II.5. This method is not usually used for eigenvalue value problems.

Method 2

The dependent variable $\phi_N(y_i)$ can also be written as

$$\phi_N(y) = \sum_{j=0}^{N} h_j(y)\phi_N(y_j), \tag{II.13}$$

where $h_j(y)$ are the polynomials of degree N defined as

$$h_j(y) = \frac{(-1)^{j+1}(1-y^2)T_N{}'(y)}{\bar{c}_j N^2 (y - y_j)}. \tag{II.14}$$

Then the derivative can be written as

$$\phi_N^{(p)}(y_i) = \sum_{j=0}^{N} d_{i,j}^{(p)} \phi_N(y_j), \tag{II.15}$$

where $d_{i,j}^{(p)} = h_j^{(p)}(y_i)$. The expression of coefficients for some $d_{i,j}^{(p)}$ are

$$d_{i,j}^{(1)} = \begin{cases} \frac{\bar{c}_i}{\bar{c}_j} \frac{(-1)^{i+j}}{(y_i - y_j)}, & 0 \leq i, j \leq N, \quad i \neq j \\ -\frac{y_i}{2(1-y_i^2)}, & 1 \leq i \leq N-1, \quad i = j \end{cases} \tag{II.16}$$

$$d_{0,0}^{(1)} = -d_{N,N}^{(1)} = \frac{2N^2+1}{6}, \tag{II.17}$$

where $\bar{c}_0 = \bar{c}_N = 2, \quad \bar{c}_j = 1$ for $1 \leq j \leq N-1$ and

$$d_{i,j}^{(2)} = \sum_{k=0}^{N} d_{i,k}^{(1)} d_{i,k}^{(1)}. \tag{II.18}$$

So that in vector form $\phi^{(p)} = D^{(p)}\phi$, where $D = d_{i,j}^{(1)}, i, j = 0, ..., N$.

Bibliography

Batchelor, G. K. & Gill, A. E. 1962 Analysis of the stability of axisymmetric jets. *J. Fluid Mech.* **14**, 529–551.

Batchelor, G. K., K., M. H. & Worster, M. G. 2000 *Perspectives in Fluid Dynamics*, 1st edn. Canbridge University Press.

Bertolotti, F. P., Herbert, T. & Spalart, P. R. 1992 Linear and nonlinear stability of the Blasius boundary layer. *J. Fluid Mech.* **242**, 441–474.

Bertram, C. D. & Pedley, T. J. 1983 Steady and unsteady separation in an approximately two-dimensional indented channel. *J. Fluid Mech.* **130**, 315–345.

Billant, P. & Gallaire, F. 2005 Generalized rayleigh criterion for non-axisymmetric centrifugal instabilities. *J. Fluid Mech.* **542**, 356–397.

Blancher, S., Creff, R. & Qur, P. L. 2004 Analysis of convective hydrodynamic instabilities in a symmetric wavy channel. *Phys. Fluids* **16 (10)**, 3726–3737.

Burridge, D. M. & Drazin, P. G. 1969 Comments on stability of pipe Poiseuille flow. *Phys. Fluids* **12**, 264–265.

Canuto, C., Hussaini, M. Y., Quarteroni, A. & Zang, T. 1987 *Spectral Methods in Fluid Dynamics*, 1st edn. Springer-Verlag.

Carpenter, P. W. & Garrad, A. D. 1986 The hydrodynamic stability of flow over kramer-type compliant surfaces. 2. flow-induced surface instabilities. *J. Fluid Mech.* **170**, 199–232.

Chandrasekhar, S. 1981 *Hydrodynamic and hydromagnetic stability*, 1st edn. Dover publication, Inc, New York.

Cherdron, W., Durst, F. & Whitelaw, J. H. 1978 Asymmetric flows and instabilities in symmetric ducts with sudden expansions. *J. Fluid Mech.* **84**, 13–31.

Choi, C. H., A., W. J. & Breuer 2003 Apparent slip flows in hydophilic and hydrophobic microchannels. *Phys. Fluids* **15 (10)**, 2897–2902.

Chu, A. K. H. 2000 Stability of incompressible Helium II: A two-fluid system. *J. Phys. Conden. Matter* **12**, 8065–8069.

Chu, A. K. H. 2003 Instability of slip flows in a peristaltic transport. *Europhys. Lett.* **64**, 435–440.

Chu, A. K. H. 2004 Instability of navier slip flow liquids. *C. R. Mec.* **332**, 895.

CLEVER, R. M. & BUSSE, F. H. 1997 Tertiary and quaternary solutions for plane Couette flow. *J. Fluid Mech.* **344**, 137–153.

CORCOS, G. M. & SELLARS, J. R. 1959 On the stability of fully developed flow in a pipe. *J. Fluid Mech.* **5**, 97–112.

DA SILVA, D. F. & MOSS, E. A. 1994 The stability of pipe entrance flows subjected to axisymmetric disturbances. *J. Fluids Eng.* **116**, 61–61.

DARBYSHIRE, A. G. & MULLIN, T. 1995 Transition to turbulence in constant mass-flux pipe flow. *J. Fluid Mech.* **289**, 83–114.

DAVEY, A. 1978 On the stability of flow in an elliptic pipe which is nearly circular. *J. Fluid Mech.* **87**, 233–241.

DAVEY, A. & DRAZIN, P. G. 1969 The stability of Poiseuille flow in a pipe. *J. Fluid Mech.* **36**, 209–218.

DAVEY, A. & NGUYEN, H. P. F. 1971 Finite-amplitude stability on pipe flow. *J. Fluid Mech.* **45**, 701–720.

DAVEY, A. & SALWEN, H. 1994 On the stability of flow in an elliptic pipe which is nearly circular. *J. Fluid Mech.* **281**, 357–369.

DAVIES, C. & CARPENTER, P. W. 1997 Instabilities in a plane channel flow between compliant walls. *J. Fluid Mech.* **352**, 205–243.

DAVIS, S. H. 1976 The stability of time-periodic flows. *Ann. Rev. Fluid Mech.* **8**, 57–74.

DRAAD, A. A., KUIKEN, G. D. C. & NIEUWSTADT, F. T. M. 1998 Laminar-turbulent transition in pipe flow for Newtonian and non-Newtonian fluids. *J. Fluid Mech.* **377**, 267–312.

DRAZIN, P. G. & REID, W. H. 1981 *Hydrodynamic Stability*. Cambridge University Press, Cambridge.

DUCK, P. W. 2005 Transient growth in developing plane and Hagen Poiseuille flow. *Proc. R. Soc. A.* **461**, 1311–1333.

EAGLES, P. M. 1965 The stability of a family of Jeffery-Hamel solutions for divergent channel flow. *J. Fluid Mech.* **24**, 191–207.

EAGLES, P. M. 1972 Supercritical flow in a divergent channel. *J. Fluid Mech.* **57**, 149–160.

EAGLES, P. M. & WEISSMAN, M. A. 1975 On the stability of slowly varying flow: the divergent channel. *J. Fluid Mech.* **69**, 241–262.

EKMAN, V. W. 1910 On the change from laminar to turbulent motion of liquids. *Ark. Mat. Astron. Fys.* **6** (12).

ELDER, J. W. 1960 An experimental investigation of turbulent spots and breakdown to turbulence. *J. Fluid Mech.* **9**, 235–246.

ELIAHOU, S., TUMIN, A. & WYGNANSKI, I. 1998 Laminar-turbulent transition in Poiseuille pipe flow subjected to periodic perturbation emanating from the wall. *J. Fluid Mech.* **361**, 333–349.

ELLINGSEN, T. & PALM, E. 1975 Stability of linear flow. *Phys. Fluids* **18 (4)**, 487–488.

FAISST, H. & ECKHARDT, B. 2003 Travelling waves in pipes. *Phys. Rev. Lett.* **91** (22), 224502.

Faisst, H. & Eckhardt, B. 2004 Sensitive dependence on initial conditions in transition to turbulence in pipe flow. *J. Fluid Mech.* **504**, 343–352.

Farrell, B. F. 1988 Optimal excitation of perturbations in viscous shear flow. *Phys. Fluids* **31**, 2093–2102.

Fasel, H. & Konzelmann, U. 1990 Non-parallel stability of a flat-plate boundary layer using the complete navier-stokes equations. *J. Fluid Mech.* **221**, 311–347.

Fearn, R. M., Mullin, T. & Cliffe, K. A. 1990 Nonlinear flow phenomena in a symmetric sudden expansion. *J. Fluid Mech.* **221**, 595–608.

Fedele, F., Hitt, D. L. & Prabhub, R. D. 2005 Revisiting the stability of pulsatile pipe flow. *European Journal of Mechanics* **24**, 237–254.

Fjortoft, R. 1950 Application of integral theorems in deriving criteria of stability for laminar flows and for the baroclinic circular vortex. *Geofys. Publ. Oslo* **17 (6)**, 1–52.

Fletcher, C. A. J. 1991*a Computational Techniques for Fluid Dynamics*, 2nd edn., , vol. I. Springer.

Fletcher, C. A. J. 1991*b Computational Techniques for Fluid Dynamics*, 2nd edn., , vol. II. Springer.

Floryan, J. M. 2003 Vortex instability in a diverging-converging channel. *J. Fluid Mech.* **482**, 17–50.

Gan, C. & Wu, Z. 2006 Short-wave instability due to wall slip and numerical observation of wall-slip instability for microchannel flows. *J. Fluid Mech.* **550**, 289–306.

Garg, V. K. 1981 Stability of developing flow in a pipe flow: non-axisymmetric disturbances. *J. Fluid Mech.* **110**, 209–216.

Gaster, M. 1968 Growth of disturbances in both space and time. *Phys. Fluids* **11**, 723–727.

Gaster, M. 1974 On the effects of boundary layer growth on flow stability. *J. Fluid Mech.* **221**, 311–347.

Gaster, M. 2000 On the growth of waves in boundary layers: a non-parallel correction. *J. Fluid Mech.* **424**, 367–377.

Gavarini, M. L., Bottaro, A. & Nieuwstadt, F. T. M. 2004 The initial stage of transition in pipe flow: role of optimal base-flow distortions. *J. Fluid Mech.* **517**, 131–165.

Geng, X., H., Y., Oguz, H. N. & Prosperetti, A. 2001 Bubble-based micropump for electrically conducting liquids. *J. Micromech. Microeng.* **11**, 270–276.

Gersting, J. M. 1974 Hydrodynamics stability of plane porous slip flow. *Phys. Fluids* **17**, 2126–2127.

Gill, A. E. 1973 The least-damped disturbance to Poiseuille flow in a circular pipe. *J. Fluid Mech.* **61**, 97–107.

Govindarajan, R. & Narasimha, R. 1995*a* Stability of spatially developing boundary layers in pressure gradients. *J. Fluid Mech.* **300**, 117–147.

Govindarajan, R. & Narasimha, R. 1995*b* Stability of spatially developing boundary layers in pressure gradients. *J. Fluid Mech.* **300**, 117–147.

Govindarajan, R. & Narasimha, R. 1997 A low-order theory for stability of non-parallel boundary layer flows. *Proc. Roy. Soc. Lond. A* **453**, 2537–2549.

GOVINDARAJAN, R. & NARASIMHA, R. 2005 Accurate estimate of disturbance amplitude variation from solution of minimal composite stability theory. *Theoretical and Computational Fluid Dynamics* **19 (4)**, 229–235.

GROSCH, C. E. & SALWEN, H. 1968 The stability of steady and time-dependent plane Poiseuille flow. *J. Fluid Mech.* **34 (1)**, 177–205.

GUPTA, S. C. & GARG, V. K. 1981 Effect of velocity distribution on the stability of developing flow in a pipe. *Phys. Fluids* **24(4)**, 576–578.

GUSTAVSSON, L. H. 1991 Energy growth of three-dimensional disturbances in plane Poiseuolle flow. *J. Fluid Mech.* **224**, 241–260.

HALL, P. 1975 The stability of Poiseuille flow modulated at high frequencies. *Proc. R. Soc. A.* **344**, 453–464.

HALPERN, D. & GROTBERG, J. 1992 Fluid-elastic instabilities of liquid-lined flexible tubes. *J. Fluid Mech.* **244**, 615–632.

HAN, G., TUMIN, A. & WYGNANSKI, I. 2000 Laminar-turbulent transition in Poiseuille pipe flow subjected to periodic perturbation emanating from the wall. part 2. late stage of transition. *J. Fluid Mech.* **419**, 1–27.

HENNINGSON, D. S. & SCHMID, P. J. 1994 A note on measures of disturbance size for spatially evolving flows. *Phys. Fluids* **6(8)**, 2862–2864.

HOF, B., VAN DOORNE, C. W. H., WESTERWEEL, J., NIEUWSTADT, F. T. M., FAISST, H., ECKHARDT, B., WEDIN, H., KERSWELL, R. R. & WALEFFE, F. 2004 Experimental observation of nonlinear traveling waves in turbulent pipe flow. *Science* **305**, 1594.

HOF, B., JUEL, A. & MULLIN, T. 2003 Scaling of the turbulence transition threshold in a pipe. *Phys. Rev. Lett.* **91**, 244502.

HOF, B., WESTERWEEL, J., SCHNEIDER, M. & ECKHARDT, B. 2006 Finite lifetime of turbulence in shear flow. *Nature* **443**, 59–62.

HORNBECK, R. W. 1964 Laminar flow in the entrance region of a pipe. *Appl. Sci. Res. A* **13**, 224–232.

HUANG, L. M. & CHEN, T. S. 1974 Stability of the developing laminar pipe flow. *Phys. Fluids* **17 (1)**, 245–247.

HUERRE, P. & ROSSI, M. 1998 Hydrodynamic instabilities in openflows. In *Hydrodynamics and nonlinear instabilities* (ed. C. Godreche & P. Manneville), pp. 81–288. Cambridge University Press.

IOOSS, G. & JOSEPH, D. D. 1989 *Elementary Stability and Bifurcation Theory*, 2nd edn. Springer-Verlag.

KARNIADAKIS, G. E. & BESKOK, A. 2002 *Micro Flows: fundamentals and simulation*. Springer-Verlag, New York, Inc.

KAWAHARA, G. & KIDA, S. 2001 Periodic motion embedded in plane Couette turbulence: regeneration cycle and burst. *J. Fluid Mech.* **449**, 291–300.

KERCZEK, C. H. 1982 The instability of oscillatory plane Poiseuille flow. *J. Fluid Mech.* **116**, 91–114.

Kerswell, R. R. & Davey, A. 1996 On the linear instability of elliptic pipe flow. *J. Fluid Mech.* **316**, 307–324.

Koch, W., Bertolotti, F., Stolet, A. & Hein, S. 2000 Nonlinear equilibrium solutions in a three-dimensional boundary layer and their secondary instability. *J. Fluid Mech.* **406**, 131–147.

Kovasznay, L. S. G., Komoda, H. & Vesudeva, B. R. 1962 Proc. heat trans. & fluid mech. inst. *Stanford University Press.* .

Kumaran, V. 1995*a* Stability of the flow of a fluid through a flexible tube at high Reynolds number. *J. Fluid Mech.* **302**, 117–139.

Kumaran, V. 1995*b* Stability of the viscous flow of a fluid through a flexible tube. *J. Fluid Mech.* **294**, 259 – 281.

Kumaran, V. 1998*a* Stability of fluid flow through a flexible tube at intermediate Reynolds number. *J. Fluid Mech.* **357**, 123–140.

Kumaran, V. 1998*b* Stability of wall modes in a flexible tube. *J. Fluid Mech.* **362**, 1–15.

Landahl, M. T. 1980 A note on an algebraic instability of inviscid parallel shear flows. *J. Fluid Mech.* **98**, 243–251.

Lauga, E., Brenner, M. P. & Stone, H. A. 2005 Microfluidics: The no-slip boundary condition. In *Handbook of Experimental Fluid Dynamics* (ed. J. Foss, C. Tropea & A. Yarin). Springer, New-York, Ch. 15.

Lauga, E. & Cossu, C. 2005 A note on the stability of slip channel flows. *Phys. Fluids* **17**, 088106.

Lessen, M., Sadler, S. G. & Liu, T. Y. 1968 Stability of pipe Poiseuille flow. *Phys. Fluids* **11**, 1404–1409.

Lin, C. C. 1955 *The theory of hydrodynamic stability*. Cambridge University Press.

Lindgren, E. R. 1969 Propagation velocity of turbulent slugs and streaks in transition pipe flow. *Phys. Fluids* **12**, 418.

Ma, B., Doorne, C. v., Zhang, Z. & Nieuwstadt, F. 1999 On the spatial evolution of a wall-imposed periodic disturbance in pipe Poiseuille flow at Re=3000. Part 1. Subcritical disturbance. *J. Fluid Mech.* **398**, 181–224.

Mackrodt, P. A. 1971 Stabilitat von hagen-poiseuille stromungen mit uberlagerter starrer rotation. PhD thesis, University of Gottingen.

Maxwell, J. C. 1879 On stresses in rarefied gases arising from inequalities of temperature. *Phil. Trans. Roy. Soc. Lond.* **170**, 231–256.

Meseguer, A. & Trefethen, L. N. 2003 Linearized pipe flow to Reynolds number 10^7. *Journal of Computational Physics* **186**, 178–197.

Min, T. & Kim, J. 2005 Effects of hydrophobic surface on stability and transition. *Phys. Fluids* **17 (10)**, 108106.

Mohanty, A. & Asthana, S. 1979 Laminar flow in the entrance region of a smooth pipe. *J. Fluid Mech.* **90**, 433–447.

Nagata, M. 1990 Three-dimensional finite-amplitude solutions in plane Couette flow: bifurcation from infinity. *J. Fluid Mech.* **217**, 519–527.

Peixinho, J. & Mullin, T. 2006 Decay of turbulence in pipe flow. *Phys. Rev. Lett.* **96**, 094501.

Piekos, E. & Breuer, K. 1995 DSMC modeling of micromechanical devices. *AIAA Thermophysics Conference, San Diego* p. 2089.

Rao, K. S., Seshadri, R. & Govindarajan, R. 2004 A minimal composite theory for stability of non-parallel compressible boundary-layer flow. *Theoretical and Computational Fluid Dynamics* **17**, 233–248.

Rayleigh, L. 1880*a* On the stability or instability of certain fluid motions. *Proc. London Math. Soc.* **11**, 57.

Rayleigh, L. 1880*b* *Scientific Papers*, , vol. 1. Dover, New York, 1964.

Reddy, S. C. & Henningson, D. S. 1993 Energy growth in viscous channel flows. *J. Fluid Mech.* **252**, 209–238.

Reshotko, E. 1958 Experimental study of the stability of pipe flow i. establishment of an axially symmetric Poiseuille flow. *JPL Progress Report* pp. 20–364.

Reuter, J. & Rempfer, D. 2004 Analysis of pipe flow transition. Part I. Direct numerical simulation. *Theoretical and Computational Fluid Dynamics* **17**, 273–292.

Reynolds, O. 1883 An experimental investigation of the circumastances which determine whether the motion of water shall be direct or sinuous and of the law of resistance in parallel channels. *Phil. Trans. Roy. Soc.* **174**, 935–982.

Sahu, K. C. 2003 Numerical computation of spatially developing flows by full-multigrid technique. Master's thesis, Jawaharlal Nehru Centre for Advanced Scientific Research, Bangalore, India.

Sahu, K. C. & Govindarajan, R. 2005 Stability of flow through a slowly diverging pipe. *J. Fluid Mech.* **531**, 325–334.

Salwen, H., Cotton, F. W. & Grosch, C. E. 1980 Linear stability of Poiseuille flow in a circular pipe. *J. Fluid Mech.* **98**, 273–284.

Sarpkaya, T. 1966 Experimental determination of the critical reynolds number for pulsating Poiseuille flow. *J. Basic Engng. Trans. A. S. M. E.* **88**, 589.

Sarpkaya, T. 1975 A note on the stability of developing laminar pipe flow subjected to axisymmetric and non-axisymmetric disturbances. *J. Fluid Mech.* **68**, 345–351.

Schmid, P. J. & Henningson, D. S. 1994 Optimal energy density growth in Hagen-Poiseuille flow. *J. Fluid Mech.* **277**, 197–225.

Schmid, P. J. & Henningson, D. S. 2001 *Stability and Transition in Shear Flows*. Springer-Verlag, New York.

Selvarajan, S., Tulapurkara, E. G. & Ram, V. V. 1999 Stability characteristics of wavy walled channel flows. *Phys. Fluids* **11 (3)**, 579–589.

SELVEROV, K. P. & STONE, H. A. 2001 Preistaltically driven channel flows with applications toward micromixing. *Phys. Fluids* **13**, 1837–1859.

SHAMES, I. H. 1992 *Mechanics of Fluids*, 3rd edn. McGraw-Hill, Inc.

SHAN, H., MA, B., ZHANG, Z. & NIEUWSTADT, F. 1999 Direct numerical simulation of a puff and a slug in transitional cylindrical pipe flow. *J. Fluid Mech.* **387**, 39–60.

SHANKAR, V. & KUMARAN, V. 1999 Stability of non-parabolic flow in a flixible tube. *J. Fluid Mech.* **395**, 211–236.

SHANKAR, V. & KUMARAN, V. 2000 Stability of fluid flow in a flexible tube to non-axisymmetric disturbances. *J. Fluid Mech.* **407**, 291–314.

SHERWIN, S. J. & BLACKBURN, H. M. 2005 Three-dimensional instabilities and transition of steady and pulsatile axisymmetric stenotic flows. *J. Fluid Mech.* **533**, 297–327.

SISAVATH, S., JING, X. & ZIMMERMAN, R. W. 2001 Creeping flow through a pipe of varying radius. *Phys. Fluids* **13**, 2762–2772.

SOUTH, M. J. & HOOPER, A. P. 2001 Linear growth in two-fluid plane Poiseuille flow. *J. Fluid Mech.* **381**, 121–139.

SPARROW, E. M., LIN, S. H. & LUNDGREN, T. S. 1964 Flow development in the hydrodynamic entrance region of tubes and duct. *Phys. Fluids* **7 (3)**, 338–347.

SQUIRE'S, H. B. 1933 On the stability of three-dimensional distribution of viscous fluid between parallel walls. *Proc. Roy. Soc.* **142**, 621–628.

SREENIVASAN, K. R. & STRYKOWSKI, P. J. 1983 An instability associated with a sudden expansion in a pipe flow. *Phys. Fluids.* **26 (10)**, 2766–2768.

STILLER, J., FRANA, K., GRUNDMANN, R., FLADRICH, U. & NAGEL, W. E. 2004 A parallel pspg finite element method for direct simulation of incompressible flow. *Parallel Processing, Springer* pp. 726–733.

STRAATMAN, A. G., KHAYAT, R. E., HAJ-QASEM, E. & STEINMAN, D. A. 2002 On the hydrodynamic stability of pulsatile flow in a plane channel. *Phys. Fluids* **14 (6)**, 1938–1944.

TATSUMI, T. 1952 Stability of the laminar inlet-flow prior to the formation of Poiseuille regim, II. *J. Phys. Soc. Japan* **7**, 495.

THEOFILIS, V., DUCK, P. W. & OWEN, J. 2004 Viscous linear stability analysis of rectangular duct and cavity flows. *J. Fluid Mech.* **505**, 249–286.

THEOFILIS, V., FEDOROV, A., OBRIST, D. & DALLMANN, U. C. 2003 The extended gortler-hammerlin model for linear instability of three-dimensional incompressible swept attachment-line boundary layer flow. *J. Fluid Mech.* **487**, 271–313.

THEOFILIS, V., HEIN, S. & DALLMANN, U. 2000 On the origins of unsteadiness and three-dimensionality in a laminar separation bubble. *Phil. Trans. Roy. Soc.* **358**, 3229–3246.

TRETHEWAY, D. C. & MEINHART, C. D. 2002 Apparent fluid slip at hydrophobic microchannel walls. *Phys. Fluids* **14(3)**, L9–L12.

TUMIN, A. 1996 Receptivity of pipe Poiseuille flow. *J. Fluid Mech.* **315**, 119–137.

VENKATESH, T. N., V. R. SARASAMMA, V. R., RAJALAKSHMY, S., SAHU, K. C. & GOVINDARAJAN, R. 2005 Super-linear speed-up of a parallel multigrid navier-stokes solver on flosolver. *Current Science* **88** (4), 589–593.

WALEFFE, F. 1995 Hydrodynamic stability and turbulence: Beyond transients to a self-sustaining process. *Society for Industrial and Applied Mathematics* **95**, 319–343.

WALEFFE, F. 1998 Three-dimensional coherent states in plane shear flows. *Phys. Rev. Lett.* **81** (19), 4140–4143.

WALEFFE, F. 2001 Exact coherent structures in channel flow. *J. Fluid Mech.* pp. 93–102.

WATANABE, K. Y. & MIZUNUMA, H. 1998 Slip of newtonian fluids at slid boundary. *JSME Int. J., Ser. B* **41**, 525–529.

WATANABE, K. Y. & UDAGAWA, H. 1999 Drag reduction of newtonian fluid in a circular pipe with a highly water-repellant wall. *J. Fluid Mech.* **381**, 225–238.

WEDIN, H. & KERSWELL, R. R. 2004 Exact coherent structures in pipe flow: travelling wave solutions. *J. Fluid Mech.* **508**, 333–371.

WILLIAMS, S. D. 2001 An investigation of the stability pf developing pipe flow. PhD thesis, University of Manchester, UK.

WILSON, S. D. R. 1969 The development of Poiseuille flow. *J. Fluid Mech.* **38**, 793–806.

WYGNANSKI, I., SOKOLOV, M. & FRIEDMAN, D. 1975 On transition in a pipe. part 2. the equilibrium puff. *J. Fluid Mech.* **69**, 283–304.

WYGNANSKI, I. J. & CHAMPAGNE, F. H. 1973 On transition in a pipe. part 1. the origin of puffs and slugs and the flow in a turbulent slug. *J. Fluid Mech.* **59**, 281–335.

YECKO, P. & ZALESKI, S. 2005 Transient growth in two-phase mixing layers. *J. Fluid Mech.* **528**, 43–52.